/
Article / Book Information

( )	
Title(English)	A study on characterization of doping profile in semiconductor devices
( )	
Author(English)	Hidehiko Yabuhara
( )	: , : , : 10344 , :2016 9 20 , : , : , , , , ,
Citation(English)	Degree:, Conferring organization: Tokyo Institute of Technology, Report number: 10344 , Conferred date:2016/9/20, Degree Type:Course doctor, Examiner:,,,,,
( )	
Type(English)	Doctoral Thesis

Doctoral Thesis

A study on characterization of doping profile in semiconductor devices

A Dissertation Submitted to the Department of
Electronics and Applied Physics
Interdisciplinary Graduate School of Science and Engineering
Tokyo Institute of Technology

August 2016

Hidehiko Yabuhara

Supervisor: Prof. Kuniyuki Kakushima
Co-supervisor: Prof. Kazuo Tsutsui

Abstract

The prediction and control of doping profiles in two or three dimensions becomes increasingly important for the miniaturization of MOSFETs and emerging semiconductor devices. In this thesis, methodologies for evaluation of the doping profiles were investigated by using computational simulations and scanning capacitance microscopy (SCM) measurements.

In order to form an ultra-shallow junction (USJ), a low-energy doping process of a few hundred electron volts or less is required. For the low-energy doping process, the Monte Carlo simulation in the binary-collision approximation or the first-principles simulation is widely used. However, the former is not accurate in surface damage generations and the latter is time-consuming for a calculation of a large structure needed for the prediction of a junction position. Therefore, a hybrid method of the tight-binding quantum chemical and the classical molecular dynamics was first applied to the prediction of an USJ position. The depth of the simulation structure of a silicon (100) crystal was 12 nm and 2500 boron atoms were independently injected into the silicon structure. For the boron doping process of 200 eV, the junction position was estimated to be 6.2 nm by using the hybrid method calculation and 6.4 nm from the experimental result. This good agreement between the simulation and the experimental result indicates that the hybrid molecular dynamics method is applicable to the low-energy doping profile prediction in a silicon substrate with a depth of more than 10 nm that is needed to evaluate USJ formations.

SCM measurement is one of the most promising methods for 2D doping profile because of its high spatial resolution and wide detection concentration range. However, its poor repeatability and reproducibility of measurements, and the lack of accurate conversion method from SCM signals to carrier/doping concentrations have been problems. In this study, the repeatable and reproducible SCM measurement was

established by using a robust and conductive diamond-coated probe and a sample preparation technique of low-temperature oxidation under UV illumination. The shift of SCM signal during successive measurements was improved to 0.2 % by using the diamond-coated probe from 5 % by the conventional metal-coated probe. A methodology of quantitative SCM measurement was proposed by using the combination of a doping concentration standard sample and 3D device simulation. The validity of this methodology was examined. The converted doping concentration profile from measured SCM signals of a boron-doped silicon sample was in good agreement over the range of four orders of magnitude, 1×10^{15} - 2×10^{19} atoms/cm^3, with the result of conventional secondary ion mass spectrometry (SIMS) measurement of the same sample. Moreover, the SCM measurement has been applied to estimate a pn junction. The position of an electrical pn junction is influenced by the applied bias voltage in SCM measurements and is usually different from the position of metallurgical one. From 3D device simulations of various type of pn junctions and SCM measurements of a UMOS power device, it was shown that the SCM measurement is applicable to the delineation of abrupt pn junctions such as p-type of 1×10^{19} and n-type of 1×10^{15} atoms/cm^3. This kind of abrupt junction position is important for the design of a drain extension profile of a MOSFET. SCM measurement was shown to be applicable to other materials: SiGe and SiGeC. The diffusivities of boron in the two materials are different and the SCM measurement directly demonstrated the difference of boron diffusion profiles in SiGe and SiGeC. A kind of matrix effect was found in SCM measurement of $Si_{1-x}Ge_x$ with different Ge mole fraction x, namely, the SCM signal intensities of the same concentration of boron in $Si_{0.9}Ge_{0.1}$ and $Si_{0.8}Ge_{0.2}$ are different.

The combination usage of the hybrid molecular dynamics method of low-energy doping process and the repeatable and quantitative SCM measurement would be effective for improvement of a doping simulation model in the lateral direction of a MOSFET and also effective for the accuracy improvement of defect analysis.

Table of Contents

Chapter 1
Introduction

1.1 Semiconductor industry

1.2 Scaling rule of MOSFET

1.3 Channel and Source/Drain engineering

1.4 Characterization and modeling of dopant profile

    1.4.1 Doping profile measurements

    1.4.2 Models for computational simulations

    1.4.3 Interface characterizations of diffusion layer and metal

1.5 Scope of this work

References

1.1 Semiconductor industry

Nowadays, a wide variety of semiconductor devices, such as LSIs, memory devices, power transistors, and LEDs, are used for many products from computers to automobiles. These products contribute to the widespread improvement of our living standards. Figure 1.1 shows the worldwide sales of semiconductor devices from 2000 to 2016 [1.1]. The world market of semiconductor industry in 2014 was 336 B$ including 92 B$ of logic devices and 79 B$ of MOS memories.
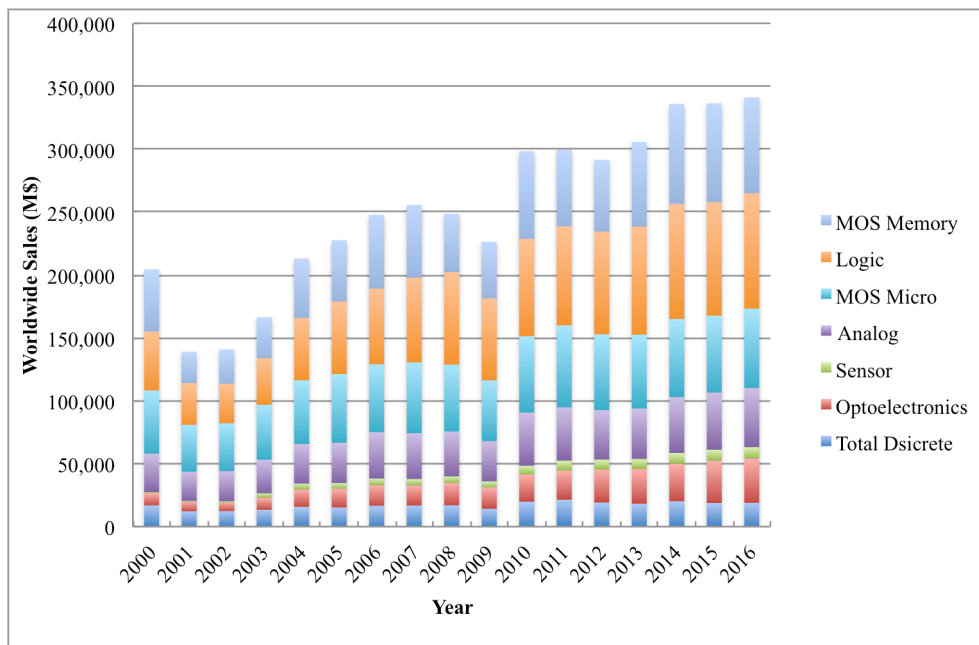
Fig. 1.1 Worldwide sales of semiconductor market from 2000 to 2016. 2015 and 2016 are forecast [1.1].

Over the past decades, the cost reduction has accelerated the worldwide use of the products and the systems. The most characteristic and important trend for production of semiconductor devices involves the reduction of cost per function of a device. The cost of apparatus including clean rooms is so high that the cost reduction of semiconductor

devices has induced a motive of competition for the maximization of the number of semiconductor chips taken out from a semiconductor wafer. The well-known Moore's law for integrated circuits (ICs), an empirical-prediction law for miniaturization of semiconductor devices, says that a device feature-size would decrease by a factor of 0.7 every two years, though it recently come down to every three years. This means that a chip area reduces by 50%, the number of chips in a wafer becomes double and the cost of a chip becomes cheaper, ideally reducing by 50% [1.2, 1.3]. The prediction has been an elegant statement of how semiconductor chips would become cheaper, faster and smaller. This law also includes the prediction of the bit-cost reduction of memory devices as shown in Fig. 1.2 [1.4].
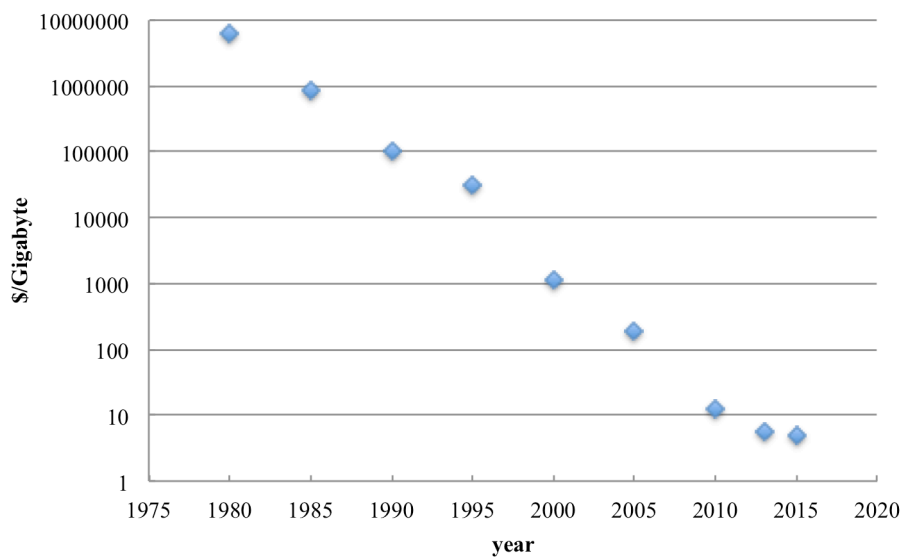
Fig. 1.2 Gigabyte cost of RAM from 1980 to 2015 [1.4].

The miniaturization of semiconductor devices has been an important direction from the viewpoint of both cost and performance. Repetition of miniaturization in the cycle of a short period of two or three years, forces companies to repeat a cycle of the design, development and manufacturing of semiconductor devices in the short term. In order to achieve this short-term repetition, process and apparatus technologies as well as

simulation, measurement and diagnosis technologies should be developed at the same time [1.5]. The miniaturization of semiconductor-device sizes according to the Moore's law becomes more difficult, and more investment is necessary to achieve the miniaturization. To continue the miniaturization, the companies need to have a return earlier for the investment.

1.2 Scaling rule of MOSFET

It has been desired that the miniaturization of ICs with high performance at low cost is achieved without losing characteristics of transistors or circuits. The short channel effect is one of the big problems for miniaturization of Metal-Oxide-Semiconductor Field-Effect-Transistors (MOSFETs) [1.6, 1.7]. To overcome the short channel effect in a smaller device, there is a scaling rule for MOSFETs. Figure 1.3 shows a scaling rule of MOSFETs [1.8, 1.9].

physical parameters	scaling factor
Channel Length (L)	$1/\kappa$
Channel Width (W)	$1/\kappa$
Gate Dielectric Thickness (Tox)	$1/\kappa$
Junction Depth (Xj)	$1/\kappa$
Impurity Concentration (N)	κ
Electric Field Intensity	1
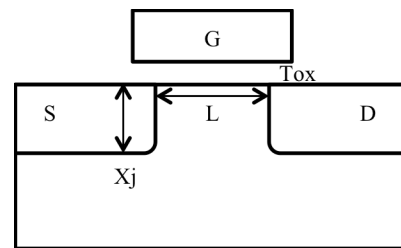
Fig. 1.3 Constant electric field scaling of a MOSFET.

One of the scaling rules is called the constant field scaling. This means that the size of the transistor must be reduced linearly together with the supply voltage, and increase the doping concentration of the source and drain regions in a way which keeps the electric field in the MOSFET constant. When the size of the gate length of a MOSFET is $1/\kappa$,

both the thickness of the gate oxide and the source/drain junction depth become $1/\kappa$, and the doping concentration becomes κ. Here, κ is a scaling factor. There are several other scaling rules [1.10, 1.11].

1.3 Channel and Source/Drain engineering

The short channel effect comes from the increase of a ratio of depletion charge supported by source/drain regions to that by a gate region as shown in Fig.1.4.

(a) Long channel
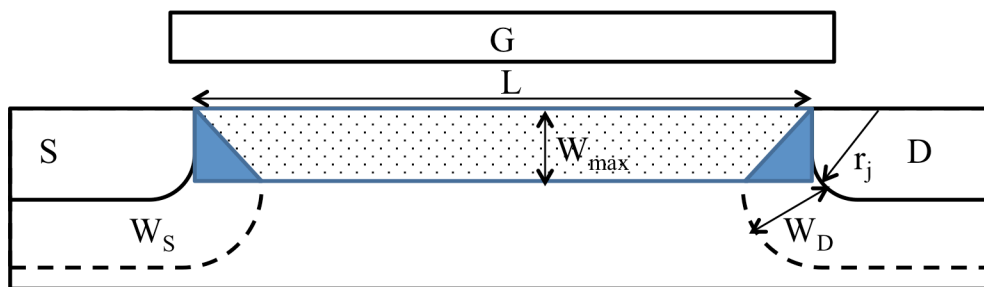
(b) Short channel
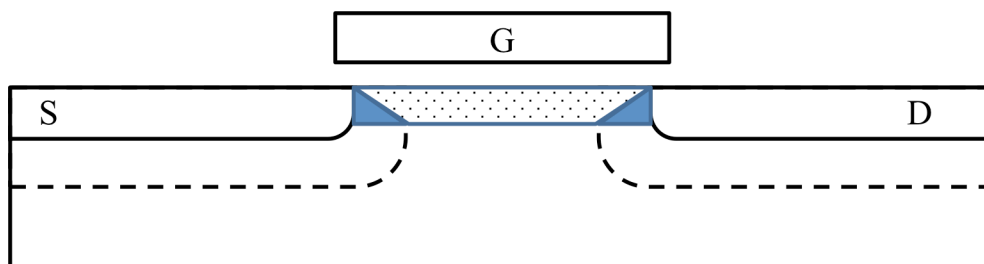
Fig. 1.4 Short channel effect of MOSFET. The gate electrode supports the depletion charge in the trapezoidal region in (a) Long channel and (b) short channel. The depletion area neighboring to S/D indicated in the triangular regions are the discrepancy from the ideal depletion region underneath the gate.

The gate electrode supports the depletion charge in the trapezoidal region shown in Fig. 1.4 (a) for a long channel and (b) for a short channel MOSFET. The depletion areas supported by source/drain region are indicated in the triangular regions, which are the discrepancy from the ideal depletion region underneath the gate. From this figure, the shift of a threshold voltage by the short channel effect in the first order approximation is shown to be $\Delta Vth = -\{qN_aW_{max}r_i/(C_oL)\} \cdot (\sqrt{1 + (2W_{max} / r_j)} - 1)$, where q is elementary charge, N_a is doping concentration, W_{max} is depletion length, r_j is junction depth, C_o is capacitance of gate oxide and L is channel length [1.12, 1.13]. To reduce the short channel effect, i.e. the depletion charge supported by the source/drain, the region is required to be shallow in vertical direction, namely, "shallow junctions". At the same time, a dopant concentration in the source/drain region should become higher because of reducing the parasitic resistance of these regions. The source/drain extensions shown in Fig. 1.5 have been introduced to effectively reduce the junction depth of the source/drain without increasing the resistance of these regions.
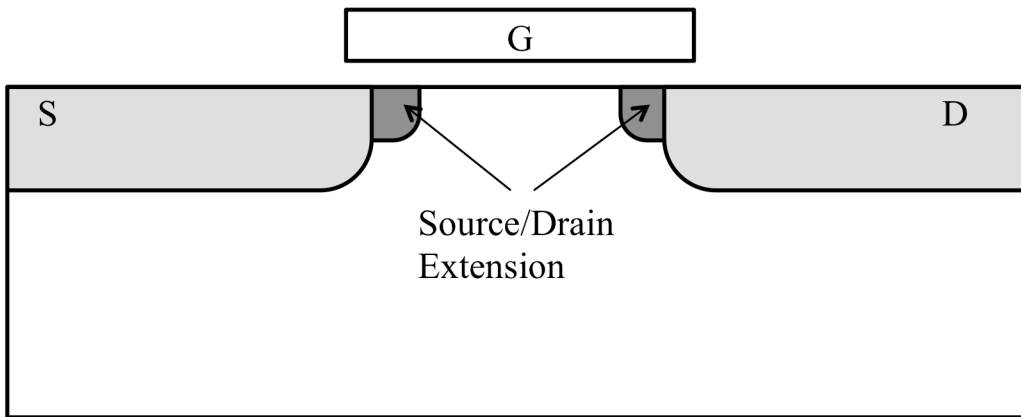
Fig. 1.5 Source/Drain extension structure of MOSFET.

There have been also many kind of source/drain engineering such as the Lightly Doped Drain (LDD) for reducing the hot carrier effect and Halo (pocket) implants for reducing the punch-through between source and drain [1.13]. Table 1.1 is a roadmap for the sizes of Logic device from the ITRS [1.14]. The junction depths have changed from 36 nm in

1999 to 12 nm in 2010, and in recent years to 8 nm or less.

Table 1.1 Roadmap of feature size and junction depth of Logic devices.

Year	1999	2003	2006	2010	2011	2012	2013	2015
Feature size (nm)	120	70	60	27	24	22	20	17
Junction depth (nm)	36	26	20	12	10	8.8	8	6.4

A design of the channel and the source/drain in the above-mentioned MOSFETs as well as a process technology for production of the designed structure are important subjects for research and development. An ion implantation and a spike rapid thermal annealing (RTA) have been widely used as a process for forming source/drain regions [1.15]. However these process technologies have a limitation in forming ultra-shallow junctions. Many process technologies have been reported to overcome the limitation [1.16].

1.4 Characterization and modeling of dopant profile

Source/drain engineering such as an ultra-shallow junction and new process technologies are required for miniaturization of MOSFETs and other devices. For this purpose, new characterization and modeling methodologies are required for precise measurement of source/drain regions in a nanometer scale and for precise prediction for designing a new device.

A dopant concentration profile and a junction position are important parameters for characterizing the diffusion layer. These parameters are sometimes predictable within the accuracy of 10 % by using a computational simulation utilizing a technology computer aided design (TCAD) software. However, the smaller a device size becomes, the more difficult the prediction of a dopant profile is [1.17]. This means that we need a methodology for both direct measurement of a doping profile in a real device and

7

accurate simulation of an ultra-shallow junction, which are required for a smaller device because of the scaling rule.

A size of a semiconductor device as well as its structure and material have been changing in these days. The structural changes are exemplified by three-dimensional Fin-FETs or vertical non-volatile memory devices [1.7, 1.18]. It is more difficult to form a doping area for Fin-FETs by using the ion implantation method in three-dimension than in conventional planar MOSFETs. In order to overcome the difficulty, a plasma doping has been a preferable alternative for isotropic doping in three-dimensions [1.19]. However, we do not have an adequate doping model in a lower energy region i.e. several hundred electron-volt range [1.20]. This low energy doping is also required for forming ultra-shallow junctions.

1.4.1 Doping profile measurements

A doping profile has been generally measured by the secondary ion mass spectrometry (SIMS) method in one dimension and optimized for a device structure through a process/device simulation. As is said in ITRS or other sources, however, measurements of a doping profile in two- or three-dimensions have been strongly desired for miniaturization of devices [1.21]. A doping profile measurement in two-/three-dimensions had been performed by a wide variety of methods as described in some review papers [1.22-1.24]. However, there was no established stable-method in 2000. Since then, many researchers have been making their efforts to develop a new method in this field. Among methods developed so far, the scanning probe microscopy (SPM) is one of the superior methods with high spatial resolution potential. The SPM measurements detect some kind of interaction between a small probe tip and a sample surface. In the measurements of a doping profile by SPMs, electrical interactions including capacitance, resistance, and surface potential are detected in scanning capacitance microscopy (SCM), scanning spreading resistance microscopy (SSRM),

and Kelvin force microscopy (KFM), respectively [1.22]. SCM has been, especially, powerful technique which can visualize a pn junction position.

The scanning capacitance microscopy (SCM) consists of a semiconductor/silicon (S), a conductive probe (M), and dielectric/oxide layer (O) between S and M [1.25]. As is shown in Fig. 1.6, this structure is a MOS capacitance.

conductive probe (Metal)

Oxide

Silicon
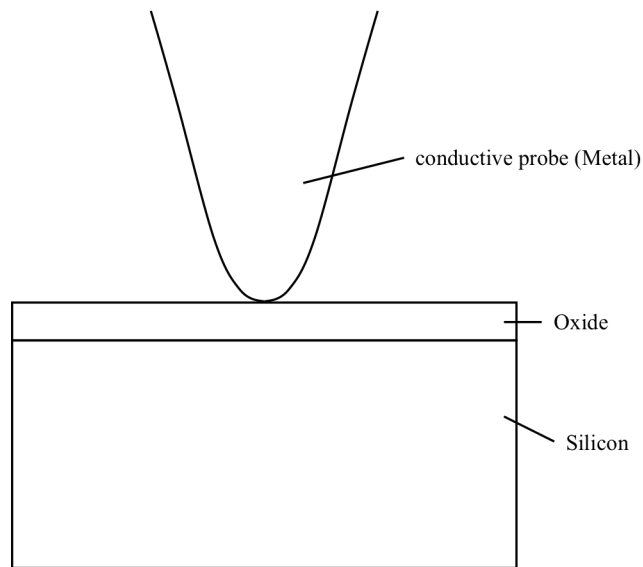
Fig. 1.6 MOS capacitance configuration in scanning capacitance microscopy.

When some dc voltage bias is applied between M and S, the depletion layer spreads in the semiconductor (S) region under the conductive probe (M), thereby changing the capacitance of this system. A small change of capacitance (dC) will occur in accordance with dV when we add some small ac bias (dV) in a frequency in addition to the dc bias. This capacitance change dC depends directly on the concentration of free carriers in the semiconductor area, and thus SCM can measure the free carrier concentrations. There are two modes including constant dC and constant dV modes. In the constant dV mode, dC changes according to a carrier density. Thus we measure the change of the width of the depletion layer. On the other hand, in the constant dC mode, ac bias voltage dV changes while keeping the depletion width constant. Moreover, considering phase

information of the dC/dV signals through a lock in amplifier detection, SCM can show the difference between n-type and p-type semiconductors. This means SCM can measure the position of a pn junction in a semiconductor. This pn junction, however, means an electrical pn junction but not metallurgical one. Therefore relationship between electrical and metallurgical pn junction should be clarified in SCM study. The capacitance measured with SCM would be affected by the topography of a conductive tip, i.e. a tip curvature and its change during the measurement, and by dielectric layer between a semiconductor and a tip. An example is the growth of a dielectric layer by anodic oxidation through carrier injections in applying a bias. These factors disturb the capacitance signal, and thereby making the SCM technology poorly reproducible and repeatable. Thus, a study of the reproducibility and repeatability of the SCM technology is necessary for making it highly reliable. Furthermore an application of the SCM technology to not only the measurement of a carrier density in a compound semiconductor instead of silicon but also the estimation of defects in a semiconductor becomes quite important.

1.4.2 Models for computational simulations

We have already had a lot of the simulation models for an ion implantation process including the dual Pearson model for 0.5 keV or higher ion implantation energy [1.15, 1.26]. However we do not have an accurate model for an ion doping process in the lower energy region that can be applicable to the plasma doping process. In the lower energy region, it is not obvious whether electrons of a doping ion affect the profile through interactions with lattice atoms or not. Accordingly, we employed a computational simulation including quantum mechanical models. A quantum molecular dynamics method is suitable for this purpose, however, it would take too much time to simulate a doping profile across several tens of nanometers in depth direction [1.27]. For the above reasons, we employed a hybrid method of classical and quantum

molecular dynamics.

Molecular dynamics is a powerful simulation method for following a trajectory of a particle, which interacts with an environment such as a silicon lattice. If the interaction is described as some kind of intermolecular potentials such as the Lennard-Jones potential u(r):

$$u(r) = 4e[(\frac{s}{r})^{12} - (\frac{s}{r})^6] \tag{1.1}$$

where e and s are parameters and r is distance between two molecules, it is called a classical molecular dynamics method. However, it is sometimes difficult to obtain the intermolecular potential correctly. In this case, the use of first principles calculation methods such as the Car-Parrinello method is a fundamental way, but it generally takes a lot of calculation time. A hybrid method of classical and quantum molecular dynamics is helpful for reducing the calculation time. In this hybrid method, an interaction between a dopant atom and its several nearest atoms in the atomic lattice of a semiconductor is treated based on the quantum calculation, while the other interactions based on the classical calculation using intermolecular potentials. The tight-binding approximation is widely used for the quantum calculation. Even if this hybrid method is employed, the doping simulation is still challenging. To predict a final doping profile, we need an annealing model such as the rapid annealing or the flash lamp annealing in a very short process time. The short process time is necessary to prevent the additional diffusion of dopant atoms in keeping an ultra-shallow doping profile. This means that the doping profile simulation in the low energy region without the annealing simulation is still significant for an ultra-shallow junction application.

1.4.3 Interface characterizations of diffusion layer and metal

It is important to control an interface of a doped silicon and a metal electrode at the source/drain area of a MOSFET device. Problems occurring at the interface sometimes

come from the diffusion of atoms from the electrode into the semiconductor and vice versa. In this case, it is the common practice to measure not only the concentration of the diffused atoms but also their electrical influence on a semiconductor i.e. the influence on a band profile at the interface of semiconductor. In order to measure both the concentration and the electrical influence of diffused atoms, X-ray photoelectron spectroscopy (XPS) is a most suitable method. We need to measure a semiconductor layer at different depths to depict a band profile. For this purpose, it would be preferable to use an angular-resolved XPS or XPS with etching of the electrode material.

Not only the diffusion layer, but also its contact interface to the electrode is important to obtain the designed device characteristics. A doped-atom is mainly included at the interface of semiconductor/electrode. However, some additional impurities might come from the environment during contact-forming processes or from the electrode itself. Moreover, the possibility of the influence of interface trap cannot be ruled out. In these cases, thermal annealing process is generally used to make ohmic contact between semiconductor and electrode. Its temperature, duration and atmosphere are important factors for keeping a doping profile unchanged and for promoting a silicidation reaction in case of silicon. However these factors also affect the mutual diffusion of atoms between semiconductor and electrode. The circumstances become more complex in emerging devices produced by using many kind of materials. In the lower temperature, silicidation for making ohmic contact does not proceed enough, thereby increasing the contact resistance. In order to clarify the reason of the high resistivity, depicting a band profile at the interface is useful. X-ray photoelectron spectroscopy (XPS) is useful for this purpose. A stacked sample of semiconductor and electrode should be used for measuring a band profile of semiconductor influenced by the electrode. However, the escape depth of a photoelectron of XPS is very shallow, and thus the resultant XPS spectra represent the condition of the top surface of a sample, typically five nanometers depth. To measure the stacked sample of

semiconductor/electrode, it is important to control the thickness of the electrode within less than a few nanometers. More precise measurement of a band profile would be performed by the use of the angular-resolved XPS.

1.5 Scope of this work

This study for the scanning capacitance microscopy measurements had been done mainly from 2000 to 2002 and that for the doping simulation from 2005 to 2007. During the course of the studies, the SPMs-based direct measurement of a 2D doping profile across cross-sectioned devices had been developed for only five years [1.28]. After that, this technology had been utilized by many researchers. However, the biggest problem involved repeatability and reproducibility for the measurement of the doping profile and its quantitative measurement by the use of SCM, SSRM and other SPM related methods [1.22, 1.24]. These problems were critical especially for manufacturing newly developed semiconductor devices as well as for improving product yields. However no one paid attention to the repeatability of SCM measurements at that time. This became a motivation that we studied an effect of the chemical treatment of the cross-sectioned samples and the repeatability of SCM measurements. We also adopted diamond-coated probes, which are usually used for SSRM, for SCM in order to prevent degradation of the probe itself during the measurements. We have improved both the sample preparations and the probes, and finally came to establish the repeatable and reproducible method. The above successful results made it possible for us to focus on a development the quantitative method by the combination of a doping concentration standard sample and 3D device simulator. In order to minimize the development time for manufacturing of a new device, we need a computational method to predict the device characteristics and its process conditions. Commercially available and house made TCAD software has been widely used to predict a doping profile. No adequate

analytical model has been reported for a low-energy doping for an ultra-shallow junction so far. Only Monte Carlo simulations have been mainly used or this purpose [1.29, 1.30]. This method usually adopts the binary collision approximation. However, the binary collision approximation is not adequate in some cases of a doping energy less than 1 keV [1.31]. Therefore our original hybrid molecular dynamics method combining tight-binding quantum mechanical model with classical one was the first example for successful application to the low energy doping process of boron into a silicon substrate which has an enough thickness for prediction of an ultra-shallow junction depth.

From the above-mentioned things, this thesis aims at diffusion layers in semiconductor devices especially from the point of developing stable and reliable characterization methods and computational simulation modeling of low energy doping for ultra-shallow junctions.

This thesis is divided in seven chapters shown in Fig. 1.7 and each chapter has the following content.

Following this introductory chapter, the modeling of low-energy boron doping into a silicon crystal will be discussed in Chapter 2 by using a hybrid of quantum and classical molecular dynamics method for ultra-shallow junctions. Basic concept of SCM and some other SPMs will be overviewed in Chapter 3. In Chapter 4, repeatability and reproducibility of SCM measurement will be discussed by using a diamond-coated tip, which is hard enough to avoid topographical change during the measurement. In this chapter, a methodology of quantitative measurement of SCM will be also proposed. In Chapter 5, SiGe and SiGeC will be treated as examples of compound semiconductors. Some problems that are characteristically observed in compound semiconductors will also be discussed. In this chapter, an application of SCM technique to a defect related problem, such as ion implantation induced defects and activation will be also discussed. In Chapter 6, the advantage and necessity of the combination of computational simulation method for the prediction of an ultra-shallow junction described in Chapter 2

and quantitative SCM technology described in Chapter 4 will be discussed. Finally in Chapter 7, this study of doping profile characterization and prediction will be concluded.

```
                    ┌─────────────────────┐
                    │    Chapter 1.       │
                    │    Introduction     │
                    └─────────────────────┘

┌─────────────────────┐          ┌─────────────────────┐
│    Chapter 2.       │          │    Chapter 3.       │
│ Simulation method for│         │ Characterization of │
│   prediction of USJ │          │   doping profile    │
│      position       │          │ SCM and other methods│
└─────────────────────┘          └─────────────────────┘

              ┌─────────────────────┐  ┌─────────────────────┐
              │    Chapter 4.       │  │    Chapter 5.       │
              │  Quantitative SCM   │  │  Application of SCM │
              │    measurement      │  │                     │
              └─────────────────────┘  └─────────────────────┘

                    ┌─────────────────────┐
                    │    Chapter 6.       │
                    │    Discussion       │
                    └─────────────────────┘

                    ┌─────────────────────┐
                    │    Chapter 7.       │
                    │    Conclusion       │
                    └─────────────────────┘
```
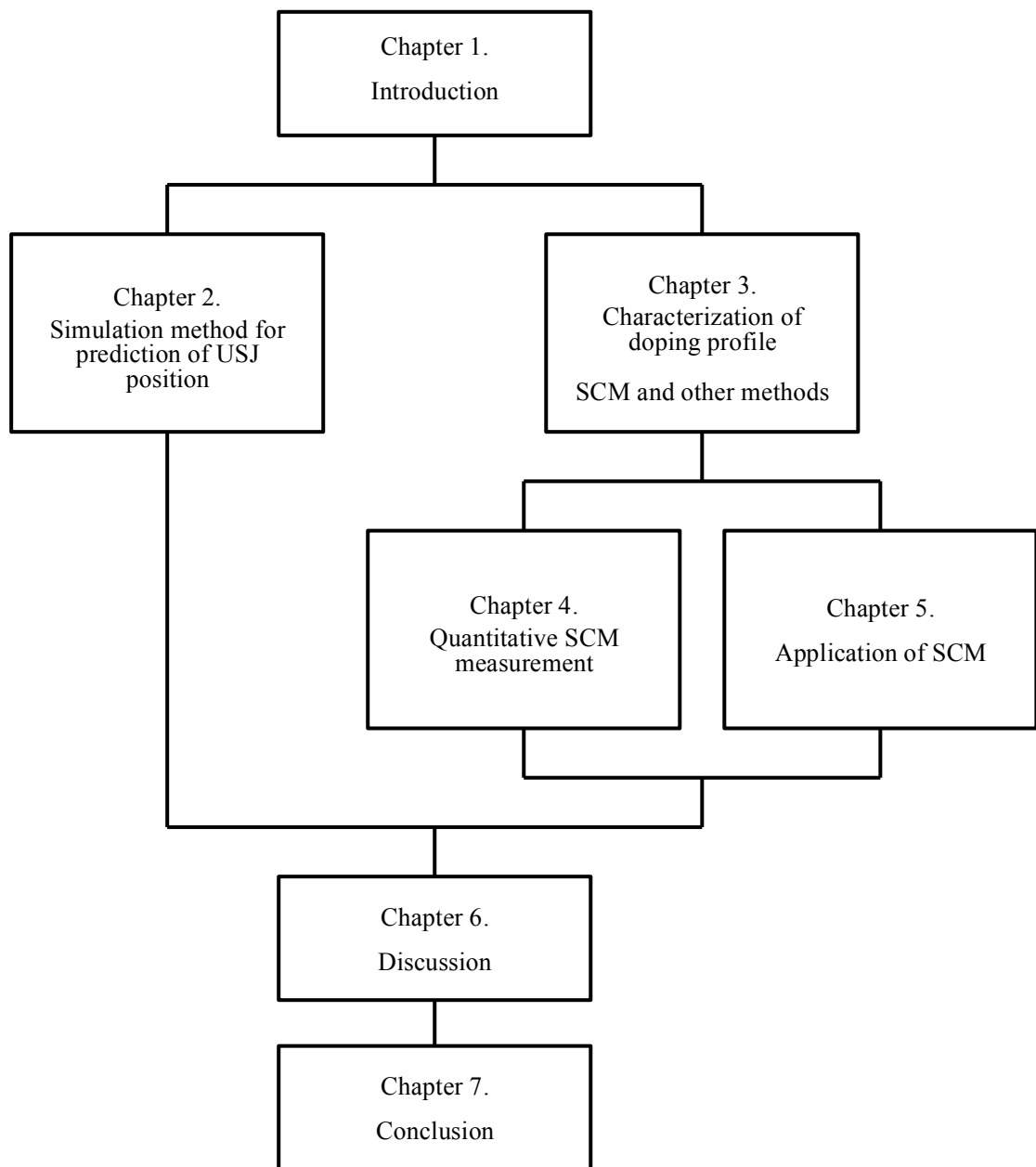
Fig. 1.7 Outline of this work.

References

[1.1] WSTS: World Semiconductor Trade Statistics, http://www.wsts.org

[1.2] G. Moore, "Cramming more components onto integrated circuits", Electronics, vol. 38, pp. 114-117, 1965.

[1.3] G. Moore, "Progress in digital integrated electronics", Electron Devices Meeting, Vol. 21, pp. 11-13, 1975.

[1.4] Average historic price of RAM, http://www.statisticbrain.com/average-historic-price-of-ram/.

[1.5] International Technology Roadmap for Semiconductor (ITRS) 2013. http://www.itrs2.net/2013-itrs.html.

[1.6] J. Ruch, "Electron dynamics in short channel field-effect transistors", IEEE Transactions on Electron Devices, vol. 19, pp. 652-654, 1972.

[1.7] X. Huang, W. C. Lee, C. Kuo, D. Hisamoto, L. Chang, J. Kedzierski, E. Anderson, H. Takeuchi, Y. K. Choi, K. Asano and V. Subramanian, "Sub 50-nm finfet: Pmos", IEDM'99. Technical Digest, pp. 67-70, 1999.

[1.8] R. H. Dennard, F. H. Gaensslen, H. N. Yu, V. L. Rideout, E. Bassous, and A. R. LeBlanc, "Design of ion-implanted MOSFET's with very small physical dimensions", IEEE Journal of Solid-State Circuits, vol. 9, pp. 256-268, 1974.

[1.9] B. Davari, R. H. Dennard and G. G. Shahidi, "CMOS scaling for high performance and low power-the next ten years", Proceedings of the IEEE, vol. 83, pp. 595-606, 1995.

[1.10] H. Iwai, "Roadmap for 22 nm and beyond", Microelectronic Engineering, vol. 86, pp. 1520-1528, 2009.

[1.11] M. Horowitz, E. Alon, D. Patil, S. Naffziger, R. Kumar and K. Bernstein, "Scaling, power, and the future of CMOS", IEDM Technical Digest, pp. 7-15, 2005.

[1.12] K. Roy, S. Mukhopadhyay and H. Mahmoodi-Meimand, "Leakage current mechanisms and leakage reduction techniques in deep-submicrometer CMOS circuits", Proceedings of the IEEE, vol. 91, pp. 305-327, 2003.

[1.13] Y. Taur and T. H. Ning, Fundamentals of Modern VLSI Devices, Cambridge Univ. Press, pp. 140-143, 1998.

[1.14] ITRS 2009, 2011.

[1.15] S. M. Sze, VLSI Technology 2nd edition, McGraw-Hill, pp. 272-374, 1988.

[1.16] S. R. Aid, S. Hara, Y. Shigenaga, T. Fukaya, Y. Tanaka, S. Matsumoto, G. Fuse and S. Sakuragi, "Formation of Ultrashallow p$^+$/n Junction in Silicon Using a Combination of Low-Temperature Solid Phase Epitaxy and Non-Melt Double-Pulsed Green Laser Annealing", Japanese Journal of Applied Physics, vol. 52, pp. 026501, 2013.

[1.17] C. Zechner, D. Matveev, A. Erlebach, S. Simeonov, V. Menialenko, R. Mickevicius, M. Foad, A. Al-Bayati, A. Lebedev and M. Posselt, "TCAD calibration of USJ profiles for advanced deep sub-μm CMOS processes", Nuclear Instrument and Methods in Physics Research B, 186, pp. 303-308, 2002.

[1.18] B. Yu, L. Chang, S. Ahmed, H. Wang, S. Bell, C. Y. Yang, C. Tabery, C. Ho, T. J. King, J. Bokor, C. Hu, M. R. Lin and D. Kyser, "FinFET scaling to 10 nm gate length", IEDM 2002, pp. 251-254, 2002.

[1.19] B. Mizuno, I Nakamura, N. Aoi, M. Kubota and T. Komeda, "New doping method for subhalf micron trench sidewalls by using an electron cyclotron resonance plasma", Applied Physics Letters, vol. 53, pp. 2059-2061, 1988.

[1.20] K. Nordlund, "Molecular dynamics simulation of ion ranges in 1-100 keV energy range", Computational Materials Science, vol. 3, pp. 448-456, 1995.

[1.21] S. Walther and L. Godet, "Plasma implanted ultra-shallow junction boron depth profiles: Effect of plasma chemistry and sheath conditions", Journal of Vacuum Science and Technology B, vol. 24, pp. 489-493, 2006.

[1.22] A. C. Diebold, M. R. Kump, J. J Kopanski and D. G. Seiler, " Characterization of two-dimensional dopant profiles: Status and review", Journal of Vacuum Science and Technology B, vol. 14, pp. 196-201, 1996.

[1.23] D. A. Bonnell, D. N. Basov, M. Bode, U. Diebold, S. V. Kalinin, V. Madhavan, L. Novotny, M. Salmeron, U. D. Schwarz and P. S. Weiss, "Imaging physical phenomena with local probes: From electrons to photons", Reviews of Modern Physics,

vol. 84, pp. 1343-1381, 2012.

[1.24] N. Duhayon, P. Eyben, M. Fouchier, T. Clarysse, W. Vandervorst, D. Álvarez, S. Schoemann, M. Ciappa, M. Stangoni, W. Fichtner, P. Formanek, M. Kittler, V. Raineri, F. Giannazzo, D. Goghero, Y. Rosenwaks, R. Shikler, S. Saraf, S. Sadewasser, N. Barreau, T. Glatzel, M. Verheijen, S. A. M. Mentink, M. Sprekeisen, T. Maltezopoulos, R. Wiesendanger and L. Hellemans, "Assessing the performance of two-dimensional dopant profiling techniques", Journal of Vacuum Science & Technology B, vol. 22, pp. 385-393, 2004.

[1.25] C. C. Williams, J. Slinkman, W. P. Hough and H. K. Wickramasinghe, "Lateral dopant profiling with 200 nm resolution by scanning capacitance microscopy", Applied Physics Letters, vol. 55, pp. 1662-1664, 1989.

[1.26] R. G. Wilson, "The pearson IV distribution and its application to ion implanted depth profiles", Radiation Effects, vol. 46, pp. 141-147, 1980.

[1.27] L. Marques, I. Santos, L. Pelaz, P. Lopez, and M. Aboy, "Atomistic modeling of ion implantation technologies in silicon", Nuclear Instruments and Methods in Physics Research B, vol. 352, pp. 148-151, 2015.

[1.28] A. Erickson, L. Sadwick, G. Neubauer, J. J. Kopanski, D. Adderton and M. Rodgers, " Quantitative scanning capacitance microscopy analysis of two-dimensional dopant concentrations at nanoscale dimensions", Journal of Electronic Materials, vol. 25, pp. 301-304, 1996.

[1.29] S. Tian, "Predictive Monte Carlo ion implantation simulator from sub-keV to

vol. 84, pp. 1343-1381, 2012.

[1.24] N. Duhayon, P. Eyben, M. Fouchier, T. Clarysse, W. Vandervorst, D. Álvarez, S. Schoemann, M. Ciappa, M. Stangoni, W. Fichtner, P. Formanek, M. Kittler, V. Raineri, F. Giannazzo, D. Goghero, Y. Rosenwaks, R. Shikler, S. Saraf, S. Sadewasser, N. Barreau, T. Glatzel, M. Verheijen, S. A. M. Mentink, M. Sprekeisen, T. Maltezopoulos, R. Wiesendanger and L. Hellemans, "Assessing the performance of two-dimensional dopant profiling techniques", Journal of Vacuum Science & Technology B, vol. 22, pp. 385-393, 2004.

[1.25] C. C. Williams, J. Slinkman, W. P. Hough and H. K. Wickramasinghe, "Lateral dopant profiling with 200 nm resolution by scanning capacitance microscopy", Applied Physics Letters, vol. 55, pp. 1662-1664, 1989.

[1.26] R. G. Wilson, "The pearson IV distribution and its application to ion implanted depth profiles", Radiation Effects, vol. 46, pp. 141-147, 1980.

[1.27] L. Marques, I. Santos, L. Pelaz, P. Lopez, and M. Aboy, "Atomistic modeling of ion implantation technologies in silicon", Nuclear Instruments and Methods in Physics Research B, vol. 352, pp. 148-151, 2015.

[1.28] A. Erickson, L. Sadwick, G. Neubauer, J. J. Kopanski, D. Adderton and M. Rodgers, " Quantitative scanning capacitance microscopy analysis of two-dimensional dopant concentrations at nanoscale dimensions", Journal of Electronic Materials, vol. 25, pp. 301-304, 1996.

[1.29] S. Tian, "Predictive Monte Carlo ion implantation simulator from sub-keV to

above 10 MeV" , Journal of Applied Physics, vol. 93, pp. 5893-5904, 2003.

[1.30] W. Moeller and W. Eckstein, "Tridyn — A TRIM simulation code including dynamic composition changes", Nuclear Instruments and Methods in Physics Research B, vol. 2, pp. 814-818, 1984.

[1.31] I. Santos, L. A. Marques, L. Pelaz, and P. Lopez, "Improved atomistic damage generation model for binary collision simulations", Journal of Applied Physics, vol. 105, pp. 083530, 2009.

Chapter 2
Computational method for prediction of USJ position

2.1 Introduction

2.2 Computational and experimental methods

 2.2.1 Computational method

 2.2.2 Plasma doping experiment

2.3 Results and discussion

 2.3.1 Doping profile and junction position

 2.3.2 Defect distribution

2.4 Conclusions

References

2.1 Introduction

The International Technology Roadmap for Semiconductors states that the depth of an ultra-shallow junction needed for a drain extension in MOSFETs is about 8 nm for the 24 nm node [2.1]. There is also need of a conformal doping for three-dimensional devices [2.2]. Plasma doping is a promising process for ultra-shallow junction formation in planar devices and for conformal doping profile formation in three-dimensional devices [2.3 − 2.5]. However, the low-energy doping mechanism has not yet been established [2.6]. Therefore, computational simulation models, particularly the analytical models typically used in commercially available technology computer-aided design (TCAD), are not well established [2.7, 2.8]. In fact, there are few established parameter tables used in analytical models applicable to doping energy less than 200 eV. On the other hand, Monte Carlo simulation is widely used in low-energy doping profile prediction [2.9, 2.10]. This method usually adopts the binary collision approximation, which ignores many-body collisions in the complex potential field of a solid. However, the binary collision approximation is not adequate in some cases of doping energy less than 1 keV, such as underestimation of displacement of atoms below about one bond length [2.11 − 2.13]. In these cases, many-body collisions of the doped atom with the surrounding atoms should be considered. Moreover, since, for doping in a low-energy region such as less than 500 eV, electron-electron interactions become important, we need a quantum mechanical model. However, the quantum mechanical calculation, such as first-principles calculation, of the dynamics of doping atoms into a silicon crystal is time-consuming even with the use of recent powerful computers. One approach to achieve an accurate and less computationally time-consuming model is the multi-scale simulation method [2.14, 2.15].

Tight-binding quantum chemical molecular dynamics has been applied to doping processes to reduce the computational time [2.16]. The analysis of energy loss processes

through the interactions between silicon atoms and a boron atom injected into silicon crystal at several injection angles has confirmed that the boron atom forms chemical bonds with its surrounding silicon atoms, resulting in the loss of its kinetic energy, and then the bonds are broken and the boron atom continues to move until the next interaction with silicon atoms. However, the thickness of the silicon crystal used in this calculation was 2 nm, which is less than the 10 nm needed to predict the ultra-shallow junction position. Moreover, for the prediction of the profile and the junction position, at least 10^3 boron atoms, hopefully more than 10^4 atoms, should be considered because the boron concentration at the junction is two or 3 orders of magnitude less than that at the peak position. For such a large silicon structure into which more than 10^3 boron atoms are injected, the adoption of the full tight-binding quantum chemical molecular dynamics method is not realistic in the point of computational time. As far as we know, there is one case in which simulations were conducted for doping profile prediction in a realistic size by the tight-binding quantum chemical method [2.17].

Therefore, we adopt a hybrid of quantum chemical and classical molecular dynamics method to enable the calculation of the boron depth profile in silicon with a sufficient thickness to predict the position of an ultra-shallow junction. In this hybrid method, quantum chemical molecular dynamics calculation is used for an injected born atom and some silicon atoms located near the boron atoms, and classical molecular dynamics calculation is used for the other silicon atoms. By using the hybrid molecular dynamics method, we are able to consider many-body collisions with the formation and dissociation of chemical bonds between an injected boron atom and silicon atoms for more than 10^3 boron injection events in a realistic computation time. We also compare the calculated profiles with the experimental results of plasma doping. Moreover, we investigated the retained dose and defect distribution in low energy doping.

2.2 Computational and experimental methods

2.2.1 Computational method

In this study, the original hybrid molecular dynamics (MD) program, "Hybrid Colors", which consists of tight-binding quantum chemical and classical MD programs, has been used. These programs have been developed by a group of Miyamoto and are commercially available [2.18, 2.19]. Their tight-binding MD program, "Colors", based on their original tight-binding approximation, is over 5000 times faster than the conventional first-principles MD method. In the "Colors" program, the total energy, E, for each atom is expressed by

$$E = \sum_{i=1}^{n} m_i v_i^2 / 2 + \sum_{k=1}^{occ} \varepsilon_k + \sum_{i=1}^{n} \sum_{\substack{j=1 \\ i>j}}^{n} Z_i Z_j e^2 / R_{ij}$$

$$+ \sum_{i=1}^{n} \sum_{\substack{j=1 \\ i>j}}^{n} E_{repul} (R_{ij}). \tag{2.1}$$

In this formula, m_i is the mass of the electron, v_i is the velocity of the electron, ε_k is the eigenvalue of the orbital calculated by the tight-binding calculation, Z_i is the atomic charge, e is the elementary electric charge, and R_{ij} is the interaction distance. In the second term the summation includes all occupied orbitals. The fourth term means the short-range exchange repulsion energy that is represented by

$$E_{repul}(R_{ij}) = (b_{ij}) \exp[(a_{ij} - r_{ij})/b_{ij}]. \tag{2.2}$$

Here, the parameters a_{ij} and b_{ij} represent the size and stiffness, respectively.

The force is calculated using Eq. (1) and is shown as

$$F_i = \sum_{\substack{j=1 \\ j \neq i}}^{n} \sum_{k=1}^{occ} C_k^T (\partial H / \partial R_{ij}) C_k + \sum_{\substack{j=1 \\ j \neq i}}^{n} \sum_{k=1}^{occ} \varepsilon_k C_k^T (\partial S / \partial R_{ij}) C_k - \sum_{\substack{j=1 \\ j \neq i}}^{n} Z_i Z_j e^2 / R_{ij}^2$$

$$+ \sum_{\substack{j=1 \\ j \neq i}}^{n} \partial E_{repul}(R_{ij}) / \partial R_{ij} \,. \qquad (2.3)$$

Here, C_k is the coefficient of the basis function, C_k^T is its transposed form, H is the Hamiltonian of the system, and S is the overlap integral of the atomic orbitals. In order to minimize the computational time, various parameters, namely, the valence state ionization potential of atomic orbital i ($I_i = -H_{ii}$) and the Slater exponent of atomic orbital i, were used [2.18]. For the off-diagonal Hamiltonian, the following H_{rs} expression is employed.

$$H_{rs} = \frac{1}{2} K S_{rs} [H_{rr} + H_{ss}] , \qquad (2.4)$$

$$K = 1 + (\kappa + \Delta^2 - \Delta^4 \kappa) \, exp\{-\delta(R - d_0)\} , \qquad (2.5)$$

$$\Delta = \frac{H_{rr} - H_{ss}}{H_{rr} + H_{ss}} . \qquad (2.6)$$

Here, κ, δ, and d_0 are the tight-binding parameters. Overlap integral S_{rs} was calculated from Slater exponent, which was fitted to the result of Density Functional Theory (DFT) calculation. The H_{rr} was also calculated by fitting to the result of DFT. The validity of the result of these parameter fittings in "Colors" program was confirmed by comparing the potential curve of Si – Si in diatomic Si_2 molecules calculated by the DFT method [2.18].

In "Hybrid Colors", an extended link-atom method was used to counter the cluster terminal effect and to obtain stable electronic structures of the quantum mechanical atoms [2.20]. In the extended link-atom method, link atoms, i.e., adjacent Si atoms of the injected boron atom and terminating hydrogen atoms, are added to balance the electron structure in the quantum mechanical calculation part.

Tsuboi et al. has shown, by using the "Colors" program, that in the low-energy

implantation of boron into a 2-nm-thick silicon layer at an initial kinetic energy of 100 eV, there is a strong correlation between the kinetic energy loss of the irradiated boron atom and the total bond population [2.16]. The loss of the kinetic energy of boron was attributed to the higher angle collisions, where the angle is measured between the scattered and incident directions of the boron atom, and the formation and dissociation of chemical bonds between the boron atom and its surrounding silicon atoms. The latter mechanism shows the importance of using a quantum chemical MD approach and also indicates that it is sufficient to adopt this approach only for small areas including a boron atom and some neighboring silicon atoms in the case of low-energy implantation. The silicon (001) substrate model with the dimensions of $2.17 \times 2.17 \times 12.0$ nm^3 shown in Fig. 2.1 was used for the doping simulation.
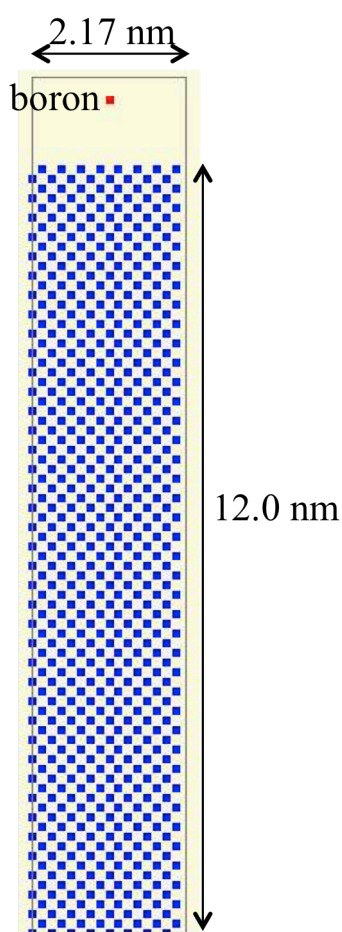
Fig. 2.1 Silicon (001) model with dimensions of $2.17 \times 2.17 \times 12.0$ nm^3.

The tight-binding quantum chemical MD calculation was used for the injected boron atom and its neighboring silicon atoms within a sphere with a radius of 0.5 nm centered at the boron atom. The radius of the quantum mechanical part should be decided from two aspects. One is the computational time and the other is balance of forces at the center atom in the extended link-atom method. In this study, the radius of the quantum mechanical part has been decided to 0.5 nm by comparing with 1.0 nm in the preliminary simulation and its value was larger than that of 0.3 nm used in the reference [2.20].

For the hybrid MD calculation, the classical MD was used for the other silicon atoms with the conventional Stillinger-Weber (SW) potential [2.21]. 2500 boron atoms were injected independently into the silicon (001) substrate at different initial positions (x, y). The initial kinetic energies were 100 and 200 eV. Simulations were performed under the periodic boundary condition in the x and y directions and the non-periodic condition in the z direction. The time step was 0.1×10^{-15} s and the temperature of the system was 300 K. The velocity rescaling method was used to control the temperature of the system, and the injected atom was excluded from this temperature control. We repeated the calculation steps for each injection position until the boron stopped in the silicon structure or the boron disappeared in the z direction by reflection from the silicon surface or by passing through the structure without stopping.

The number of defects generated during boron doping processes was also estimated by using another silicon (001) substrate model with smaller dimensions of $0.77 \times 0.77 \times 2.13$ nm^3. This silicon structure is smaller than the previous one, because we do not need a depth that includes the junction position to determine the defect distribution. The boron injection was repeated 50 times and the number of silicon atoms that moved from their initial positions and had a bond population of less than 4, resulting in the formation of defects, was determined [2.16]. The initial kinetic energies were 50, 100, and 200 eV.

2.2.2 Plasma doping experiment

The simulation results were compared with the experimental results of plasma doping obtained by Sasaki et al [2.22]. Figure 2.2 shows the secondary ion mass spectrometry (SIMS) profiles of as-doped boron in silicon substrates measured with 250 eV O_2^+ primary beam. The ion doping energy was estimated to be 120 and 200 eV for the two profiles.
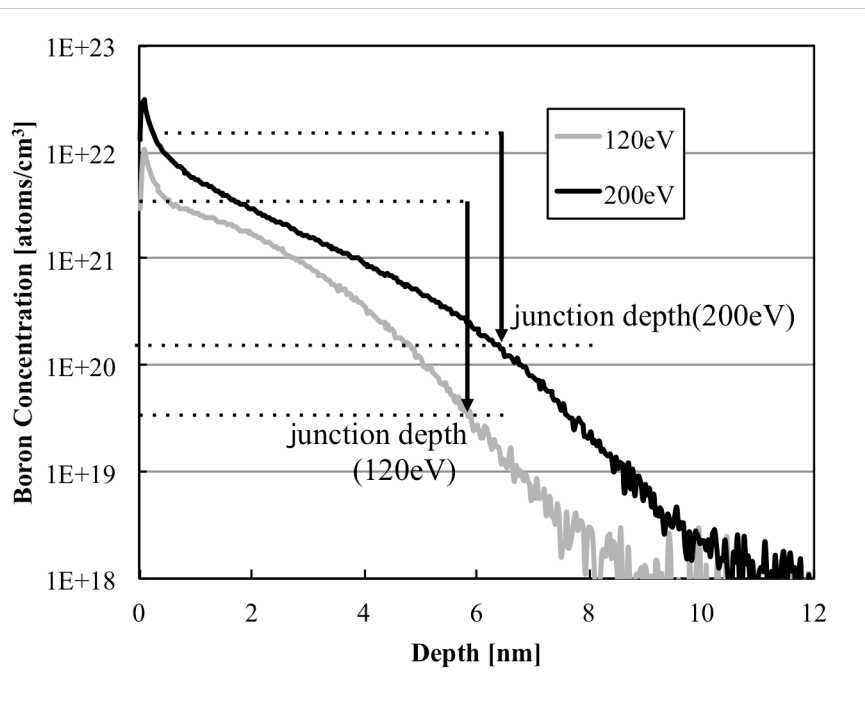

Fig. 2.2 Secondary ion mass spectrometry profiles of as-doped boron in silicon substrates in plasma doping experiment with estimated doping energies of 120 and 200 eV.

2.3 Results and discussion

2.3.1 Doping profile and junction position

Figure 2.3 is an example of the simulation result of low-energy boron doping. Open red circles in this figure show the trajectory of the injected boron atom. The boron atom was injected into the silicon surface from the initial position and stopped at the final position in the silicon substrate shown in Fig. 2.3.
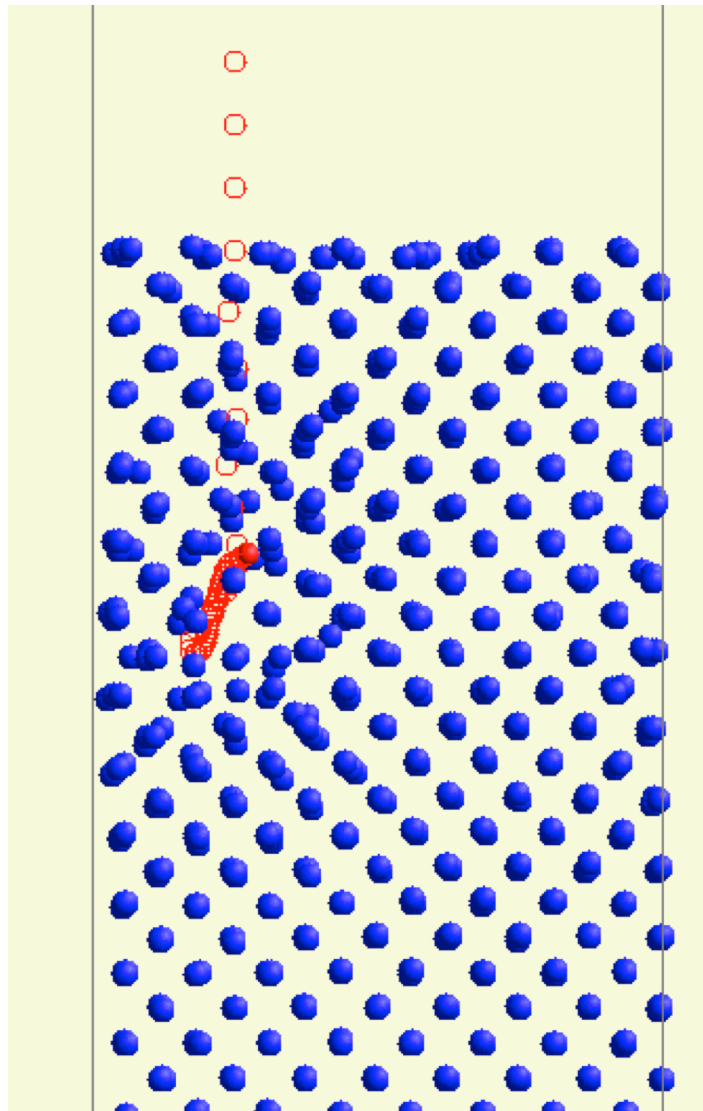
Fig. 2.3 Example of simulation result. Open red circles represent the trajectory of the injected boron with time.

We repeated this kind of simulation 2500 times with different boron initial positions for each initial energy and estimated doped boron profiles. Figures 2.4(a) and 2.4(b) showed the simulated distribution profiles in depth below the silicon surface at which the doped boron atoms stopped after being injected normally into the Si(001) surface at initial energies of 100 and 200 eV, respectively. The lateral axis shows the depth below the silicon surface, and the longitudinal axis the number of doped boron atoms on a log scale.

(a)
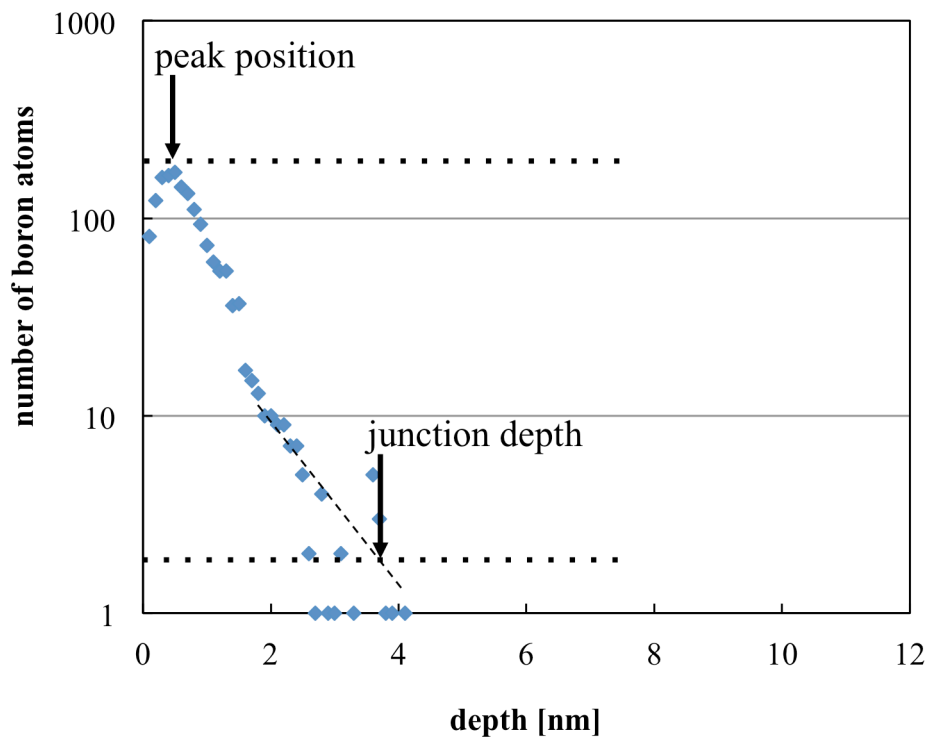
Fig. 2.4 (a) Simulated distribution profile of the stopped positions of doped boron atoms with initial energy of 100 eV.

(b)
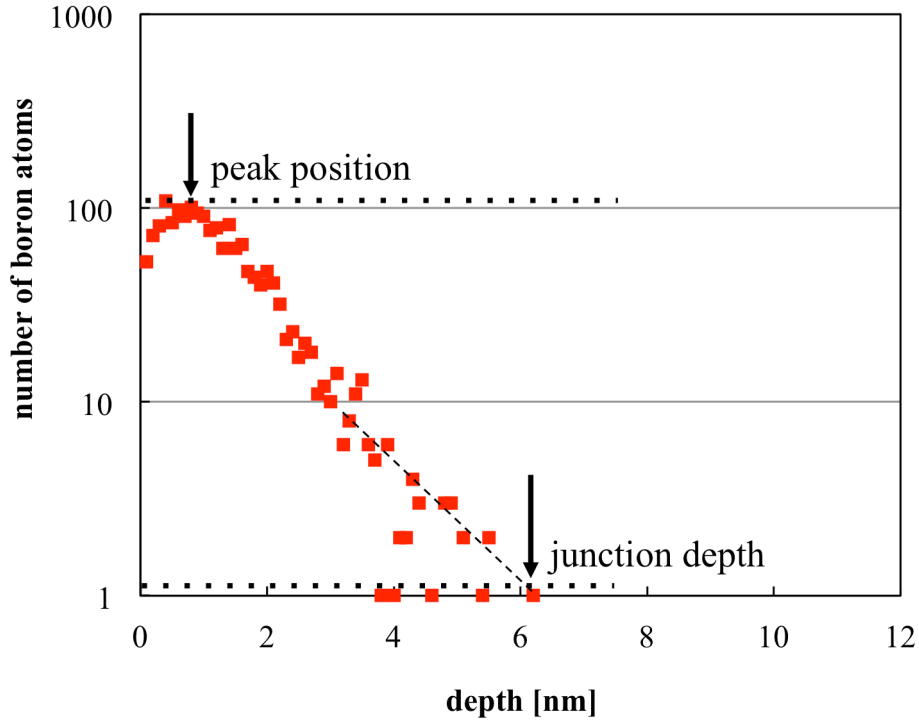
Fig. 2.4 (b) Simulated distribution profile of the stopped positions of doped boron atoms with initial energy of 200 eV.

The two dotted lines in Figs. 2.4(a) and 2.4(b) indicate the boron concentration of the peak and that of two orders of magnitude less than the peak. The peak positions of the profiles were 0.5 nm for 100 eV and 0.8 nm for 200 eV. The junction depth, where the boron concentrations are two orders of magnitude less than that at the peak position, was estimated to be 3.8 nm for 100 eV and 6.2 nm for 200 eV. The total number of retained boron atoms in the silicon substrate was 1621 for 100 eV and 1779 for 200 eV. Since the number of injected boron atoms was 2500 in these simulations, about 35% for 100 eV and 29% for 200 eV of the injected atoms were found to be reflected from the silicon surface. As the implanted retained dose for boron increases with implantation

energy as determined by SIMS measurement, the simulation results indicated the same tendency for lower implantation energy [2.23].

The peak positions and junction positions of the simulated profiles shown in Fig. 2.4 were compared with the experimental results shown in Fig. 2.2. The dotted lines in Fig. 2.2 indicate the maximum boron concentration and that two orders of magnitude less than the maximum for 120 and 200 eV. For the peak positions of the profiles, the simulated results were in good agreement with the experimental ones, which include an artificial effect of SIMS measurements on the surface and which also have lower-energy boron atoms in the plasma doping process [2.22]. The junction positions, where boron concentrations are two orders of magnitude less than that at peak positions in this study, were 3.8 nm for boron doping at an initial kinetic energy of 100 eV and 6.2 nm for 200 eV in the simulation results, and 5.8 nm for 120 eV and 6.4 nm for 200 eV in the experimental results. This comparison indicates that our simulation results were in good agreement with experimental ones. Since the number of boron atoms at the junction positions in the simulation results is one or two in this study, a larger number of boron atoms should be considered in future work to improve the simulation accuracy.

2.3.2 Defect distribution

The final junction position is determined by activation annealing processes following doping processes. In the annealing process, the distribution of defects generated by the doping process would influence not only on the diffusion of doped atoms but also on the optical absorption in short-time optical annealing.

Figures 2.5(a) and 2.5(b) show the simulated distributions of doped boron atoms and the defects generated in the doping process, respectively. The number of the injected boron atoms was 50 and the initial kinetic energy of doped boron atoms was 50, 100, and 200 eV. Since the depth of the simulation structure was 2.13 nm, the number of boron atoms exceeded this depth is shown at the position of 2.0 nm in Fig. 2.5(a). The

longitudinal axis of Fig. 2.5(a) is the ratio of the number of boron atoms at each depth to the total injected 50 boron atoms, and that of Fig. 2.5(b) is the ratio of the number of silicon defects at each depth to the total number of defects. Here, bond populations of each silicon atom were analyzed for the simulation results and silicon atoms with bond populations not equal to 4 were defined as silicon defects [2.16].
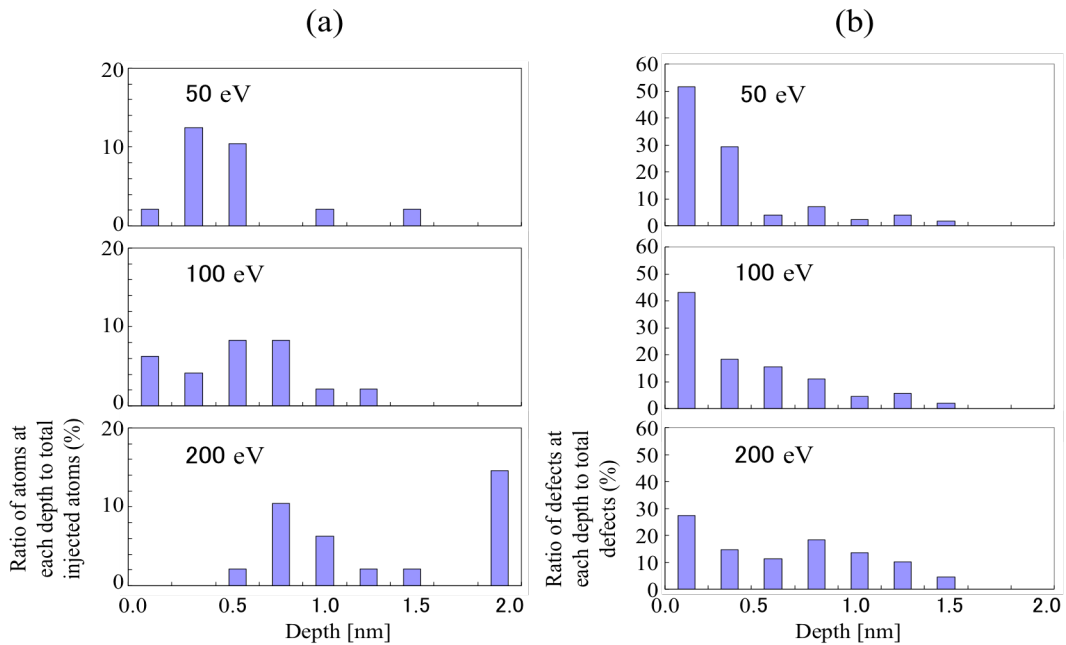

Fig. 2.5 Simulated distributions of (a) boron atoms and (b) generated defects with initial kinetic energies of 50, 100, and 200 eV.

Though the number of injected boron atoms and the depth of the silicon structure were smaller and shallower than those used for the junction position calculations, the peak positions of the boron profiles in Fig. 2.5(a), 0.6 nm for 100 eV and 0.8 nm for 200 eV, were nearly equal to the results of the junction position calculations in Fig. 2.4, 0.5 nm for 100 eV and 0.8 nm for 200 eV.

From Fig. 2.5(a), the ratio of boron atoms that penetrated into the silicon substrate

was 29.2, 31.2, and 37.5 % for the injection energy of 50, 100, and 200 eV, respectively. This means that the ratio of retained boron atoms in the silicon substrate increased with the injection energy. These results indicated the same tendency as those of the large silicon structure simulation, but the ratios of retained boron were smaller. One reason was the smaller number of injected boron atoms. Detail analysis of trajectories of reflected boron atoms in the simulation results revealed that some boron atoms were reflected at the silicon surface without invasion into silicon substrate and others were reflected from inside the silicon substrate after colliding with silicon atoms in the substrate. Although the final locations of reflected boron atoms were not investigated in this study, some of them might be finally absorbed at silicon surface.

Figure 2.5(b) indicated that the highest defect ratio was at the silicon surface for initial kinetic energies from 50 to 200 eV. In particular, 80% of defects were concentrated at the surface in the case of 50 eV. This result implies that boron atoms with low injection energy, such as 50 eV, lost their energy at the silicon surface, resulting in silicon defects, and were reflected from the surface without penetration into the silicon substrate. For the injection energy of 200 eV, the ratio of defects at the surface was still high, but it was less than 50%. On the other hand, about 35% of defects were located at around the peak concentration position of the doped boron atoms. This analysis revealed that at an extremely low injection energy, such as 50 or 100 eV, defects at the silicon surface were dominant, and that at a higher energy, such as 200 eV, defects around doped atoms became dominant.

2.4. Conclusions

Our novel hybrid method of quantum molecular dynamics and classical molecular dynamics was first applied to a low-energy boron doping process used for ultra-shallow junction formation. It was shown that this method was applicable to a silicon structure

with a depth of more than 10 nm that is needed to directly predict the junction position of an ultra-shallow junction. Good agreement was obtained between the simulated and experimental junction positions in the as-doped boron depth profile of 200 eV. This hybrid method also reproduced the increase in the retained boron dose with increasing initial energy in the lower energy region of less than 200 eV. Moreover, this method is also applicable to three-dimensional devices by using different incident angles of boron atoms.

The final junction position is determined by the activation annealing process after doping. To restrict additional diffusion in the case of ultra-shallow junctions, short-time activation, such as by flash lamp annealing, is required. However, simulation models of optical absorption in the annealing process have not yet been established. The proposed method in this study would also be applicable in the future to activation and diffusion processes induced by the absorption of light because the defects formed by the doping process could be handled by the quantum molecular dynamics method shown in the present study.

References

[2.1] http://www.itrs.net

[2.2] D. Pham, L. Larson, and J. W. Yang, "FINFET Device Junction Formation Challenges", International Workshop Junction Technology 2006, pp. 73-77, 2006.

[2.3] T. Izumida, K. Okano, T. Kanemura, M. Kondo, S. Inaba, S. Itoh, N. Aoki, and Y. Toyoshima, "Advantage of Plasma Doping for Source/Drain Extension in Bulk Fin Field Effect Transistor", Japanese Journal of Applied Physics, vol. 50, pp. 04DC15, 2011.

[2.4] Y. Sasaki, C. G. Jin, K. Okashita, H. Tamura, H. Ito, B. Mizuno, H. Sauddin, R. Higaki, T. Satoh, K. Majima, Y. Fukagawa, K. Takagi, I. Aiba, S. Ohmi, K. Tsutsui, and H. Iwai, "New method of Plasma doping with in-situ Helium pre-amorphization", Nuclear Instrument Methods and Physics Research B, vol. 237, pp. 41-45, 2005.

[2.5] S. B. Felch, Z. Fang, B. W. Koo, R. B. Liebert, S. R. Walther, and D. Hacker, "Plasma doping for the fabrication of ultra-shallow junctions", Surface Coatings Technology, vol. 156, pp. 229-236, 2002.

[2.6] E. J. H. Collart, K. Weemers, D. J. Gravesteijn, and J. G. M. van Berkum, "Characterization of low-energy (100 eV–10 keV) boron ion implantation", Journal of Vacuum Science and Technology B, vol. 16, pp. 280-285, 1998.

[2.7] C. Zechner, D. Matveev, A. Erlebach, S. Simeonov, V. Menialenko, R. Mickevicius, M. Foad, A. Al-Bayati, A. Lebedev, and M. Posselt, "TCAD calibration of

USJ profiles for advanced deep sub-μm CMOS processes", Nuclear Instrument and Methods in Physics Research B, 186, pp. 303-308, 2002.

[2.8] C. Zechner, A. Erlebach, A. Terterian, A. Scholze, and M. Johnson, "New implantation tables for B, BF2, P, As, In and Sb", Proceedings of the 14th International Conference on Ion Implantation Technology, pp. 567-570, 2002

[2.9] S. Tian, "Predictive Monte Carlo ion implantation simulator from sub-keV to above 10 MeV", Journal of Applied Physics, vol. 93, pp. 5893-5904, 2003.

[2.10] W. Moeller and W. Eckstein, "Tridyn - A TRIM simulation code including dynamic composition changes", Nuclear Instruments and Methods in Physics Research B, vol. 2, pp. 814-818, 1984.

[2.11] I. Santos, L. A. Marques, L. Pelaz, and P. Lopez, "Improved atomistic damage generation model for binary collision simulations", Journal of Applied Physics, vol. 105, pp. 083530, 2009.

[2.12] L. Bukonte, F. Djurabekova, J. Samela, K. Nordlund, S. A. Norris, and M. J. Aziz, "Comparison of molecular dynamics and binary collision approximation simulations for atom displacement analysis", Nuclear Instruments and Methods in Physics Research B, vol. 297, 23-28, 2013.

[2.13] G. Hobler and G. Betz, "On the useful range of application of molecular dynamics simulations in the recoil interaction approximation", Nuclear Instruments and Methods in Physics Research B, vol. 180, pp. 203-208, 2001.

[2.14] L. Pelaz, L. Marques, M. Aboy, I. Santos, and P. Lopez, "Simulation of p-n junctions: Present and future challenges for technologies beyond 32 nm", Journal of Vacuum Science and Technology B, vol. 28, pp. C1A1-C1A6, 2010.

[2.15] L. Marques, I. Santos, L. Pelaz, P. Lopez, and M. Aboy, "Atomistic modeling of ion implantation technologies in silicon", Nuclear Instruments and Methods in Physics Research B, vol. 352, pp. 148-151, 2015.

[2.16] H.Tsuboi, A. Sagawa, H. Iga, K. Sasata, T. Masuda, M. Koyama, M. Kubo, E. Broclawik, H. Yabuhara, and A. Miyamoto, "Tight-Binding Quantum Chemical Molecular Dynamics Study on Depth Profile Prediction in Low Energy Boron Implantation Process", Japanese Journal of Applied Physics, vol. 44, pp. 2288-2293, 2005.

[2.17] I. Karmakov, I. Chakarov, and A. Konova, "Depth profile characterization of low-energy B+- and Ge+-ion-implanted Si", Applied Surface Science, vol. 211, pp. 270-279, 2003.

[2.18] T. Yokosuka, K. Sasata, H. Kurokawa, S. Takami, M. Kubo, A. Imamura, Y. Kitahara, M. Kanoh, and A. Miyamoto, "A Theoretical Study on the Realistic Low Concentration Doping in Silicon Semiconductors by Accelerated Quantum Chemical Molecular Dynamics Method", Japanese Journal of Applied Physics, vol. 42, pp. 1877-1881, 2003.

[2.19] http://www.rsi.co.jp/kagaku/cs/miyamoto/program.html#colors

[2.20] T. Masuda, H. Tsuboi, M. Koyama, A. Endo, M. Kubo, E. Broclawik, and A.

Miyamoto, "Development of Hybrid Tight-Binding Quantum Chemical Molecular Dynamics Method and Its Application to Boron Implantation into Preamorphized Silicon Substrate", Japanese Journal of Applied Physics, vol. 45, pp. 2970-2974, 2006.

[2.21] F. Stillinger and T. Weber, "Computer simulation of local order in condensed phases of silicon", Physical Review B, vol. **31**, pp. 5262-5271, 1985.

[2.22] Y. Sasaki, "A Study on Conformal Plasma Doping Process with Self-regulating Characteristics for Source/drain Extension", Doctoral Thesis, Department of Electronics and Applied Physics, Tokyo Institute of Technology, Tokyo, 2012.

[2.23] Y. S. Lee, W. J. Lee, M. H. Lee, and S. K. Rha, "Study of Implanted B+ and P+ Ions into Si (100) for Ultra-shallow Junction by SIMS", Journal of Surface Analysis, vol. 14, pp. 420-423, 2008.

Chapter3
Characterization of doping profile:
Scanning capacitance microscopy and other methods

3.1 Overview of the techniques for doping profiles and scanning capacitance microscopy

3.2 Scanning capacitance microscopy method

3.3 Problems of SCM measurements

    3.3.1. Poor repeatability and reproducibility

    3.3.2. Conversion method

    3.3.3. Contrast reversal

3.4 What we should improve in SCM measurements around year 2000

References

3.1. Overview of the techniques for doping profiles and scanning capacitance microscopy

As the size of a semiconductor device such as a MOSFET is in the order of deep sub-microns, a measurement of a doping profile has been getting more difficult. One reason is the requirement of the very high spatial resolution less than 10 nm which could be applicable to ultra-shallow junctions (USJs). Another reason is the need for a precise measurement of the doped atoms in the lateral direction of a MOSFET or a mapping of them in two or three dimensions for optimization of complex doping designs and annealing processes. The other reason is the need for wide dynamic range of doping concentration from 10^{15} atoms/cm^3 to 10^{20} atoms/cm^3.

There are a lot of methods for measuring a doping profile in one-, two-, and three-dimensions. In developing semiconductor devices, one-dimensional doping profiles are widely used in determining parameters of ion implantation and thermal annealing processes. In the one-dimensional measurement, we would have a depth profile of doped atoms. In this case, the important characteristics required for the measurements are high depth resolution and sensitivity for dopant concentration. When we apply one-dimensional method to a device structure, we could only get averaged information of wide area. In two-dimensional measurements, there are two types of view for the measuring area. One is top surface view and the other is cross-sectional view of a semiconductor device. In both cases, the important characteristics required for the measurements are spatial resolution in two-dimensions and wide range of measured dopant concentration. For three-dimensional measurements of doping profiles, there are not so many techniques so far. A three-dimensional atom probe is one of the promising candidates but not yet developed enough for a reliable measurement. Slice and view or etch and view method is another way of getting a three-dimensional profile. This could be deemed as the application of two-dimensional measurement. Therefore,

two-dimensional doping profile measurement is the most important so far. Table 3.1 shows major methods of doping profiles in two dimensions.

Table 3.1. Comparison of measurement methods of 2D doping profiles.

Method	Spatial resolution in 2D	Detection range [cm^{-3}]	Measurement
SIMS	>100nm	10^{15} - 10^{21}	destructive
Electron holography	Debye length-limited	>10^{18}	nondestructive
SCM	Debye length-limited	10^{15} - 10^{20}	nondestructive
SSRM	10nm	10^{15} - 10^{20}	destructive

Secondary ion mass spectrometry (SIMS) is one of the most widely used methods. The advantage of SIMS is its high sensitivity detecting doping concentration as low as 10^{15}atoms/cm^3. It has, however, low spatial resolution of a few hundred nanometers. Therefore, SIMS is generally used as a one-dimensional doping profiler. The other disadvantage of SIMS, especially dynamic SIMS, is less precise measurement of outermost and near surface, which is crucial for ultra-shallow junction [3.1].

Electron holography is an interference-based transmission electron microscopy (TEM) technique [3.2]. It has sub-10 nm spatial resolution suitable for USJs. However, its lower limit of doping concentration is the order of 10^{18} atoms/cm^3. The interference-based method could be also influenced by a strain in a device.

Scanning probe microscopy based methods have basically good spatial resolution. In particular a scanning capacitance microscopy (SCM) and a scanning spreading resistance microscopy (SSRM) has also wide detection range from 10^{15} atoms/cm^3 to 10^{20} atoms/cm^3. SCM is a non-destructive technique based on the MOS capacitance measurement and the quality of the oxide or insulator layer on semiconductor strongly influence on the results. On the other hand, SSRM is a destructive measurement using a

hard-material probe such as a diamond-coated silicon probe that is pushed into the sample surface with high pressure in the order of GPa. Another disadvantage of SSRM is that it is not able to distinguish between n-type and p-type doping atoms. In the SSRM measurements, the scanning dust is basically generated from a sample surface during scanning the probe, which is pushed into the sample with high pressure. The scanning dust, for example amorphous silicon or silicon dioxide in the case of a silicon device sample, has usually high electric resistivity. The dust caught between the probe and the sample during a scanning makes the measured resistivity higher than real one. This prevents repeatable and reproducible measurements of the SSRM.

In the measurements of semiconductor devices, especially in failure analysis, the area that is available to the analysis is limited. Repeatable measurements in the same area are essential for failure analysis. Therefore, a nondestructive method is required. SIMS is basically a destructive measurement utilizing sputtering of the surface. Electron holography, SCM and SSRM are also destructive in the meaning of that a cross-section sample is needed. After cross-sectioning process is performed, the electron holography and the SCM could measure the cross-sectioned sample surface in nondestructive way. In the SSRM measurement, a hard diamond or diamond-coated probe is pushed into the cross-sectioned sample surface and scanned. So the SSRM is basically the destructive measurement. Nondestructive electron holography and SCM measurements are suitable for the failure analysis.

From the viewpoint of high spatial resolution, wide detection range and nondestructive measurement of cross-sectioned samples, SCM would be one of the most promising techniques in two-dimensional measurements.

3.2. Scanning capacitance microscopy method

The SCM is one of the applications of the atomic force microscopy (AFM). By scanning a probe over a sample surface with electrical ac bias between the probe and the sample, it makes a two-dimensional image of capacitance changes (dC/dV) from change of the depletion layer width in the semiconductor. We usually use not infinitesimal voltage dV, but finite voltage change ΔV, for example one volt. Therefore measured capacitance change is not really dC/dV which means differential, but $\Delta C/\Delta V$. However, the notation "dC/dV" is widely used in the same meaning of $\Delta C/\Delta V$ in this field. Therefore "dC/dV" notation is used in this thesis.

Figure 3.1 shows a schematic diagram of a SCM system. The probe tip consists of a conductive material, generally a silicon cantilever coated with a metal. A sample is semiconducting material and a thin dielectric layer is formed on the surface of the sample. Therefore MIS or MOS capacitor is consisted from the conductive probe, the dielectric layer, and the semiconductor sample. Applying an ac bias on the sample changes the depletion width in the sample according with carrier concentration in the semiconductor. This change of the depletion layer is detected as a change of capacitance, which is detected at a capacitance sensor shown in the Fig. 3.1.
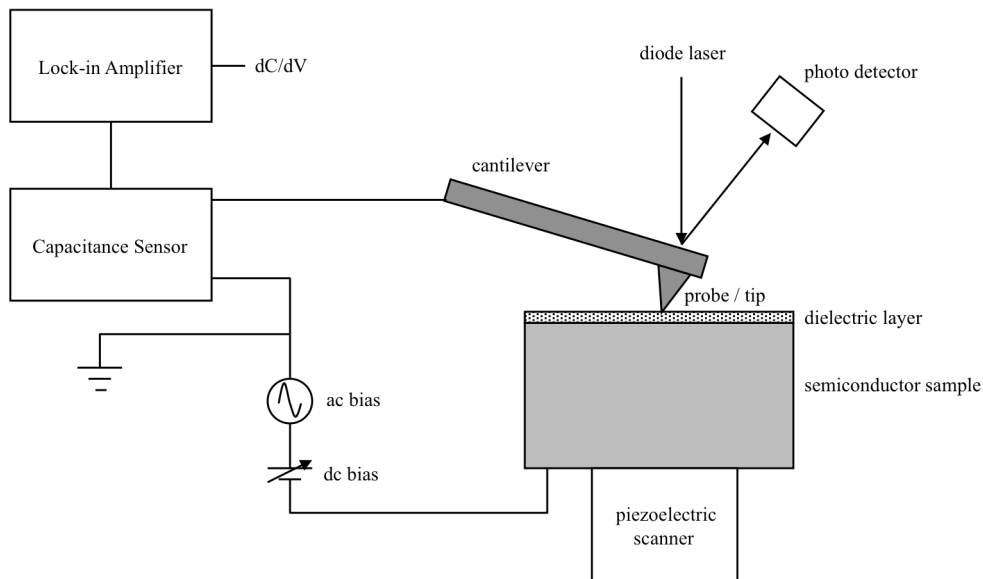
Fig. 3.1 Schematic diagram of a SCM system.

An example circuit of the capacitance sensor is shown in Fig. 3.2. This sensor consists of an oscillator of a gigahertz, a resonator, and a detecting circuit. The capacitance between the probe and the sample is a part of the resonator. Therefore a change of the probe-sample capacitance changes the resonant frequency of the resonator. This change of the resonant frequency makes change of amplitude of a wave, i.e. output voltage, which starts from the oscillator to the detector through the resonator.
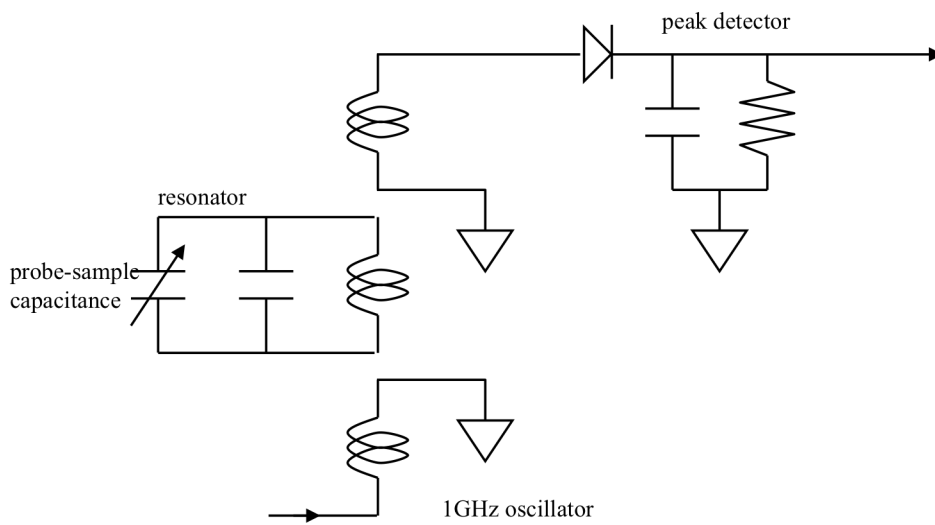
Fig. 3.2 An example circuit of a capacitance sensor of SCM. This sensor consists of an oscillator of a gigahertz, a resonator, and a detecting circuit.

The carrier concentration measurement by SCM has two modes, namely, the constant dV mode and the constant dC mode. In the constant dV mode, we measure the capacitance change with a constant ac voltage between the probe and the sample. This mode has a merit that an interpretation of measured data is straightforward. This comes from the direct measurement of the capacitance, i.e. depletion width. There is a demerit, however, that spatial resolution would change depending on carrier concentrations. On the other hand, in the constant dC mode, applying ac bias changes so that a width of a depletion layer keeps constant. This mode has a merit that the spatial resolution is

constant over different carrier concentrations and a demerit that this mode needs a feedback loop to the probe in order to keep the depletion width constant. In this thesis, the constant dV mode is discussed on its measurement and data interpretation, while the constant dC mode is not discussed.

Figure 3.3 shows typical capacitance-voltage curves in a C-V measurement of n-type semiconductors with different doping concentration. For an applied ac voltage (dV), a capacitance changes according to this curve. This capacitance change (dC) is different from each other for different doping concentration as is shown in Fig. 3.3. Generally, the higher the concentration is, the smaller the dC becomes. The dC also depends on an applied dc bias, as is shown in Fig. 3.4.
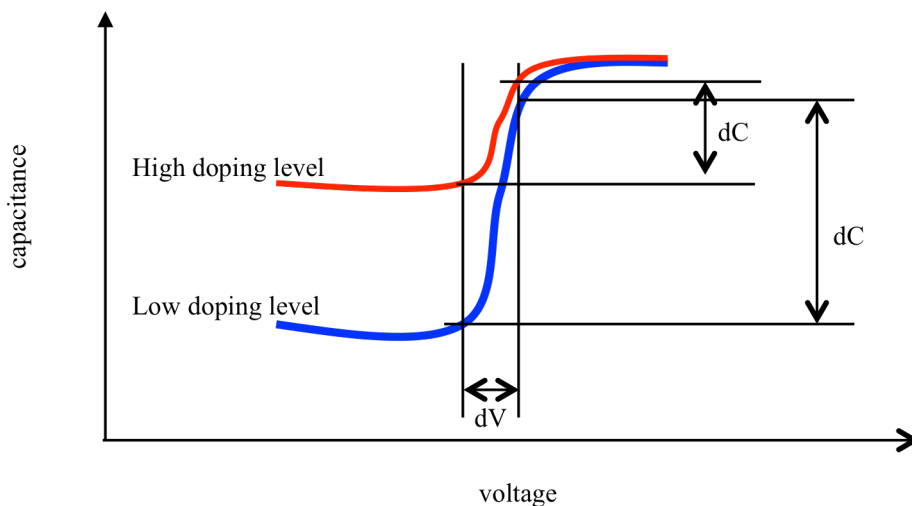
Fig. 3.3 Capacitance-voltage curves in C-V measurements of high doped and low-doped n-type semiconductors.

Because of the difference of the flat-band voltage for different doping concentration, the choice of the dc bias in a SCM measurement sometimes produces contrast reversal of a SCM image. In the case of the contrast reversal, the dependency of dC/dV signal on doping concentration becomes reversed, i.e. the dC/dV signal intensity increases in

increasing of the doping concentrations. This effect disturbs a proper analysis of a doping profile.
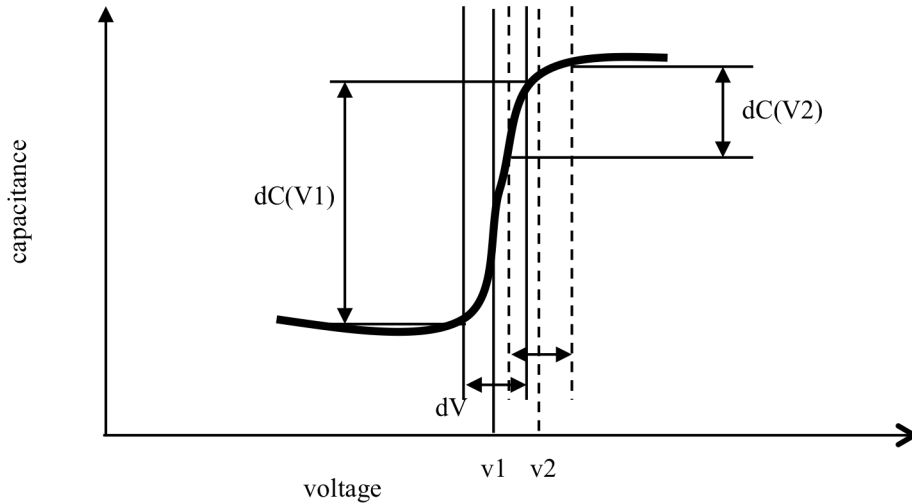
Fig. 3.4 dC signal dependence on Vdc. dC(V1) is larger than dC(V2).
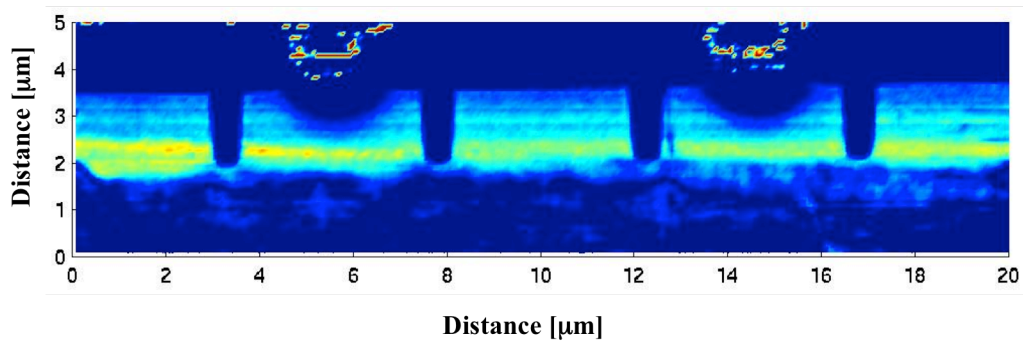
Figure 3.5 shows an example of SCM measurement of a cross-sectioned silicon power device, UMOS. The dark blue area in the figure indicates higher doping concentration area and the light blue area indicates lower concentration area. For comparison, an AFM topography image of a selectively wet-etched cross-sectioned surface of the same sample is shown in Fig. 3.6. From this kind of SCM measurement in two-dimensional, we could reveal a two-dimensional doping distribution in a device with the high spatial resolution. Moreover this information of two-dimensional doping profile would make us possible to build a transverse diffusion model of dopant in a semiconductor device for a process simulation, which are widely used in device design in semiconductor manufacturing.

The measured SCM, i.e. dC/dV, signals and images could be used directly in the comparison of doping profiles between devices having the same structure. In a failure analysis on a device, doping profiles of a good and a failed device could be

distinguished directly from the SCM images of the two devices. However, for a design of a semiconductor device, not only qualitative doping distribution but also quantitative doping concentration would be needed. For this purpose, a methodology of quantitative SCM measurement is required. This would be achieved by using a "standard sample" and a computational simulation, as will be discussed in Chapter 4.

Fig. 3.5 An example of SCM measurement of a cross-sectioned silicon device, UMOS. The dark blue area indicates higher doping concentrations area and the light blue area indicates lower concentrations area. Both in horizontal and vertical axis are distance in micrometers.
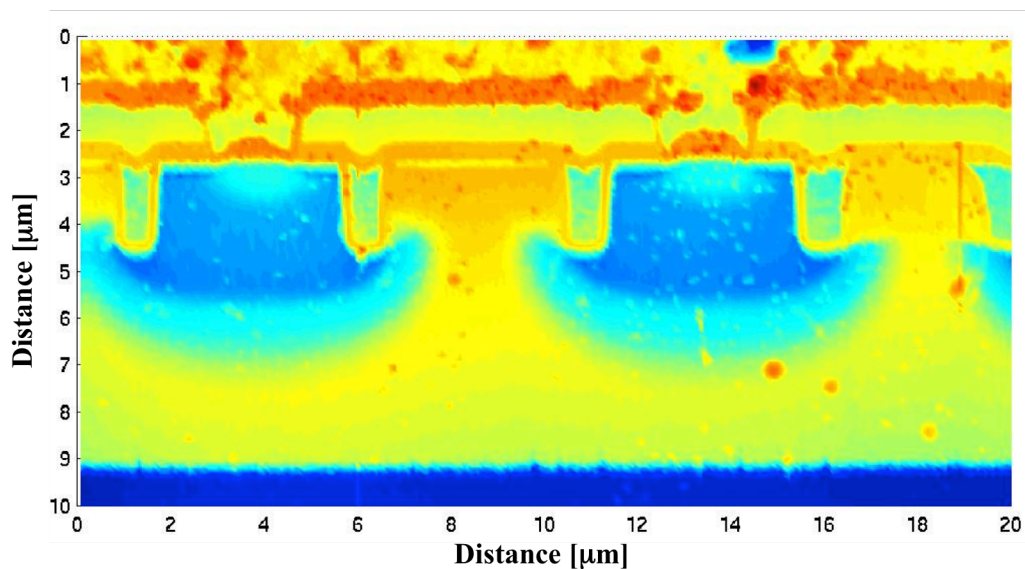
Fig. 3.6 AFM topography image of the selectively wet-etched cross-sectioned surface of the UMOS device same as Fig. 3.5.

The spatial resolution of SCM measurement is influenced by many factors. The probe radius and the dopant concentration are two main factors. In addition to these, the oxide thickness, the humidity in measurement environment that relates to water meniscus around the tip, and configuration of dopant distribution in a sample would also influence on the spatial resolution. A sharp tip would improve the spatial resolution in high concentration area. However, the sharp tip reduces the contact area as an electrode of capacitance and therefore decreases the SCM signal intensity. Generally, the tip radius is dominant in high concentration measurement, and depletion width is dominant in low concentration for the spatial resolution of SCM measurement.

3.3. Problems of SCM measurements

Here we describe the situation of SCM measurement around the year 2000 since when this study was started.

From the emerging of SCM in 1989, this measurement technique has been widely expected as a powerful two-dimensional carrier/doping profiler of a cross-sectioned semiconductor device [3.3]. Comparing with the SIMS analysis, it has higher spatial resolution in a cross-sectioned area, which had been expected to reveal lateral diffusion of source/drain and extension diffusion layer. This lateral diffusion model had been required for process simulation. Because people had mainly used a simple model in lateral diffusion, such as a constant number, e.g. 50 %, times depth diffusion length. Since SCM directly measures a depletion layer variation that depends on carrier concentration, not on doping concentration, this characteristic had been expected to be useful in the estimation of activation ratio of dopant atoms in a real device.

In order to achieve the above-mentioned expectation of SCM, there had been the following problems at that time:

(1) Poor repeatability and reproducibility of the measurements,

(2) Lack of the conversion method from measured dC/dV data to carrier concentration for wide range,

(3) Contrast reversal, i.e. non-monotonic relation between carrier concentrations and dC/dV signals.

3.3.1. Poor repeatability and reproducibility

The repeatability and reproducibility of SCM technique depends on many factors, especially on a probe, a sample surface condition, a sample preparation, and also on environment during a measurement such as humidity around tip-air-insulator configuration.

As a metal of the MOS capacitor in SCM, many kind of conductive probes have been used. Especially, Trecker et al. had performed systematic study of probes and indicated easy wear-out property of metal-coated probes in SCM measurements [3.4]. The probe should fulfill the following requirements as a reliable 2D-profiler.

- Sharp tip shape with a radius of curvature of ten nanometers or less for high spatial resolution.
- Good electrical conductivity especially for measurements of highly doped semiconductors.
- Hardness of tip material enough not to change its shape and conductivity during scans over sample surfaces in contact mode. It is important for reliable measurement.

As mentioned, a metal-coated probe or tip has been generally used in a SCM measurement. Highly doped Si tips and solid metal tips have been also used for high spatial resolution. Although a metal-coated probe, in which metal such as Pt-Ir or Pt-Cr covers Si tip surface, has good conductivity of metal and sharp tip shape, it easily

changes its shape during scans because of easy wear-out of the metal coating. This is crucial even for a qualitative measurement. The solid metal probe of sharp tip radius has been developed and has better spatial resolution than metal-coated one. However, the hardness was not enough and the usage of the tip has been restricted.

A silicon probe is widely used in an atomic force microscope and has a good robustness. Electrical conductivity had been improved by using highly doped silicon but native oxide on the tip surface was found to influence on measured signals thorough a thickness-change of the oxide layer in the MOS capacitor configuration [3.5].

In SCM measurements, we are mostly interested in a doping profile over a cross section of a semiconductor device. Therefore a surface of the cross section of the semiconductor device should be cleaved or polished. An oxide or other insulating layer should be formed on the cleaved or polished surface for a SCM measurement and there had been a lot of techniques of the oxidation reported [3.6, 3.7]. Different oxides, such as native, thermal, chemical, ultra-violet or the oxide grown by their combination have been widely adopted. There are some restrictions in forming an oxide layer for SCM measurement. The most important one is a process temperature. High quality oxide could be formed rather easily with a high temperature process, but it makes re-diffusion of doped atoms in the sample. Therefore, we needed to focus on low-temperature oxidation methods.

There had been few researches for oxides from the point of view of repeatability and reproducibility of SCM measurements. One reason was the poor repeatability of metal-coated probes themselves. When a SCM signal changed, we could not distinguish whether the change came from the probe or the oxide (or the sample). This is the reason why a robust probe should be used for a comparison and optimization of oxidation and sample preparation methods. In this work, a diamond-coated silicon probe, which has been generally used in a SSRM measurement requiring a surface contact with high pressure, was adopted for an improvement of repeatability and reproducibility of SCM

measurements. Moreover, by using a robust probe, merits and demerits of some low-temperature oxidation for a sample preparation would be clearly shown.

3.3.2. Conversion method

Another problem of the SCM measurement had been a conversion of a SCM signal into a doping concentration. The SCM signal is a capacitance change, dC/dV, of a MOS capacitance consisting of a SCM conductive probe and a semiconductor on which an oxide layer formed. The first direct comparison of a SCM signal to a SIMS depth profile was performed by Erickson in 1996 [3.8]. In their work, SCM signals were converted into carrier concentrations by using SIMS depth profile data. They also showed that the relation of SCM signals and carrier concentrations were in good agreement with the simple analytical model of C-V equation of a MOS capacitance. However, the value of peak concentration was simply fitted by normalization. Moreover, the simple analytical model is reasonable only in the uniform distribution of dopant atoms, because the component of a probe-surface fringe effect of the capacitance is not ignorable in non-uniform distribution or at a p-n junction.

A computational simulation has been a powerful tool for the theoretical understanding of SCM signals and also for a quantitative analysis [3.9, 3.10]. However, it had not been used in practical usages in a conversion from dC/dV signals into carrier concentrations.

3.3.3. Contrast reversal

There had been several reports on the contrast reversal, i.e. non-monotonic relation between the intensity of dC/dV signals and carrier concentrations [3.11]. This phenomenon would lead to a wrong estimation of a doping profile even in a qualitative analysis. This contrast reversal tends to appear in measuring a highly doped area with a low-doped probe in which depletion would occur. A full metal probe does not have this

problem because of no depletion layer in a metal probe. However, a metal-coated silicon probe sometimes has this problem. For repeatable and reproducible measurements, we use a diamond-coated probe, which have a possibility of depletion in the probe, but no study had been performed.

3.4. What we should improve in SCM measurements around year 2000

Causes of the poor repeatability and reproducibility of SCM measurements had not been identified, because several instabilities were included such as a surface condition and a tip condition. Therefore, what we needed was simplify the situation when we started the study. One of instability factor was easy wear-out property of a metal-coated silicon tip. Hence a usage of a stable probe would become one solution. A diamond or diamond-coated silicon tip would be a candidate for its hardness, however few researches had been performed. Moreover few systematic and quantitative researches had been done for "repeatability" itself. We could not discuss a stability of a sample surface distinguished clearly from a degradation of a probe, unless using a stable probe. The stability of the probe also made us possible to compare oxidation methods of silicon sample surface. Moreover both of the stable probe and the sample surface with high quality oxide finally made us possible to establish a qualitative SCM measurement with conversion from measured SCM data to carrier concentrations.

A nonlinear conversion relationship, shown in Fig. 3.7, between the SCM signal and carrier (or doping) concentration considering a three-dimensional interaction among a probe, insulator surface and an air region between them should be constructed.
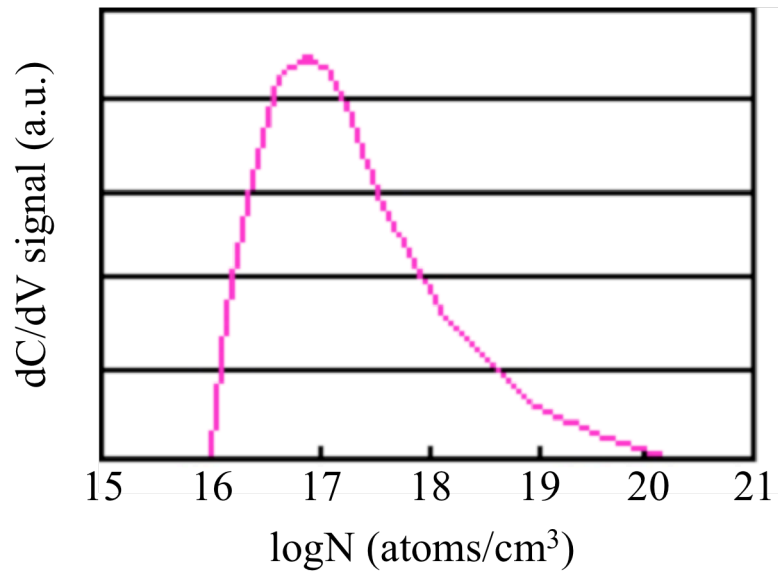
Fig. 3.7 Nonlinear conversion relationship between the SCM signal, i.e. dC/dV signal, and carrier (or doping) concentrations N.

In order to make the conversion from SCM signals into carrier concentration, two methods were mainly adopted. One was a conversion method with a computational simulation and the other was one with a reference sample including different known doping concentrations [3.12]. Even in using the simulation method, some kind of calibration based on measurements would be needed for fixing simulation parameters.

Under the circumstance, we have developed a new method of the conversion using both a computational simulation and a concentration-standard sample. In this method, two samples of the standard and a device having an unknown doping profile would be glued into the single sample and polished to make a cross-sectional surface as shown in Fig. 3.8. For this sample, we have carefully estimated how wide area of the cross-sectioned was suitable for reproducible and quantitative measurements. We have also shown for the first time the diamond-coated probe could make high contrast images without contrast reversal by selecting a proper dc bias. This has opened a practical way of SCM for quantitative measurement in industrial usages, which require repeatable and

stable measurements.
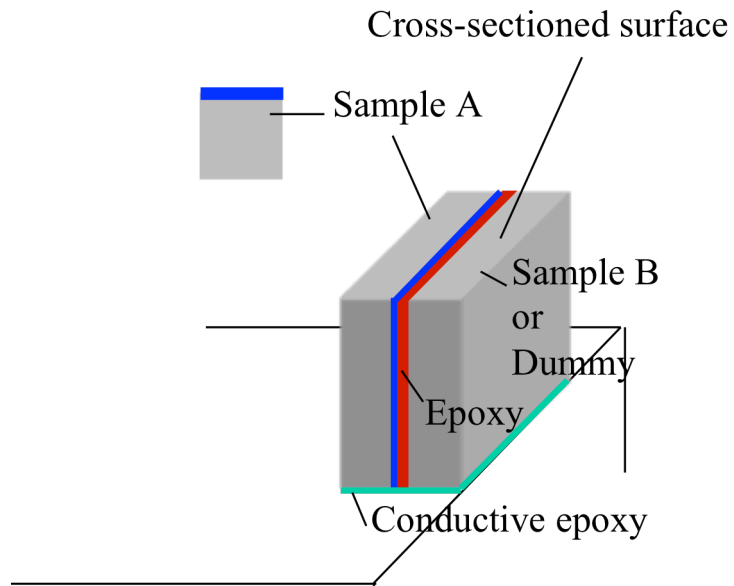
Fig. 3.8 Glued two samples attached on sample holder to make cross-sectional surface for SCM measurements.

References

[3.1] W. Vandervorst, T. Janssens, B. Brijs, T. Conard, C. Huyghebaert, J. Fruhauf, A. Bergmaier, G. Dollinger, T. Buyuklimanli, J. A. VandenBerg and K. Kimura, "Errors in near-surface and interfacial profiling of boron and arsenic", Applied Surface Science, vol. 231, pp. 618-631, 2004.

[3.2] P. Formanek and M.Kittler, "Electron holography on silicon microstructures and its comparison to other microscopic techniques", Journal of Physics: Condensed Matter, vol. 16, pp. 193-200, 2003.

[3.3] C. Williams, W. Hough and S. Rishton, "Scanning capacitance microscopy on a 25 nm scale", Applied Physics Letters, vol.55, no. 2, pp. 203-205, 1989.

[3.4] T. Treker, T. Hantschel, R. Stephenson, P. De Wolf, W. Vandervorst, L. Hellemans, A. Malave, D. Buchel, E. Oesterschulze, W. Kulish, P. Niedermann, T. Sulzbach and O. Ohlsson, "Evaluating probes for "electrical" atomic force microscopy", Journal of Vacuum Science & Technology B, vol. 18, pp. 418-427, 2000.

[3.5] V. V. Zavyalov, J. S. McMurray and C. C. Williams, "Advances in experimental technique for quantitative two-dimensional dopant profiling by scanning capacitance microscopy", Review of Science Instruments, vol.70, pp. 158-165, 1999.

[3.6] J. S. McMurray, J. Kim, C. C. Williams and J. Slinkman, "Direct comparison of two-dimensional dopant profiles by scanning capacitance microscopy with TSUPREM4 process simulation", Journal of Vacuum Science & Technology B, vol. 16, no. 1, pp. 344-348, 1998.

[3.7] O. Bowallius and S. Anand, "Evaluation of different oxidation methods for silicon for scanning capacitance microscopy", Material Science in Semiconductor Processing, vol. 4, pp. 81-84, 2001.

[3.8] A. Erickson, L. Sadwick, G. Neubauer, J. Kopanski, D. Adderton and M. Rogers, "Quantitative Scanning Capacitance Microscopy Analysis of Two-Dimensional Dopant Concentrations at Nanoscale Dimensions", Journal of Electronics Materials, vol. 25, no. 2, pp.301-304, 1996.

[3.9] J. F. Marchiando, J. J. Kopanski and J. R. Lowney., "Model database for determining dopant profiles from scanning capacitance microscope measurements", Journal of Vacuum Science & Technology B, vol.16, no.1, pp. 463-470, 1998.

[3.10] J. F. Marchiando, J. J. Kopanski and J. Albers, "Limitations of the calibration curve method for determining dopant profiles from scanning capacitance microscope measurements", Journal of Vacuum Science & Technology B, vol.18, no.1, pp. 414-417, 2000.

[3.11] R.Stephenson, A. Verhulst, P. De Wolf, M. Caymax and W. Vandervorst, "Contrast reversal in scanning capacitance microscopy imaging", Applied Physics Letters, Vol. 73, no. 18, pp. 2597-2600, 1998.

[3.12] L. Ciampolini, M. Ciappa, P. Malberti and W. Fichtner, "SCaMsim, a new three-dimensional simulation tool for scanning capacitance microscopy", Characterization and metrology for ULSI technology 2000 international conference, CP550, pp. 647-651, 2001.

Chapter 4
Quantitative SCM measurement

4.1 Repeatability and reproducibility of SCM

    4.1.1 Introduction

    4.1.2 Sample preparation

    4.1.3 SCM measurements

    4.1.4 Results

    4.1.5 Summary

4.2 Methodology for quantitative SCM measurement

    4.2.1 Problems in quantitative measurements

    4.2.2 Comparison of two samples

    4.2.3 SCM measurements

    4.2.4 Conversion methodology of SCM data

    4.2.5 Comparison to SIMS result

    4.2.6 PN junction

References

4.1 Repeatability and reproducibility of SCM

4.1.1 Introduction

Scanning Capacitance Microscopy (SCM) is a scanning probe technique that provides one- and two- dimensional doping profile measurements of semiconductor devices. Some investigations have demonstrated that the use of metal-coated (Cr-alloy, Pt-Ir) silicon probes leads to scarcely reproducible results and to contrast reversal effects [4.1]. These problems are mainly related to the fast wear-out of the metal-coated probe operated in contact mode, namely the degradation of the tip radius and the fast peel-off of the metallization as described in the previous chapter. Both degradation mechanisms have detrimental effects on the reproducibility of qualitative and quantitative SCM measurements.

We chose diamond-coated silicon probes in order to improve both the endurance of the coating layer and the shape stability of the probes undergoing tribologic stresses. Robust probes are also essential for reducing the measurement time, especially when characterizing multiple samples or a large sample area. The time reduction in measurements is important for industrial usages.

In spite of their robustness, diamond-coated probes have been hardly used in SCM measurements [4.2]. We performed for the first time a systematic investigation of the SCM response of diamond-coated probes. A comparison with the conventional metal-coated probes has demonstrated the superior repeatability and reproducibility of the measurements performed by diamond-coated probes. Furthermore, the behavior of diamond-coated probes has been investigated for different oxide layers grown by both dry and wet oxidation process on the cross-sectioned samples. Due to the good reproducibility of diamond-coated probes, we were able to compare the large-area homogeneity of ultra-thin oxide layers grown by both dry and wet oxidation.

4.1.2 Sample preparation

The SCM measurement is strongly influenced by the surface condition of a sample. Surface contaminations would lead to a low signal-noise ratio of SCM signals. Oxide fixed charges would make a shift of the flat-band in a C-V curve that changes the optimal V_{dc} value in a SCM measurement. Interface traps would affect a C-V curve by stretching the transition region between accumulation and inversion that influences on a measurable range of doping concentration and that sometimes produces the contrast reversal effect. The surface condition of a sample is mostly influenced by the sample preparation. Though cleanroom technologies for a device fabrication are basically desirable, there are some constraints for sample making of the SCM measurement. In this section, we will describe a sample preparation method that is suitable for the SCM measurement.

In this study, we used a p-type and an n-type epitaxial staircase sample developed and manufactured at IMEC [4.3]. They consist of a number of (six for p-type and five for n-type) 5 μm thick epitaxial layers with different doping concentration (4.0×10^{15} - 6.0×10^{19} atoms/cm^3 for p-type and 5.0×10^{14} - 2.0×10^{19} atoms/cm^3 for n-type), spaced by a 1 μm buffer layer with higher doping concentrations. The details of these samples are shown in Table 4.1.

Table 4.1 Structure of p-type and n-type staircase samples

Type	Concentrations (atoms/cm^3)					
p-type	4.0×10^{15}	4.0×10^{16}	1.3×10^{17}	4.0×10^{18}	1.3×10^{19}	6.0×10^{19}
n-type	5.0×10^{14}	5.0×10^{16}	1.0×10^{17}	1.0×10^{18}	2.0×10^{19}	

Each staircase sample is glued on a dummy silicon chip by using a high-temperature resistant epoxy resin. This dummy silicon was used for preventing corner rounding of the staircase sample during the polishing. Before polishing of one side of the sample,

the opposite side was roughly polished and thin gold film was sputtered to improve electrical contact to a conductive sample holder. Then the set of samples was glued to the sample holder with the gold sputtered side down by using conductive epoxy paste as shown in Fig.4.1, same as Fig.3.8. This sample holder was used both for polishing and measurements. Cross-sectioning of these samples was performed by a standard polishing method [4.4].   The rough polishing of the cross-sectioning sample was performed by diamond lapping films down to 0.1 μm. The surface condition of the sample during the polishing was checked roughly by an optical microscopy. In this study, 0.05 μm colloidal silica suspension was used in the final polishing process. The colloidal silica suspension with alkaline solution has an etching effect of silicon and etching rate depends on doping concentration. The reduction of the etch rate of silicon with boron is larger than that with phosphorus [4.5,4.6]. Therefore, too much polishing with colloidal silica produces topographical change of the sample surface. To prevent this, the polishing time with colloidal silica suspension was approximately 10 seconds. The mean square surface roughness (R_{ms}) of the cross-sectioned after the final polishing was measured by an atomic force microscopy at 1.0 μm × 1.0 μm area on the staircase sample side excluding the epoxy resin area. The measured R_{ms} was 0.11 nm. This flatness of the sample surface is important to prevent topographical effect in SCM measurements and 0.11 nm is small enough to the measurements. Before oxidation, the native oxide layer has been removed by 5 % diluted hydrofluoric acid.
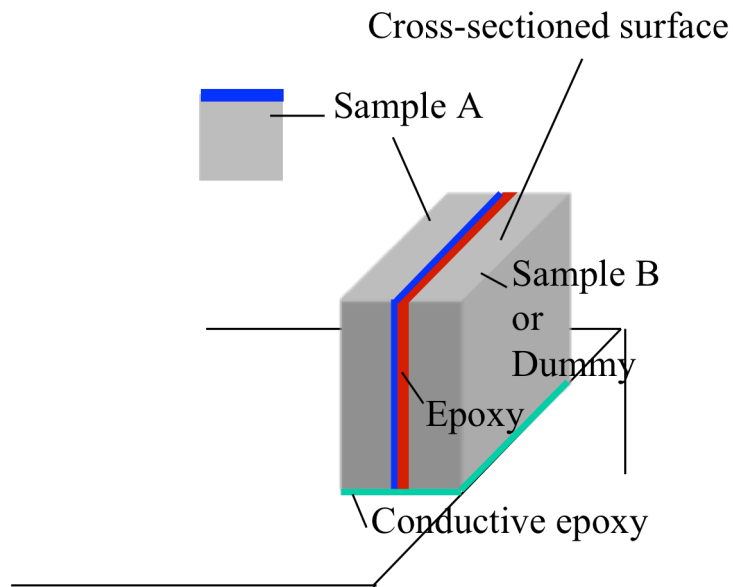
Fig. 4.1 (Same as Fig. 3.8) Glued two samples attached on sample holder to make cross-sectional surface for SCM measurements.

In order to perform reproducible and repeatable SCM measurements of a device sample, a good quality and stable oxide layer should be deposited on the cross-sectioned surface. There are some constraints in a sample preparation for the SCM measurements. The following terms are the main constraints required for the sample preparation processes.

✓ Process temperatures should be low enough to prevent re-distribution of doped atoms in a device.

✓ Processes should have no dopant concentration dependency.

✓ Processes should be performed with some kind of epoxy resin.

✓ Processes should be performed with a sample holder of aluminum or some metal because of arranging a sample cross-sectioned surface and a sample holder in parallel to keep the configuration of a probe and a sample constant.

High-temperature oxidation technique is suitable for a high quality oxide layer. However, the high-temperature oxidation makes additional diffusion of dopant and also affects the epoxy resin. Therefore low-temperature oxidation should be performed to keep doping profile unchanged during sample preparation. Two low-temperature oxidation techniques were performed. One is low-temperature dry oxidation under UV illumination, and the other is wet oxidation [4.7, 4.8]. For the dry oxidation, the sample was heated up to 300 °C on a hot plate in air under UV illumination for 40 minutes. For the wet oxidation, the sample was immersed into a 35 % hydrogen peroxide (H_2O_2) solution at 70 °C for 10 minutes. The obtained oxide thickness is 3 nm for the dry oxidation and about 2 nm for the wet oxidation [4.9]. The low-temperature dry oxidation technique with UV illumination has been reported by many researchers to enhance growth rate of high quality silicon oxide [4.10]. Under UV illumination, photo-induced transitions of electrons from the Si valence and conduction bands into the SiO_2 conduction band would occur. These electrons would enhance the formation of O^- from O atoms and/or O_2^- from O_2 molecules in the oxide layer [4.11]. The role of UV illumination was also reported to help unreacted oxygen ions combining with Si and silicon suboxides to create silicon dioxide [4.12].

It has been reported that silicon oxide layer formed by H_2O_2 has suboxides from FT-IR ATR spectra [4.13]. These suboxides would have possibility to work as trap states that cause the poor repeatability of the wet oxide in SCM measurements.

For both dry and wet oxidation techniques, no morphological steps among different dopant concentration areas on the standard sample were observed by atomic force microscopy measurement after removing the oxide layer.

4.1.3 SCM measurements

SCM measurements were performed using a Dimension 3100 with Nanoscope IIIa setup from Digital Instruments [4.14]. In the SCM measurements, dc and ac bias is

applied to a sample and the capacitance modulation (dC/dV) corresponding to the ac bias is detected using an UHF capacitance sensor described in the Section 3.2. Commercially available diamond-coated probes and metal-coated probes from NANOSENSORS were used. The diamond-coated probe is a silicon probe coated with boron-doped diamond. The typical thickness of the polycrystalline diamond layer is 100 nm and its resistivity is in the 0.003 to 0.005 ohm-cm range. The metal-coated probe is a silicon probe with a 40 nm thick Cobalt alloy layer. SCM images of the staircase sample were produced by scanning a 40 μm by 2.5 μm area including all staircases of different doping concentrations. Each one-dimensional profile shown in this section was the result of averaging over 2.5 μm along with the direction parallel to sample top surface. An example of 2D image and averaged 1D profile is shown in Fig. 4.2. The scan rate during acquisition was 1 Hz.
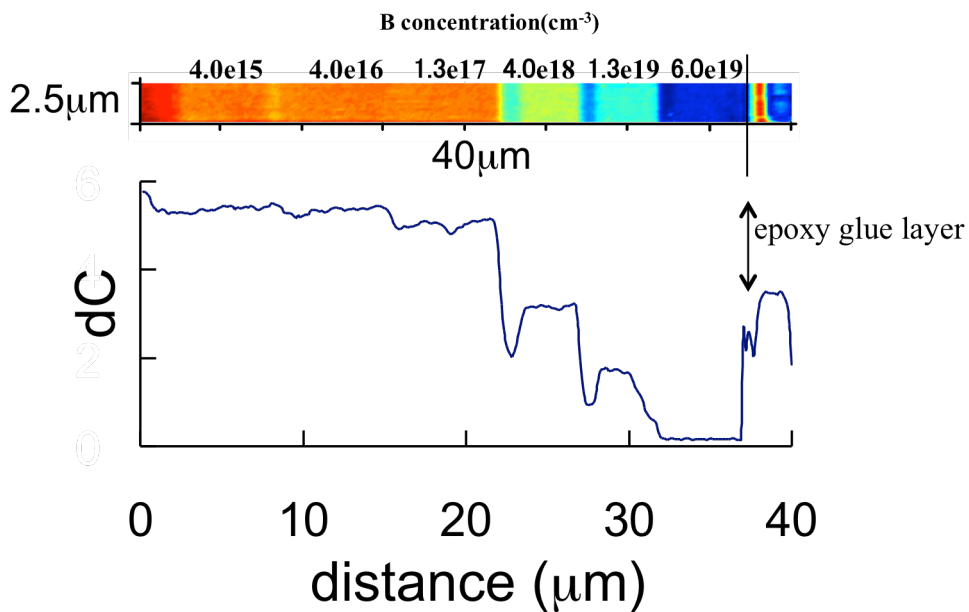
Fig. 4.2 An example of 2D SCM image and averaged 1D profile of the p-type stair case sample.

4.1.4 Results

Multiple measurements were performed on the same area at same working set points in order to evaluate the influence on the SCM image of charge trapping and interface state formation. Figures 4.3 (a) and (b) shows the results of 10 successive measurements of the p-type staircase sample submitted to the dry and to the wet oxidation, respectively. The amplitude of the ac bias (V_{ac}) applied to the sample was 1.0 V and the dc bias (V_{dc}) was 0 V. During the 10 successive measurements, the dC/dV signal decreased by an amount depending on the doping concentration. The variation was in the 0.2 to 8 % range in the case of the dry oxidation and in the 7 to 18 % range for the wet oxidation.

Figure 4.4 shows the relative dC/dV signal shift (R1) during the 10 successive measurements defined as

$$R1 = \frac{\left.\dfrac{dC}{dV}\right|_{10th-meas} - \left.\dfrac{dC}{dV}\right|_{1st-meas}}{\left.\dfrac{dC}{dV}\right|_{1st-meas}} \times 100 \qquad (4.1)$$

as function of V_{dc} for both the dry and the wet oxidation technique. The R1 depends both on V_{dc} and the doping concentration. In particular, the signal variation is smaller in the dry oxidation than in the wet oxidation case. This signal variation, i.e. decrease of dC/dV signal, might come partially from growth of oxide layer during successive measurements [4.15]. Figure 4.4 also includes the result of 10 successive measurements using a brand new metal-coated probe with dry oxidation. The variation was 5 to 15 %. By comparing the dC/dV signal shift with that observed in the case of a diamond-coated probe, one can conclude that the variation is due to the tip coating layer and to the oxidation process.

Ten successive measurements were also performed for the n-type staircase sample using a diamond-coated tip. The result indicates that diamond-coated probes are suitable

for measuring both p- and n-type samples and that they provide an intensive dC/dV signal. Furthermore, the monotonic decrease of the signal intensity with increasing doping concentration demonstrated that there is no contrast reversal effect due to the depletion of the diamond tip [4.16].
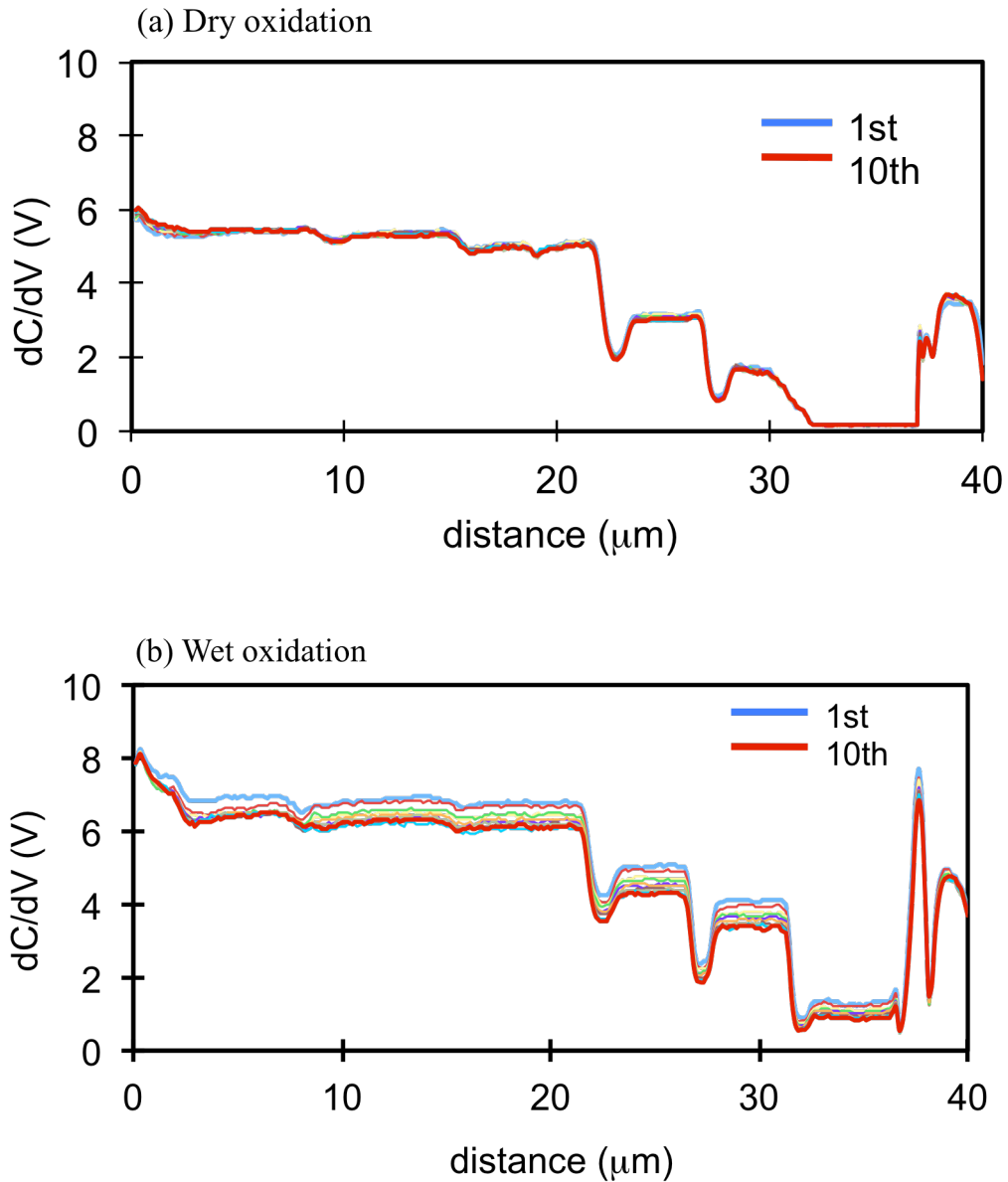
Fig. 4.3 Results of 10 successive measurements of the p-type staircase sample submitted to (a) dry and to (b) wet oxidation.
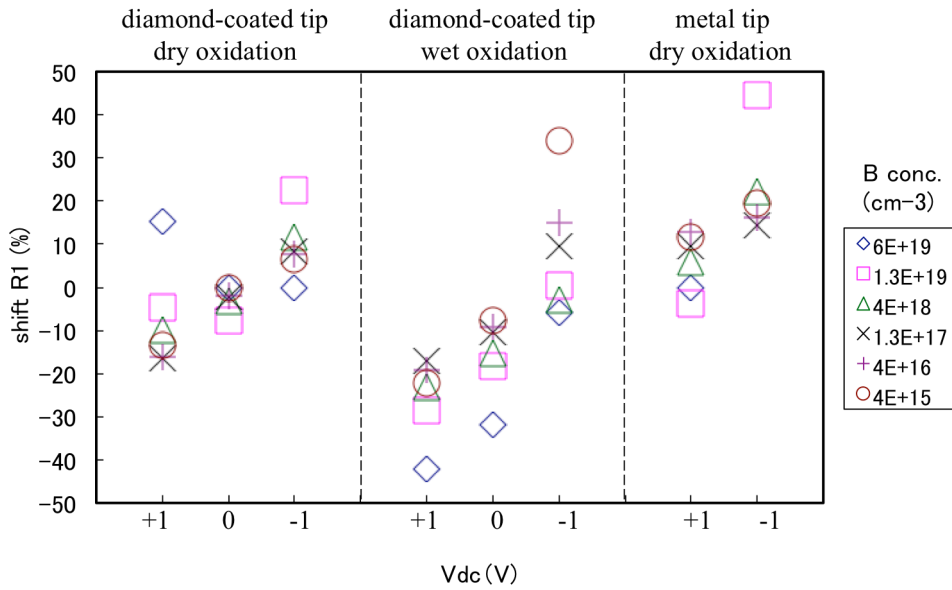
Fig. 4.4 Relative dC/dV signal shift (R1) during the 10 successive measurements.

The dC/dV-V_{dc} characteristics were measured by using a diamond-coated tip for both oxidation techniques. The results show that the ultra-thin oxides grown by wet oxidation exhibit a bell-shaped curve with a clearly defined peak located at $V_{dc} = 0$ V shown in Fig. 4.5. On the contrary, ultra-thin oxides produced by dry oxidation result into a flat characteristic shown in Fig. 4.6. However, dC/dV curves of wet-oxidized samples were non-monotonic for negative V_{dc}, indicating the appearance of contrast reversal effects.

The homogeneity of the ultra-thin oxide properties over the sample surface was investigated in the nine different locations across a p-type staircase sample by using a diamond-coated tip. The measurement locations consisted of three groups separating at least 200 μm each other and each group included three locations separating 10 μm each other. The homogeneity (R2) of the ultra-thin oxide films defined as

$$R2 = \frac{\left.\dfrac{dC}{dV}\right|_{\max} - \left.\dfrac{dC}{dV}\right|_{\min}}{\left.\dfrac{dC}{dV}\right|_{\max} + \left.\dfrac{dC}{dV}\right|_{\min}} \times 100.$$ (4.2)
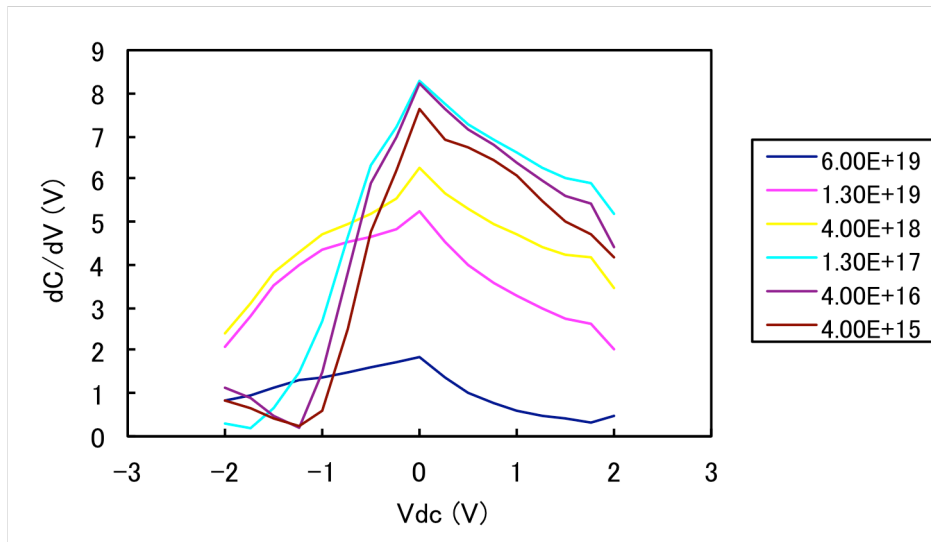
Fig. 4.5 dC/dV-V$_{dc}$ characteristics of the sample with the ultra-thin oxide layer grown by wet oxidation. The sample has six-staircase type of boron concentrations.
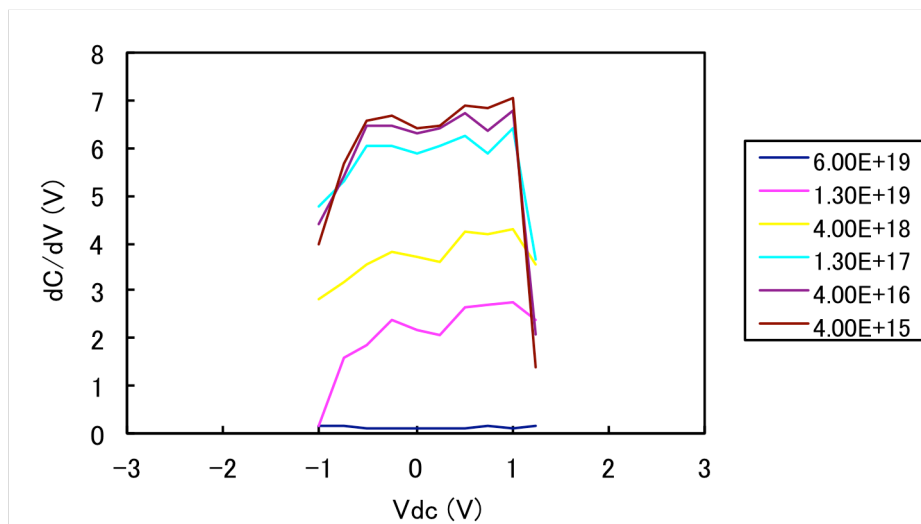
Fig. 4.6 dC/dV-V$_{dc}$ characteristics of the sample with the ultra-thin oxide layer grown by dry oxidation. The sample has six-staircase type of boron concentrations.

The R2 for the two oxidation techniques is represented in Fig. 4.7. It is evident that the homogeneity is much better in the case of the wet oxidation, especially for high doping concentrations.
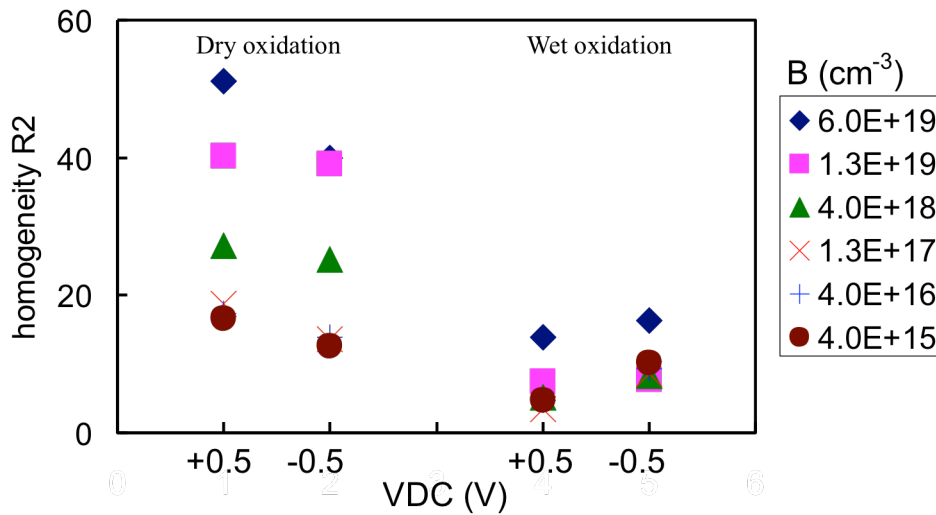
Fig. 4.7 Homogeneity R2 of SCM measurements for dry and wet oxidation.

The present investigation showed that diamond-coated probes are suitable for SCM applications. The SCM response in terms of dC signal intensity of the diamond-coated probes was similar to that of a brand new metal-coated tip but showing much better endurance properties. As a result of the very high B concentration, diamond-coated tips did not introduce additional contrast reversal effects produced by the depletion of the probe. A unique dependence of the dC signal on the doping level can be achieved by selecting the correct V_{dc} bias.

The excellent endurance provided by diamond-coated probes permits the application of SCM for the characterization of 2D doping profile. In the past, metal-coated probes have been demonstrated to be prone to metallization removal, leading to non-monotonic dC signals as a function of the doping concentration and to a very poor reproducibility of the measurements [4.17]. Furthermore, the brittleness of metal- coated probes was a

severe limit when measuring composite samples with a non-flat topography. This impeded reliable SCM measurements on composite samples consisting in the sample itself glued on the top of a calibration chip (e.g. staircase).

No abnormal behavior of the diamond-coated probes has been observed for both ultra-thin oxides grown by dry and wet oxidation, respectively. The differences, which have been observed between the SCM response of dry and wet ultra-thin oxides, could not be attributed to the use of diamond-coated tips. In particular, repeated measurements on the same oxide area revealed that dry ultra-thin oxides provide a better reproducibility than wet oxides, and further on a wider doping concentration range. This was probably due to the fact that wet oxides are usually thinner and have more interface traps than dry oxides as described in the Section 4.1.2. Due to the improved endurance provided by diamond-coated probes, it has been demonstrated that the wet oxidation provides a better homogeneity over extended areas. This makes wet oxidation very suitable for qualitative SCM imaging of large structures as for instance power devices [4.18]. Similar to metal-coated probes, large discrepancies between the measured and the theoretical dC/dV-V curves have been observed. Also in this case, the non-idealities are not due to the diamond-coated probes but they can be attributed to the poor quality of the ultra-thin oxide layers grown at low temperatures and to the smearing effect produced by the UHF sensor in the detector.

4.1.5 Summary

In summary, diamond-coated probes produce adequate intensity of the dC signal and high contrast images for both p-type and n-type silicon samples without implying contrast reversal effects. The excellent wear-out properties of diamond-coated probes opened new applications of SCM. The use of diamond-coated probes in combination with the dry oxidation technique can provide a good reproducibility of the results. Nevertheless, the non-idealities observed in the dC/dV-V measurements, indicated that

there is still a room for improving the quality of the ultra-thin oxides.

4.2 Methodology for quantitative SCM measurement

4.2.1 Problems in quantitative measurements

The SCM has a difficulty in a quantitative measurement, because of the nonlinear relation between the measured dC/dV signal and the carrier concentration [4.19]. In this section, the methodology of quantitative measurement of SCM will be described. There are two main problems in using a SCM for a quantitative measurement of carrier concentration. One is the conversion of SCM signals into carrier concentration and the other is the stability in SCM measurement. The latter problem has been discussed in Section 4.1. Here the first one is discussed. Basic concept of the quantitative measurement is to obtain relationship between a change of capacitance, i.e. SCM signal, and carrier concentration. One idea for this is to prepare several samples whose carrier concentrations are known in advance, and make relation between the measured data and the known concentrations [4.3]. Here, the sample whose carrier concentration is known in advance is called as standard sample. This method is effective for an area that does not include pn junctions, however it is not enough for an area including pn junctions. In order to make a quantitative measurement for the area including pn junctions, the method that uses both the standard sample and computational simulation would be suitable. This method will be described in detail.

4.2.2 Comparison of two samples

In the SCM measurement or generally in the SPM measurement, it is sometimes difficult to compare two samples, which have been measured separately, because of the changes of surface condition of the samples and the changes of probes during each measurement [4.1]. Therefore a sample that has unknown carrier distribution should be measured at the same time with the above-mentioned standard sample. This is possible for example by gluing two samples each other on their surface following by cross sectioning. In this case, we should estimate how wide area of both samples is in the same measurement conditions. In order to estimate the wideness of the area, two exactly same samples were prepared and glued each other on each surface, and then cross-sectioned. The sample was the p-type staircase sample in this study. The way of cross sectioning was described in Section 4.1.2.
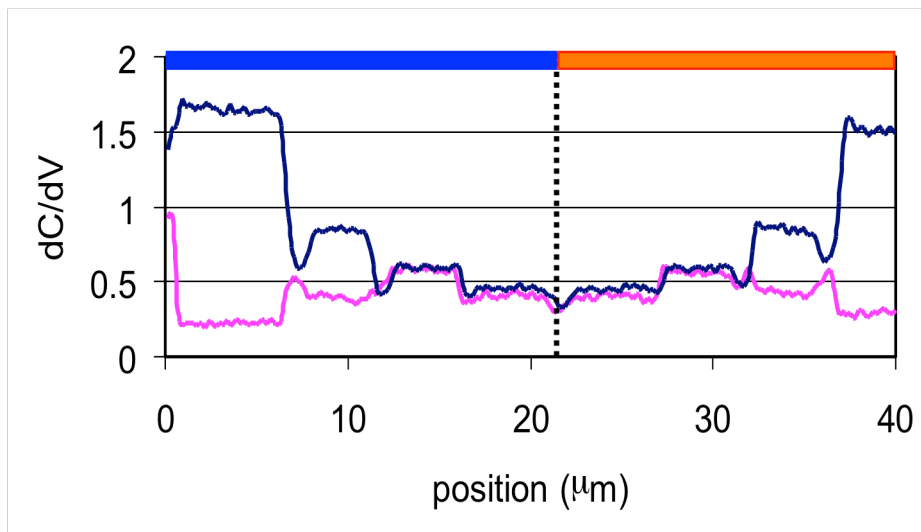
Fig. 4.8 The results of SCM measurement of the glued samples with two different dc bias conditions shown in dark blue and pink line. The dotted line indicates glued surfaces of the two samples shown in blue and red bar area at the top of this figure.

Figure 4.8 shows the results of SCM measurement of the glued samples with two different dc bias conditions. The dark-blue line was measured at Vdc = 0 V, and the

pink line at Vdc = -1 V. The dotted line indicates glued surface of the two samples. The center part of the measured area, about 13 μm both sides of the dotted line for each sample, showed the same SCM signal intensities for the samples. However, far sides from the dotted line of the SCM result showed different SCM signal intensities, even if the both samples were measured at the same time. This might come from the difference of the overlapping area between the probe and the sample that caused different parasitic capacitance described below. From the result shown in Fig. 4.8, the area where SCM measurement of the sample at the same time produces the same result is approximately 26 μm. This area or length is wide enough to measure not only a latest small CMOS device but also a large power device. Therefore we can conclude that the same concentration region in the two samples measured at the same time give the same SCM signal intensity.

The configuration of a diamond-coated probe and a sample is shown in Fig. 4.9. The probe consists of a silicon cantilever and a conductive cover layer of polycrystalline diamond. The conductive diamond layer is supported by a metal bar thorough which the probe is connected to a capacitance sensor. The silicon cantilever part generally does not influence on a SCM measurement unless the conductive diamond layer would deplete itself in measuring a high-doped sample. As shown in Fig. 4.9, there is an overlapping area between a cantilever and a sample that causes parasitic capacitance. The overlapping area was roughly 30 μm (the width of the typical cantilever) × 50 μm (the length of the cantilever floating on the sample) and the distance from the sample surface to the cantilever was about 500 μm. On the other hand, the tip-top area contacting to the sample was about 100 nm × 100 nm and the distance from the tip to the sample surface was 3 nm that is equal to the oxide thickness. Capacitance is roughly proportional to $\varepsilon S/d$. Here ε is the dielectric constant, S is the area of overlap and d is the distance. The dielectric constant is 3.9 for silicon oxide and 1.0 for air. Therefore the parasitic capacitance of the overlapping area is about one tenth of the capacitance under

74

the tip-top with some fringe capacitance component. This means that the parasitic capacitance of the cantilever is sometimes not negligible.
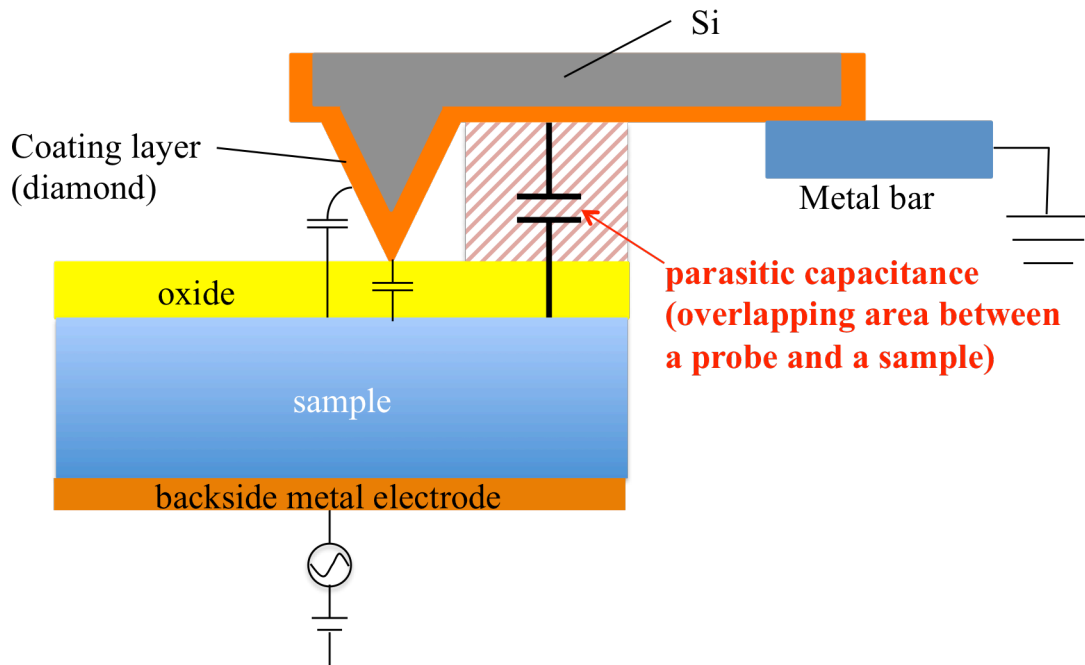

Fig. 4.9 Schematic configuration of a diamond-coated probe and a sample. There is a parasitic capacitance from overlapping area between the probe and the sample.

4.2.3 SCM measurements

Here the quantitative SCM measurement method will be described by using a boron implanted Si sample whose carrier distribution is unknown and the concentration-standard sample, which was epitaxialy grown several layers with different B concentrations described in Section 4.1.2. The matrix effect in SIMS analysis of the concentration standard sample was canceled out by using a calibration sample of constant boron concentration in silicon. As for the B implanted sample, B was implanted into an n-type Si wafer with the acceleration energy of 200 keV and the dose of 1×10^{15} atoms/cm^2, followed by annealing in 900 °C for 30 minutes. Both of the B implanted and the standard sample were glued each other on the top surface by the epoxy resin. The glued sample was cross-sectioned in the way described in Section

4.1.2. An ultra-thin oxide layer was deposited by using the dry oxidation technique, 300 °C under UV illumination. The result of a SCM measurement of the cross-sectioned sample is shown in Fig. 4.10. The SCM measurement condition was $V_{dc} = 0$ V, $V_{ac} = 0.5$ V, and scan rate of 1 Hz. The left side of the glue layer in Fig. 4.10 shows the result of the standard sample and the right side shows the B implanted sample. The four different B concentration layers of the standard epitaxial sample were 6.0×10^{19}, 1.3×10^{19}, 4.0×10^{18}, and 1.3×10^{17} atoms/cm^3 from the glue layer, respectively. First of all, the relation of the four different concentrations and the measured SCM signal intensity was estimated by using device simulation. The following is the brief description of the simulation.
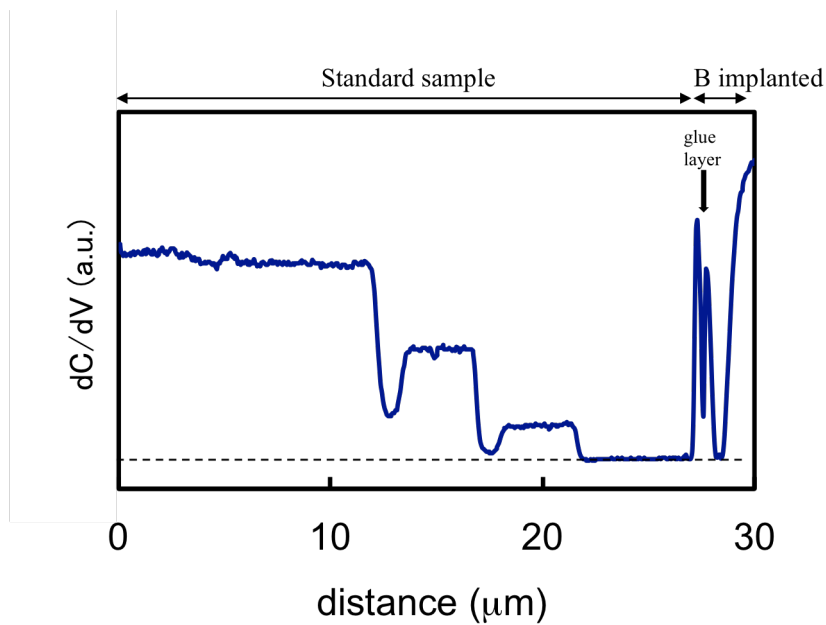
Fig. 4.10 The result of the SCM measurement of the cross-sectioned sample consisting of the B implanted and the standard samples, which has 1.3×10^{17}, 4.0×10^{18}, 1.3×10^{19}, and 6.0×10^{19} atoms/cm^3.

4.2.4 Conversion methodology of SCM data

The methodology of a conversion from SCM signals to carrier/dopant concentrations is shown in Fig. 4.11 schematically. There are two important points in this methodology. One is the SCM measurement of a sample having unknown dopant profile and the concentration standard sample at the same time as described in the previous section. The other is the data set of C-V curves through the device simulation considering three-dimensional effect in the probe – sample configuration. The concentration standard sample has two purposes. One is the calibration of the simulation model parameters and the other is the monitoring of a measurement condition. In case of getting very low signal or contrast reversal at the measurement of the standard sample, we should check the probe and the sample surface. As for the validity of carrier/dopant concentration of the standard sample itself, in this study we have a maximum concentration of 6×10^{19} atoms/cm^3. This concentration is low enough to being fully activated and the carrier concentration is equal to the dopant concentration.
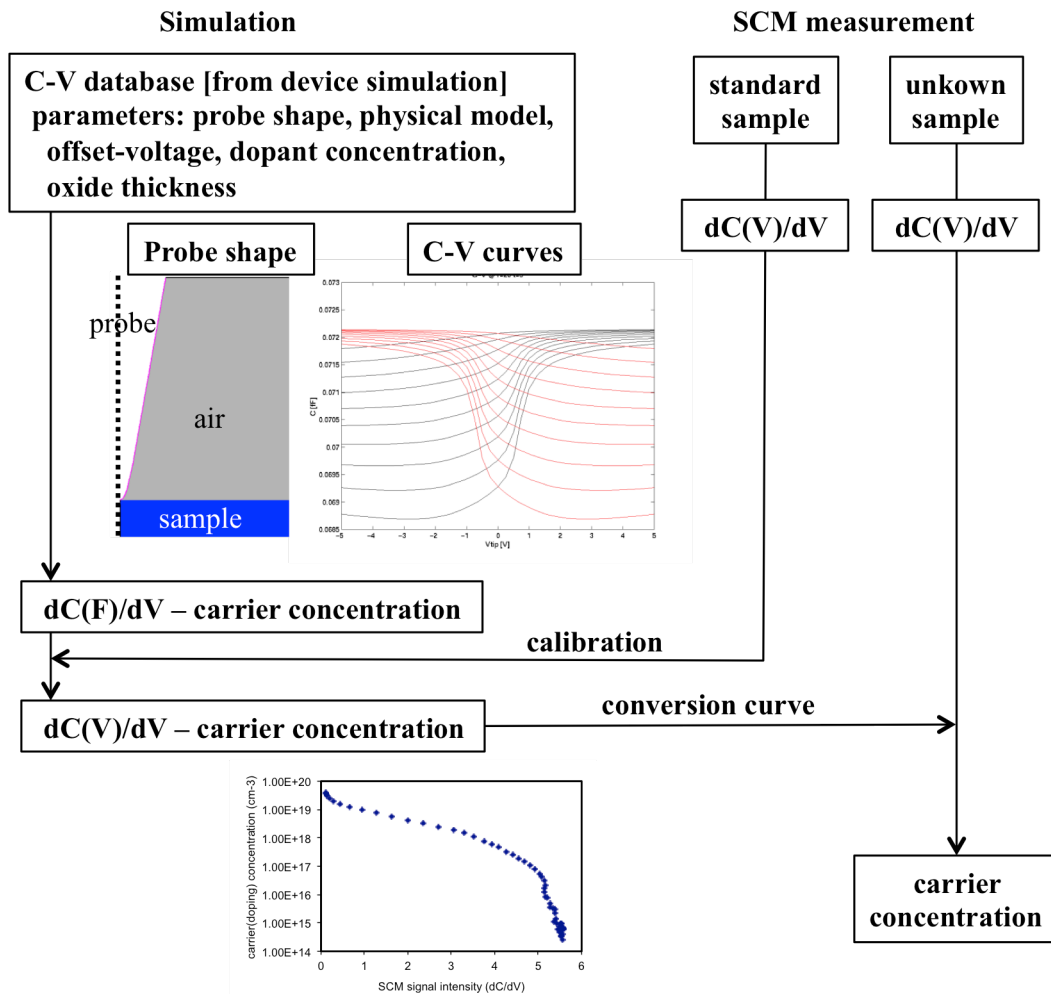
Fig. 4.11 Schematic diagram of the methodology of a conversion from SCM signals to carrier concentrations.

For the simulation, device simulator DESSIS of Synopsys Inc. and SCaMsim package developed by Ciampolini were used [4.20]. The structure used in the simulation, shown in Fig. 4.12, consists of the tip of the probe, Si substrate with uniform doping, and a dielectric layer in cylindrical coordinate system. The tip was characterized by parabolic curve. The dielectric layer was silicon oxide whose dielectric constant is 3.9 and the area between the probe and the silicon dioxide layer was assumed to be air whose dielectric constant is 1.0. The Si substrate had four different B concentrations corresponding to the standard sample. After the setting of electrodes on the bottom of

the Si substrate and the probe surface, ac small signal analysis was performed by using the device simulator. C (capacitance) and V (voltage used in SCM measurement) obtained from the result of the ac small signal analysis, and then dC/dV - V curve was derived from this C - V curve. In the device simulation, the parameters such as the curvature of the tip, thickness of silicon oxide, dielectric constant of the oxide, and interface traps were prepared with variations. The curvature of the tip was directly measured by using the deconvolution method. In this method, a sample including a wide variety of roughness in height and width was measured with the probe in topography mode. From the measured image, the three-dimensional tip shape was reversely derived. Though the curvature of the tip was fitted from the measured result, the variation of 10 or 20 nm was added in the simulation because the real tip shape is not conformal in cylindrical direction. There were also variations of oxide thickness with one or two nm that included the variations of both physical thickness and dielectric constant of the silicon oxide. The dataset of C-V curves were calculated with these parameters including the variations of each parameter and dC/dV values was derived from the C-V dataset.
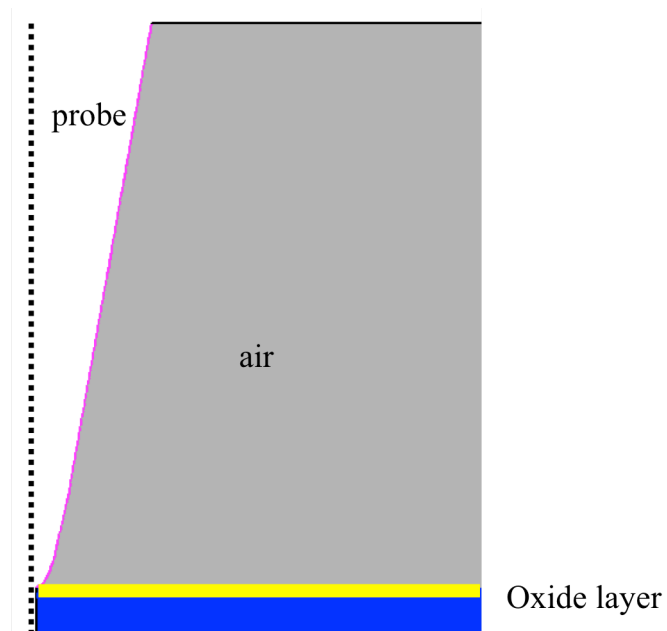
Fig. 4.12 Structure used in the device simulation in cylindrical coordinate system.

By calibrating the simulated dC/dV value at the applied dc bias in SCM measurement to the measured SCM result of the standard sample, parameters such as silicon dioxide thickness, curvature of the tip, and device models were adjusted. Finally, the relationship between dC/dV and B concentrations was determined as shown in Fig. 4.13.
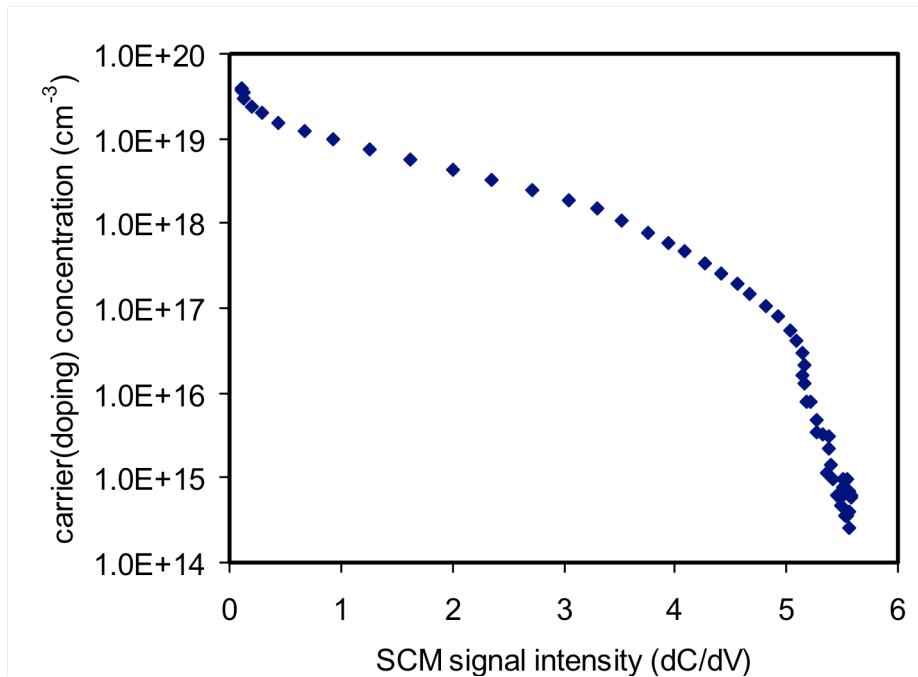
Fig. 4.13 Relationship between dC/dV and B concentration determined the simulation and SCM results of the standard sample.

4.2.5 Comparison to SIMS result

Then the result of the SCM measurement of the B implanted sample whose carrier concentration was unknown (shown in Fig. 4.14) was converted into B or carrier concentration based on the dC/dV and B concentration relation obtained from the standard sample measurement and the simulation. The result was compared with secondary ion mass spectrometry (SIMS) measurement for the same sample. The SIMS measurement was performed with 2 keV O_2^+ primary ion beam to reduce the knock-on effect. The result of SCM and SIMS is shown in Fig. 4.15. The converted SCM signal was in good agreement with the SIMS measurement over the range of four orders of magnitude, 1×10^{15} - 2×10^{19} atoms/cm^3. The error of the SCM data to SIMS data was within 10 % from 0.6 μm to 1.2 μm. This error value is almost the same of SIMS measurements. There were, however, three discrepancies between the doping profiles

obtained by SCM and SIMS: (1) from the surface to the peak of the B profile, the SCM result was lower than the SIMS result and the error was about a factor of 2, (2) the peak value of the profile in SCM and SIMS were different, and (3) there was a small peak in the SCM results around 1×10^{15} atoms/cm^3 of the B concentrations.
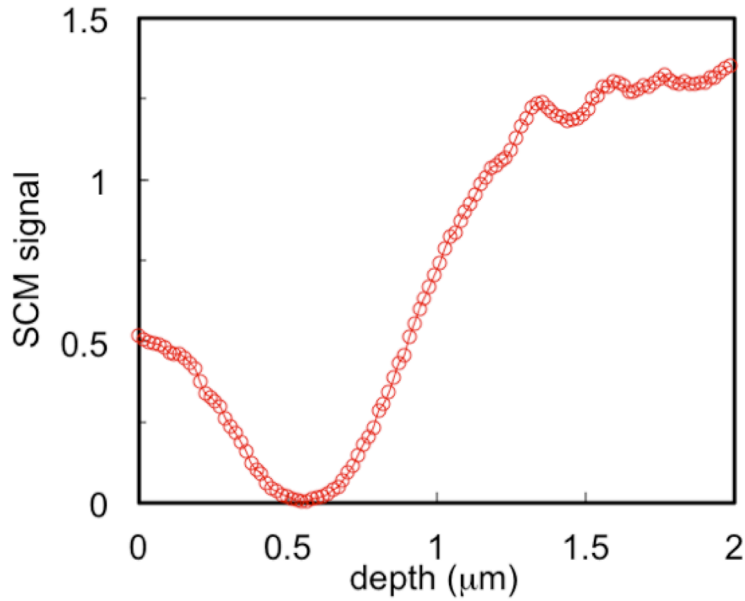
Fig. 4.14 The result of the SCM measurement of the B implanted sample.

For (1), it is assumed that corner rounding of the sample in the cross-sectioning caused the lower concentrations. The B implanted sample and the standard sample were tried to be glued each other without a gap between them. However there might be a thin gap and this made the corner round during the polishing. This corner rounding made the angle between the probe and the sample surface non-90 degrees, while the angle between them in the simulation was 90 degrees.

For (2), depletion in the probe itself might be the reason. In the peak region where B concentrations close to 1×10^{20} atoms/cm^3 in the B implanted sample, a semiconductor character of the probe that coated by B doped diamond could not be ignored. Another reason for the discrepancy (2) is detection limit of SCM for higher concentration than

6.0×10^{19} atoms/cm^3. As was shown in Fig. 4.10, SCM signal intensity for 6.0×10^{19} atoms/cm^3 was equal to or less than lower detection limit of SCM indicated in dashed line in the figure.

For (3), this might be affected by the existence of a pn junction. This will be discussed in the next section in the detail.
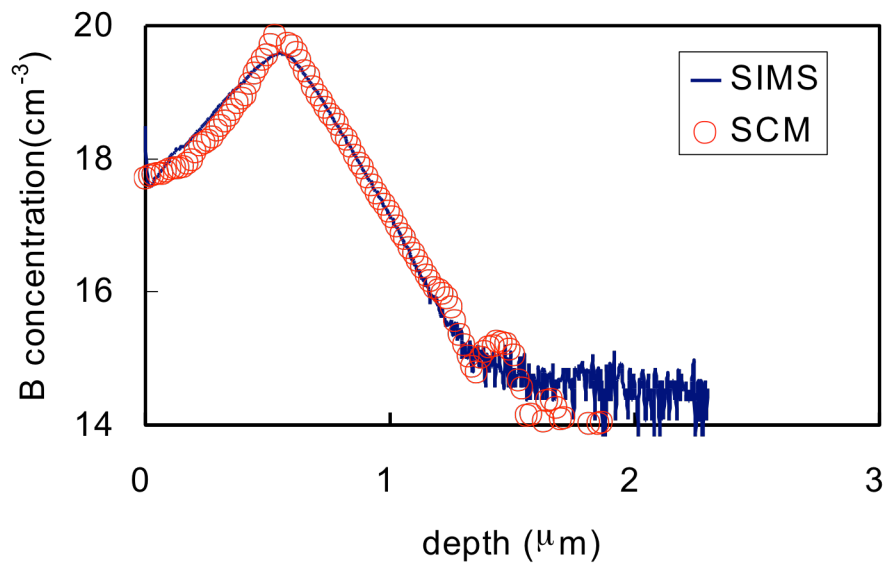
Fig. 4.15 Comparison the results of converted SCM measurement and SIMS of the

B implanted sample.

4.2.6 PN junction

Delineation of pn junction in a device is one of the most important and interesting things for device design. SCM is one of the powerful techniques for this purpose. There are, however, several difficulties for the delineation of the pn junction. One of the difficulties is the difference between metallurgical pn junction and electrical one. Another is spatial resolution of the SCM measurement. Fig. 4.16 shows results of SCM measurements of the B implanted sample with several dc voltages. The metallurgical pn junction is shown in Fig. 4.16 with dotted line. On the other hand, electrical pn junction positions, where SCM signal become zero, changed according with dc bias voltage: -0.1

µm from the metallurgical pn junction position for V_{dc}=-0.5 V and +0.4 µm for V_{dc}=+0.5 V. Electrical pn junction position should coincide with metallurgical one under flatband voltage condition of MOS capacitor consisting of the sample, the dielectric layer, and the probe. This shift of measured electrical pn junction position depended not only on the applied dc bias, but also on doping concentration.
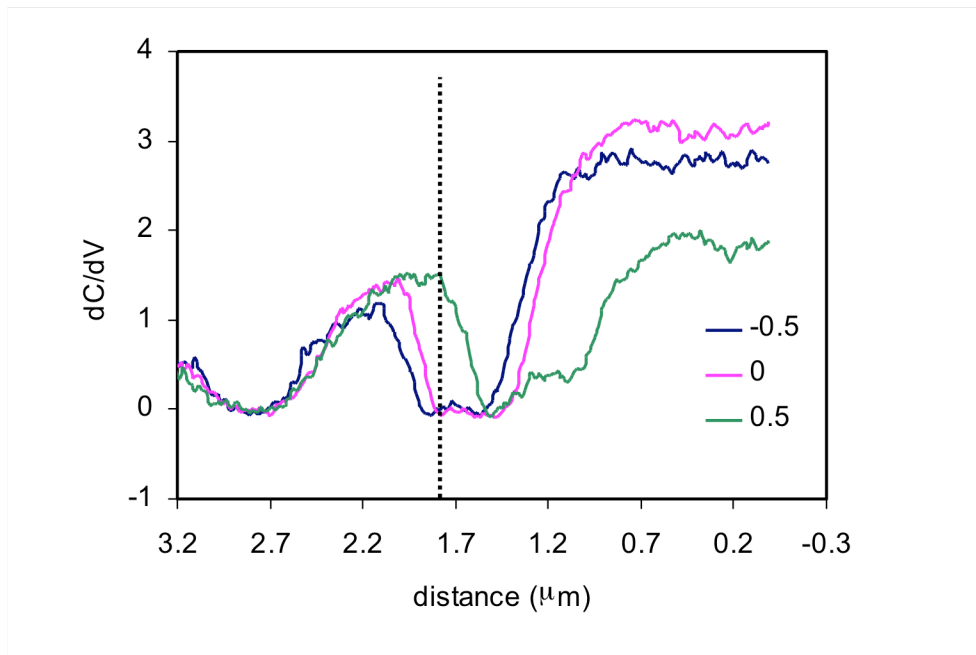
Fig. 4.16 Results of SCM measurements of the B implanted sample with several dc voltages; -0.5 , 0 , +0.5 V. The dotted line shows the metallurgical junction position.

If the doping concentration at the pn junction is high, change of the depletion width is small so that the electrical pn junction position changes slightly. On the other hand, if the doping concentration at the pn junction is low, change of the depletion width is large so that the electrical pn junction position changes largely. The doping concentration also affects spatial resolution of SCM measurement. Fig. 4.17 shows maximum depletion width in one-dimension, which is calculated by the following expression.

$$W_{max} = 2\sqrt{\varepsilon\phi_F / qN_a} \,, \qquad\qquad (4.3)$$

$$\phi_F = (kT/q)\ln(N_a/n_i), \qquad\qquad (4.4)$$

where N_a is doping concentration and n_i is intrinsic carrier concentration [4.21]. This relationship between doping concentration and maximum depletion width indicates that the spatial resolution is close to 100 nm in the low doping concentration, while the spatial resolution in high concentration area is limited by the probe tip size (10 nm).
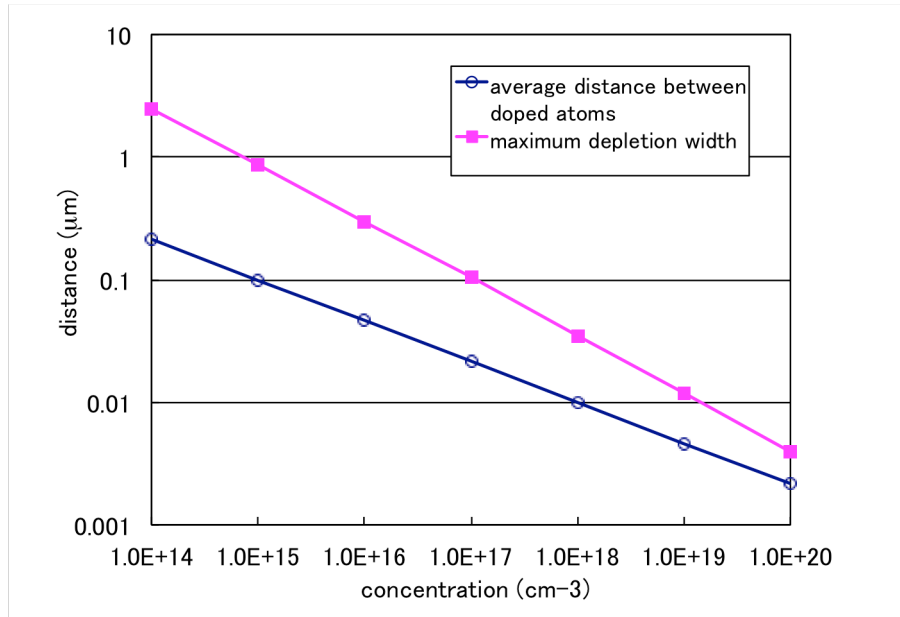
Fig. 4.17 Relationship between doping concentration and maximum depletion width calculated in 1d model. The spatial resolution of SCM is limited by depletion width depending on the doping concentration.

From the dependency of the spatial resolution on the dopant concentration and that of electrical junction position on the applied voltage, it would be concluded that SCM measurement is suitable to the delineation of an abrupt junction with high and low dopant concentration areas. To confirm this, we applied the SCM measurement to a UMOS power device. As illustrated in Fig. 4.18, the UMOS has several kinds of pn junction. The abrupt junction in the UMOS locates at Source(n$^+$)/Channel(p), and the

gradually changing junction at Channel(p)/Drain(n). The result of the SCM measurement was shown in Fig. 4.19. The abrupt junction at Source(n^+)/Channel(p) was clearly indicated. The Contact(p^+)/Channel(p) position was also clearly observed. On the contrary, the junction at Channel(p)/Drain(n) was not clear. These results strongly support our conclusion.
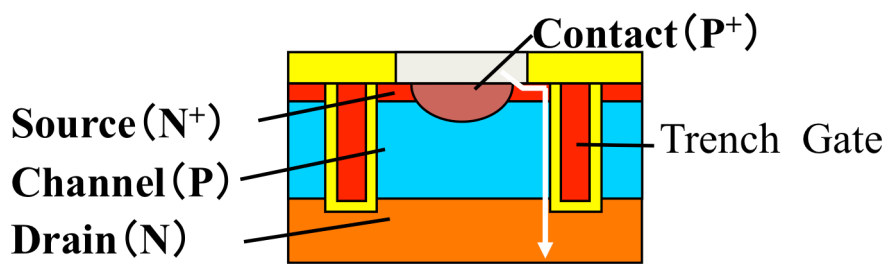
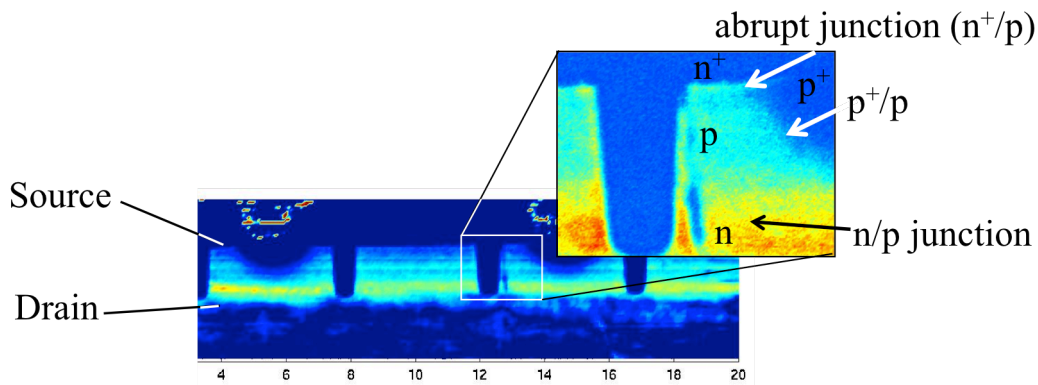**Fig. 4.18 Illustrated structure of an UMOS power device.**

Fig. 4.19 SCM image of the UMOS device. There is the abrupt junction at Source(n^+)/Channel(p).

Since the device simulation used in making the SCM signal – concentration conversion curve has used a simulation structure of a constant doping concentration, it is not possible to apply it directly to the prediction of the pn junction position which would be changed with applied voltage. To indicate the change of the junction position in a low dopant concentration area more clearly, we investigated the conduction band

energy profile, which could be used for a rough estimation of the depletion width, across a pn junction with the SCM probe. Figures 4.20 and 4.21 shows the configuration of a probe and a silicon sample with a pn junction, and simulation results of the
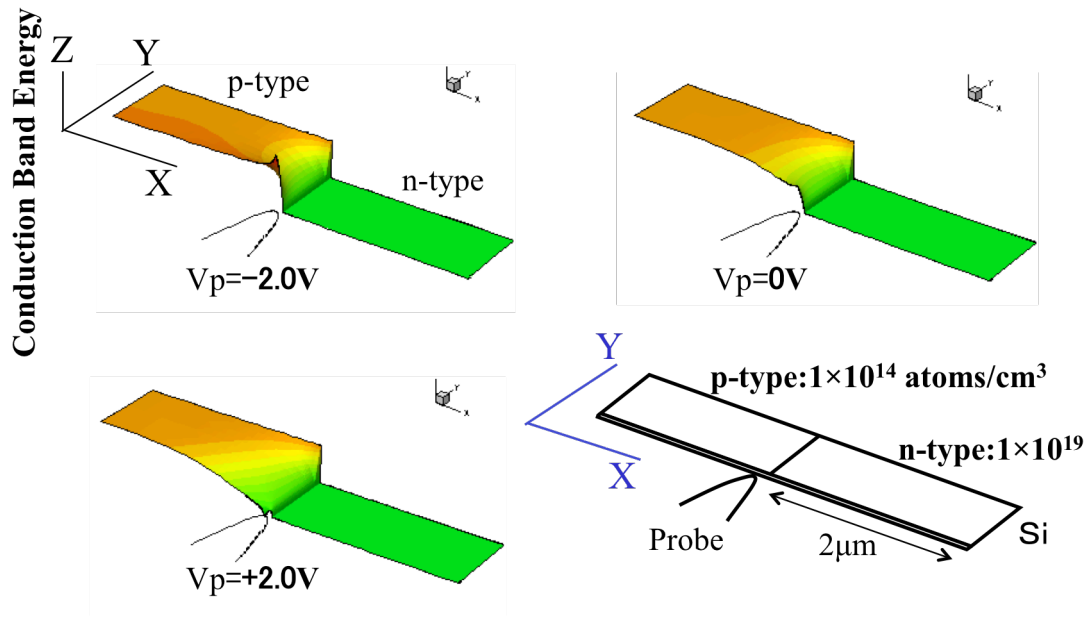
Fig. 4.20 Simulation results of conduction band energy with the probe position at 0.2 μm in the p-type region from the metallurgical junction.

conduction band energy with different dc bias voltage (V_p). The z-axis indicates the conduction band energy of the silicon sample. In Figs. 4.20 and 4.21, the dopant concentration of p-type region was 1×10^{14} atoms/cm^3 and that of n-type was 1×10^{19}. These simulations could help us to estimate the depleted area. The probe position was 0.2 μm to the p-type region from the metallurgical junction in Fig. 4.20 and 0.1μm to the n-type region from the metallurgical junction in Fig. 4.21. At the low concentration of p-type region, the conduction band energy was influenced even at about 1.0 μm from the metallurgical junction at the sample surface. On the other hand, at the high concentration of n-type region, the conduction band energy was influenced locally at the probe. By using these kinds of simulation, it would be possible to indicate the pn junction position even for non-abrupt junctions.
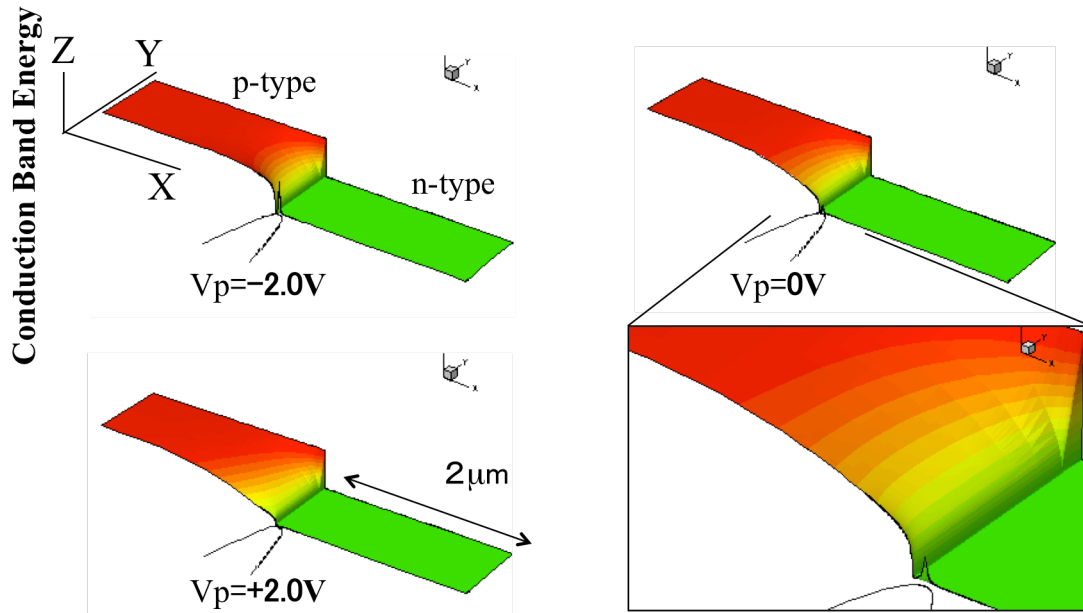
Fig. 4.21 Simulation results of conduction band energy with the probe position at 0.1 µm in the n-type region from the metallurgical junction.

In SCM measurements of low dopant concentration less than 1×10^{15} atoms/cm^3, there are several crucial problems. One is the small number of carriers under a tip. That makes difficult to detect the capacitance itself. Another is the low spatial resolution. The depletion width spreads about 1 µm at 1×10^{15} atoms/cm^3. Improvement of the detection circuit would be one idea to overcome the detection limit. The constant dC mode, mentioned in Section 3.2, would improve the spatial resolution in the lower concentration range though it has disadvantage in the higher concentration.

Recently, a scanning microwave microscopy (SMM) and a scanning nonlinear dielectric microscopy (SNDM) have been reported having a possibility to measure lower dopant concentration range than SCM. These new technologies will be described in Chapter 7.

The discussions conducted thus far were on the assumption that a sample has a uniform dopant concentration in a silicon layer in vertical direction under the probe to the bottom electrode as shown in Fig. 4.22 (a). In the case of having non-uniform
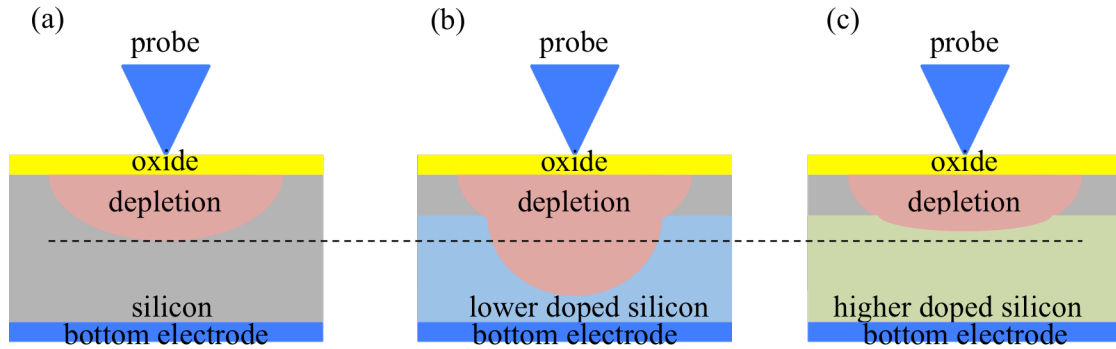

Fig. 4.22 Schematic pictures of depletion region in (a) uniformly doped layer, (b) stacked two layers with lower doped layer at the bottom and (c) with higher doped layer.

dopant concentration in vertical direction, it becomes more complex to analyze SCM signals. The simple cases are shown in Fig. 4.22 (b) and (c). In these figures, samples have two silicon layers of different dopant concentrations in vertical direction. As indicated in Fig. 4.22, depletion widths are different for three cases. Therefore, SCM signals, which come from the changes of depletion width with the applied ac bias, become different each other though they have the same dopant concentration at the upper layer. If the thickness of the upper layer of Fig. 4.22 (b) and (c) are wider than the depletion width, it would be possible to make the quantitative analysis unless the resistivity of the lower layer is high to distort a C – V curve.

References

[4.1] P. Malberti, L. Ciampolini, M. Ciappa and W. Fichtner, "Quantification of scanning capacitance microscopy measurements for 2D doping profiling", Microelectronics Reliability, vol. 40, pp. 1395-1399, 2000.

[4.2] T. Trenkler, T. Hantschel, R. Stephenson, P. De Wolf, W. Vandervorst, L. Hellemans, A. Malave, D. Buchel, E. Oesterschulze, W. Kulish, P. Niedermann, T. Sulzbach and O. Ohlsson, "Evaluating probes for electrical AFM", Journal of Vacuum Science and Technology B, vol. 18, pp. 418-427, 2000.

[4.3] T. Clarysse, M. Caymax, P. De Wolf and W. Vandervorst, "Epitaxial staircase structure for the calibration of electrical characterization techniques", Journal of Vacuum Science and Technology B, vol. 16, pp. 394-400, 1998.

[4.4] G. Pietsch, G. Higashi and Y. Chabal, "Chemiomechanical polishing of silicon: surface termination and mechanism of removal", Applied Physics Letters, vol. 64, pp. 3115-3117, 1994.

[4.5] H. Seidel, L. Csepregi, A. Heuberger and H. Baumgärtel, "Anisotropic etching of crystalline silicon in alkaline solutions II. Influence of dopants", Journal of the Electrochemical Society, vol. 137, pp. 3626-3632, 1990.

[4.6] M. Forsberg, K. Niclas and O. Jörgen, "Effect of dopants on chemical mechanical polishing of silicon", Microelectronic engineering, vol. 60, pp. 149-155, 2002.

[4.7] V. Ukraintsev, F. Potts, R. Wallace, L. Magel, H. Edwards and M. Chang, "Silicon

surface Preparation for two-dimensional dopant characterization", Proceedings of the Characterization and Metrology for ULSI Technology, pp. 736-740, 1998.

[4.8] T. Ohmi, "Very high quality thin gate oxide formation technology", Journal of Vacuum Science and Technology A, vol. 13, pp. 1665-1670, 1995.

[4.9] D. Cole, J. Shallenberg, S. Novak, R. Moore, M. Edgell, S. Smit, C. Hitzman, J. Kirchof, E. Principe, W. Nieveen, F. Huang, S. Biswas, R. Bleiler and K. Jones," SiO2 thickness determination by XPS, AES, SIMS, RBS, TEM, and ellipsometry", Journal of Vacuum Science and Technology B, vol. 18, pp. 440-444, 2000.

[4.10] Y. Ishikawa, T. Shibamoto and I. Nakamichi, "Low-Temperature Oxidation of Silicon in Dry O_2 Ambient by UV-Irradiation", Jpn. J. Appl. Phys., vol. 31, pp. 1148 – 1152, 1992.

[4.11] A. Kazor and I. W. Boyd, "Growth and modeling of cwUV induced oxidation of silicon", J. Appl. Phys., vol. 75, pp. 227 – 231, 1994.

[4.12] J. Y. Zhang and I. W. Boyd, "Low temperature photo-oxidation of silicon using a xenon excimer lamp", Appl. Phys. Lett., vol. 20, pp. 2964 – 2966, 1997.

[4.13] T. Ohwaki, M. Takeda and Y. Takai, " Characterization of silicon native oxide formed in SC-1, H2O2 and wet ozone processes", Jpn. J. Appl. Phys., vol. 36, pp. 5507 – 5513, 1997.

[4.14] Support note No. 289, Rev. A, Digital Instruments Veeco Metrology, 2000

[4.15] E. S. Snow, W. H. Juan, S. W. Pang and P. M. Campbell, "Si nanostructure fabricated by anodic oxidation with an atomic force microscope and etching with an electron cyclotron resonance source", Applied Physics Letters, vol. 66, pp.1729-1731, 1995.

[4.16] R.Stephenson, et al., "Contrast reversal in scanning capacitance microscopy imaging", App. Phys. Lett., Vol. 73, no. 18, pp. 2597-2600 (1998).

[4.17] P. Malberti, L. Ciampolini, M. Ciappa and W. Fichtner, "Experimental investigation and 3D simulation of contrast reversal effects in scanning capacitance microscopy", Proceedings of the Characterization and Metrology for ULSI technology, pp. 652-656, 2001.

[4.18] M. Buzzo, "Dopant imaging and profiling of wide bandgap semiconductor devices", Doctoral dissertation, Technische Wissenschaften, Eidgenössische Technische Hochschule ETH Zürich, Nr. 16756, 2007.

[4.19] T. Fujita, A. Karen, H. Ito and D. Fujita, "Industrial standardization and quantification of the carrier concentration in semiconductor devices using electric SPM", Journal of Surface Analysis, vol. 19, pp. 76-80, 2012.

[4.20] L. Ciampolini, M. Ciappa, P. Malberti and W. Fichtner, "SCaMsim, a new three-dimensional simulation tool for scanning capacitance microscopy", Characterization and Metrology for ULSI Technology, CP550, pp. 647-651, 2001.

[4.21] J. Singh, Semiconductor Devices An Introduction, McGraw-Hill, 1994.

Chapter 5
Application of SCM

5.1 Application of SCM to compound semiconductor materials

5.2 SCM measurement and analysis of SiGe

    5.2.1 SiGe in HBTs

    5.2.2 Experimental

    5.2.3 Simulation for different Ge Mole fraction and abrupt pn junction

    5.2.4 Results

5.3 Comparison of B diffusion in SiGe and SiGeC

References

5.1 Application of SCM to compound semiconductor materials

In the previous chapter, the methodology of stable and quantitative SCM measurement was described by using silicon samples. In this chapter, application of the SCM measurement to non-Si materials, especially compound semiconductors such as SiGe and SiGeC, will be discussed. These materials are different from silicon in the point of a dielectric constant and an oxide growth rate which have dependency on the composition ratios x or y in $Si_{1-x}Ge_x$ or $Si_{1-x-y}Ge_xC_y$. Both dielectric constant and oxide thickness are important parameters in the capacitance measurement of SCM.

5.2 SCM measurement and analysis of SiGe

5.2.1 SiGe in HBTs

SiGe is one of the key materials for high-speed semiconductor devices, for example hetero bipolar transistors (HBTs) and MOSFETs. In HBTs, SiGe is used as a base layer (Fig. 5.1) and it includes boron as a dopant. The B profile in the base layer should be controlled precisely in order to achieve shorter transit time for higher speed performance [5.1].
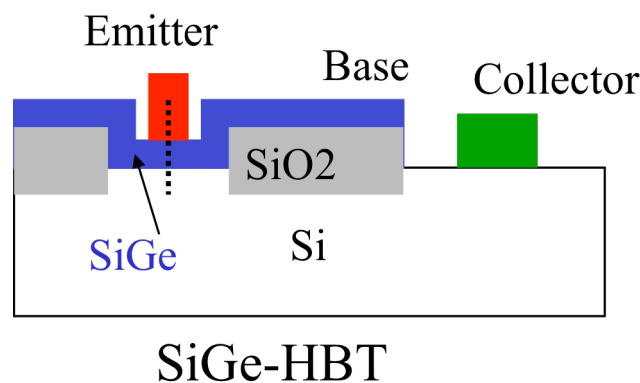
Fig. 5.1 Structure of SiGe-HBT. The base region is SiGe.

This boron profile is usually measured by SIMS in wide area, such as a test element group (TEG), but not in the HBT device itself. This makes difference between the measured B profile in the TEG and the real one in the device because of structure-oriented effects such as a stress dependent diffusion [5.2]. To improve this situation, the direct measurement of B profile in SiGe-HBTs has been expected. One of the direct measurement methods is scanning probe microscopy, especially scanning capacitance microscopy (SCM). However, there had been not enough study in SCM measurement of SiGe [5.3]. The "matrix effect", which is usually mentioned in SIMS measurement to describe different secondary ion yields among different materials, has been observed in the SIMS measurement of $Si_{1-x}Ge_x$ with different Mole fraction x [5.4]. This makes difficult to make quantitative measurement of B profile especially in graded Ge base, in which Ge Mole fraction x gradually changes spatially, of HBTs [5.5]. Though it is different from the matrix effect in SIMS measurement, there is also expected some kind of "matrix effect" in SCM measurement of $Si_{1-x}Ge_x$. This comes from different dielectric constant of $Si_{1-x}Ge_x$ with different Mole fraction x and/or a different native oxide thickness on $Si_{1-x}Ge_x$ surface [5.6]. In this section, we focus on how to measure and analyze B profile across SiGe layers with different Ge concentrations.

5.2.2 Experimental

There are two typical features of B profiles in HBTs. As is shown in Fig. 5.2, one is an abrupt pn junction in SiGe base layer and the other is B profile across graded Ge profile. From these points, we prepared two kinds of sample. One was a silicon epitaxial sample, which included six different boron concentrations layers from 2×10^{18} to 1×10^{19} atoms/cm^3. Each layer was about 60 nm of the thickness. The other sample was an epitaxialy deposited SiGe sample consisted of seven different Ge Mole fractions from 1 to 14%. For this sample, B concentration was expected to be constant across all layers

in the epitaxial process. Both epitaxial layers developed on the n-type silicon substrates. The details of these samples were shown in Table 5.1.
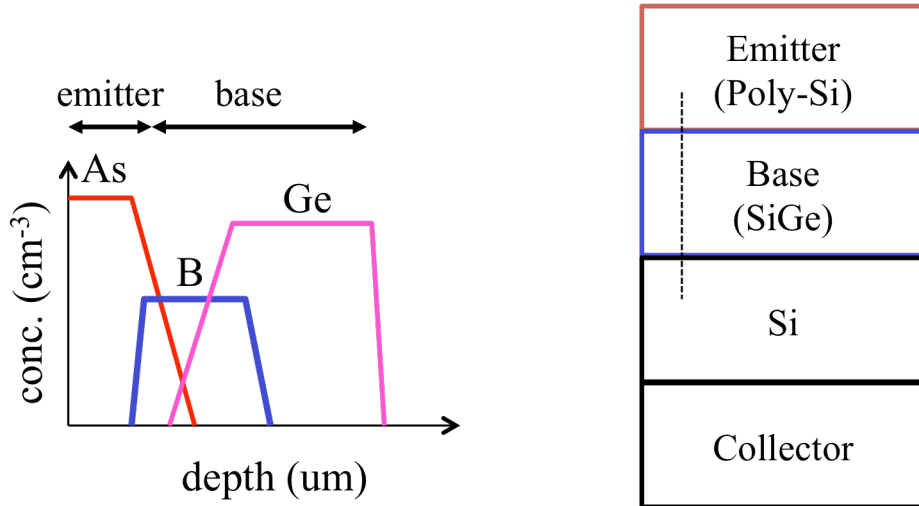

Fig. 5.2 Schematic illustration of boron profile in SiGe-HBT. The right side shows 1D structure of SiGe-HBT and the left side shows profiles of As, B and Ge across the Base region of HBT (along the dotted line in the 1D structure).

Table 5.1 Sample structures. (a) Si epitaxial sample with different boron concentrations from 2.0×10^{18} to 1.0×10^{19} atoms/cm^3. (b) SiGe epitaxial sample with different Ge Mole fraction from 1.0 to 14.0 %. Both samples developed on n-type silicon wafers.

(a) Silicon epitaxial sample

layer	B concentrations (atoms/cm^3)	thickness (nm)
a cap Si layer without boron		
1	2.0×10^{18}	60
2	4.0×10^{18}	60
3	5.0×10^{18}	60
4	7.0×10^{18}	60
5	9.0×10^{18}	60
6	1.0×10^{19}	60
silicon substrate		

(b) SiGe epitaxial sample

layer	Ge Mole fraction (%)	thickness (nm)
a cap Si layer		
1	1.0	120
2	4.0	120
3	6.0	120
4	8.0	120
5	10.0	120
6	12.0	120
7	14.0	120
silicon substrate		

These samples were measured by secondary ion mass spectrometry (SIMS). Figures 5.3 and 5.4 are results of the SIMS measurements for the silicon epitaxial sample and the SiGe epitaxial sample respectively.
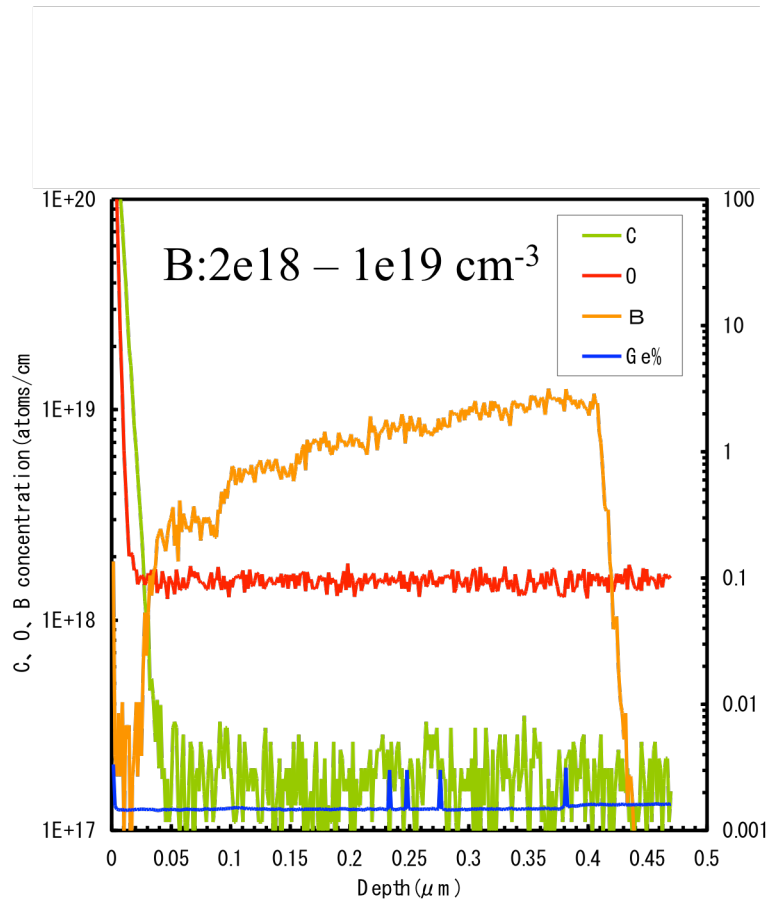

Fig. 5.3 The result of SIMS measurements for the silicon epitaxial sample.

B profile in the SiGe sample, shown in Fig. 5.4, was not constant, but looked like staircases. In this stage, we do not know whether this B staircase-like profile is real one or artificial one produced by matrix effect in SIMS measurement. Scanning capacitance microscopy (SCM), D3100 of Veeco, was applied to these samples. The two samples glued each other on their surface and cross-sectioned in order to measure both samples

at the same time according to Chapter 4. This kind of treatment was required for comparing two SCM images because SCM signals could be easily affected by surface condition of samples, tip shape, humidity in measurement and so on. The scanning area was 2 μm, parallel to the sample surfaces, by 5 μm, perpendicular to the sample surfaces. The measured two-dimensional image signal was averaged across 2 μm into one-dimensional SCM signal. On the cross-sectioned surface, there was native oxide layer and no additional insulating layer was deposited for SCM measurement in this study.
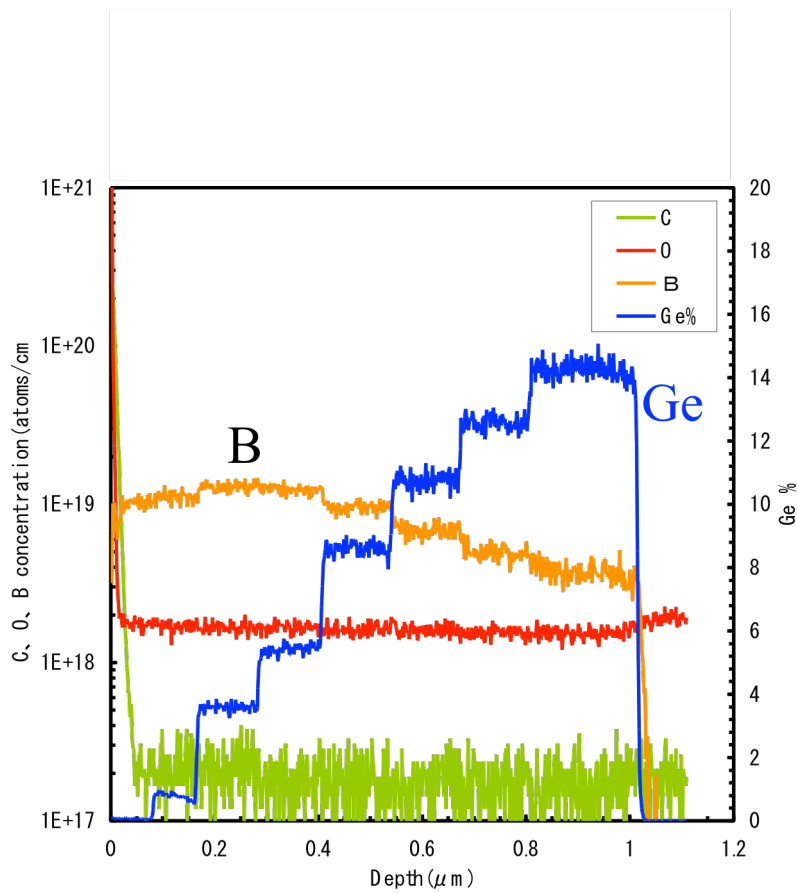
Fig. 5.4 The result of SIMS measurements for the SiGe epitaxial sample. Boron concentrations in epitaxial process had been constant in design.

5.2.3 Simulation for different Ge Mole fraction and abrupt pn junction

As described in the previous section, the SCM measurement of B doped SiGe has had possibility that SCM signal intensity in measuring same B concentration in SiGe with different Ge Mole fraction was different. In order to clarify this possibility, three-dimensional device simulation of SCM measurements was performed. In this simulation, a conductive tip of SCM, an oxide layer, and a SiGe semiconductor substrate were arranged with cylindrical symmetry. The tip radius was 30 nm and oxide thickness was 2 nm. In the device simulator, DESSIS of Synopsys, ac small signal analysis has been performed under the condition that dc voltages ramped from -2 V to $+2$ V and ac frequency was 10 kHz. From the simulation results, i.e. voltage-capacitance curve, dC/dV corresponding to SCM signal was calculated.

The device simulation was also used to explain SCM signal behavior across an abrupt pn junction. In the simulation, high doped (1×10^{19} atoms/cm^3) p-type region and low doped (1×10^{14} atoms/cm^3) n-type region made the abrupt pn junction, and a tip was located in the distance 0.05, 0.1, 0.15, and 1.0 μm from the metallurgical junction in p-type region and in the distance 0.05, 0.2, 0.5, 1.0, 1.5, and 2.0 μm from the junction in n-type region.

5.2.4 Results

Figure 5.5 shows the result of SCM measurement of the Si epitaxial sample, which has different boron concentrations in six layers whose SIMS analysis was shown in Fig. 5.3. The horizontal axis shows the depth from the top surface of the sample indicated in "0" position. The minus area in this axis is the gluing region between the two samples described in the Section 5.2.2. The vertical axis of the figure is intensity of dC/dV signal of the SCM in arbitrary unit. From the top surface of the Si epitaxial sample, SCM signal increased rapidly to about 0.1 μm depth and then decreased gradually to about 0.4 μm. After that the signal rapidly increased to 0.6 μm and again decreased.
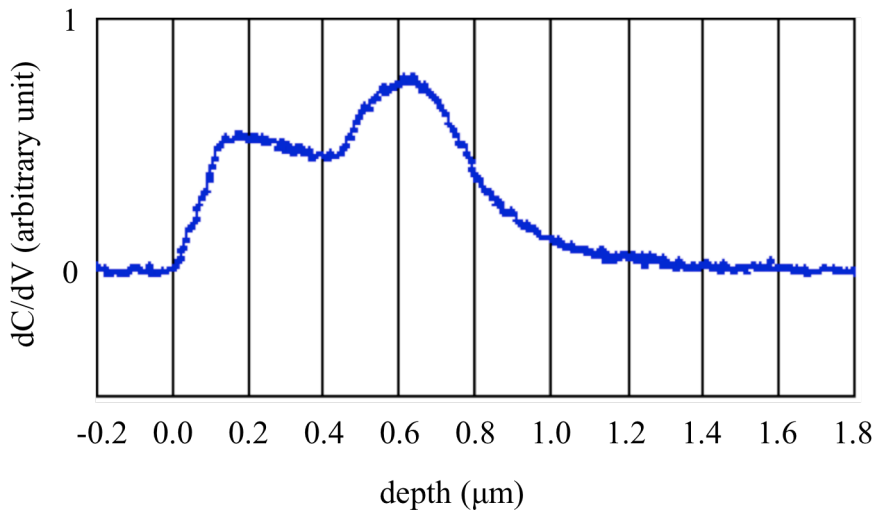
Fig. 5.5 The result of SCM measurement of the Si epitaxial sample, which has different boron concentrations in six layers (Table 5.1(a), Fig. 5.3).
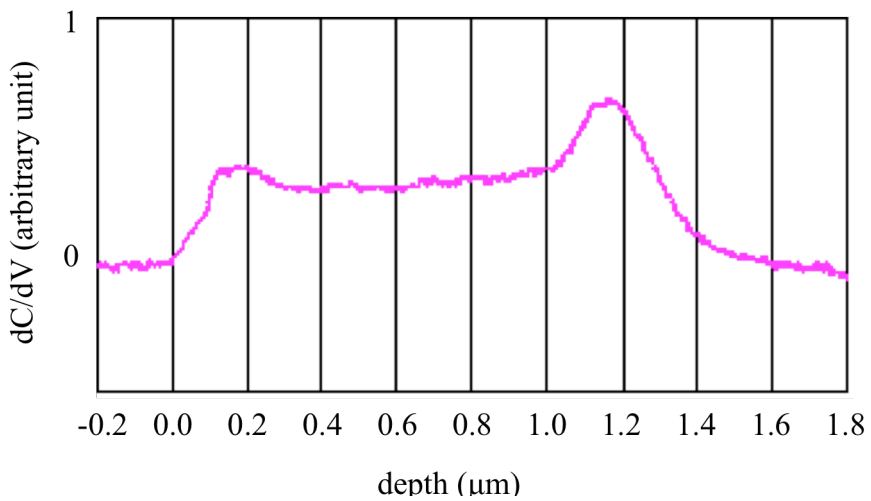

Fig. 5.6 The result of SCM measurement of the SiGe epitaxial sample, which has seven different Ge Mole fraction layers (Table 5.1(b), Fig. 5.4).

Figure 5.6 shows the result of SCM measurement of the SiGe epitaxial sample, which has seven different Ge Mole fraction layers whose SIMS analysis was shown in

Fig. 5.4. SCM signal increased rapidly from the top surface, and then decreased to about 0.3 μm. From 0.3 μm the signal increased gradually to 1.0 μm and then rapidly increased and again decreased. These SCM results shown in Figs. 5.5 and 5.6 indicated the same behavior, i.e. rapid increase and decrease of the SCM signals, at both ends of the boron doped epitaxial layers, i.e. at the surface of the sample and at the interface of n-type silicon substrate where corresponded to metallurgical junction position.

In order to figure out the reason of this behavior, we performed device simulations modeling the interface of the boron doped epitaxial layer and the n-type silicon substrate. Fig. 5.7 shows the device simulation result of the abrupt pn junction delineation.
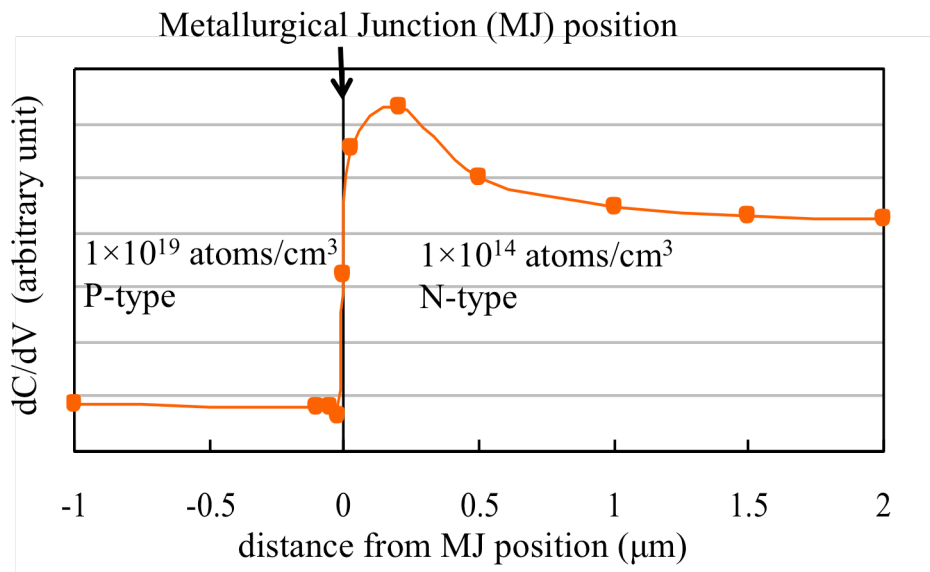

Fig. 5.7 The device simulation result of abrupt pn junction delineation. The origin of the horizontal axis is metallurgical junction potion of the sample.

The horizontal axis shows a distance from the metallurgical junction position locating at the origin. The left side of this figure is a boron high-doped (1×10^{19} atoms/cm^3) area and the right side is an n-type low-doped (1×10^{14} atoms/cm^3) area. From left to right in the figure, the SCM signal started low intensity over high-doped boron region and

increased rapidly at the metallurgical pn junction in low concentration n-type region then gradually decreased. This result was in good agreement qualitatively with measured results shown in the Figs. 5.5 and 5.6. Because the simulation result does not include phase information, the total SCM signal is sum of the SCM signal for p-type and for n-type, as is shown schematically in Fig. 5.8(a). While the SCM measurement results include phase information so that SCM signal equals SCM signal for p-type minus for n-type, as is shown in Fig. 5.8(b).

Figure 5.9 shows the simulation results of $dC/dV - V_{dc}$ curve with different Ge Mole fraction and B concentrations. The dC/dV signal of $Si_{0.9}Ge_{0.1}$ was larger than that of $Si_{0.8}Ge_{0.2}$ in the negative V_{dc} range. On the contrary, the dC/dV signal of $Si_{0.9}Ge_{0.1}$ was smaller than that of $Si_{0.8}Ge_{0.2}$ in the positive V_{dc} range. These results indicate that the same B concentration shows different dC/dV signal intensity in different Ge Mole fraction region and at different V_{dc} bias. Moreover this difference of dC/dV signal intensity also depended on B concentration. These are the "matrix effect" in SCM measurement. Here, we compared the measured result shown in Fig. 5.6 and the simulation result shown in Fig. 5.9. In Fig. 5.6, the intensity of dC/dV was the value at the fixed Vdc = -0.5 V. In the measured data, there was difference of dC/dV signal intensity by 33 % over all the different Ge Mole fraction regions. In the simulation data, there was approximately 20% difference in dC/dV signal intensity of the same B concentrations and different Ge Mole fractions at V_{dc} = -0.5 V, at which the SCM measurement was performed. This comparison indicates that the B concentration were actually different at different Ge Mole fraction layers in this sample, because that the difference of the measured data, i.e. 33 %, was larger than that of the matrix effect, i.e. 20 %.
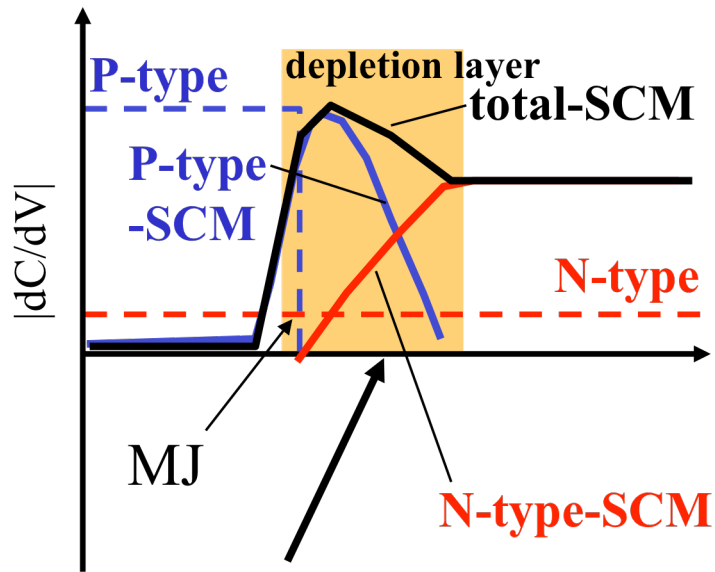
(a) Simulation (without phase)
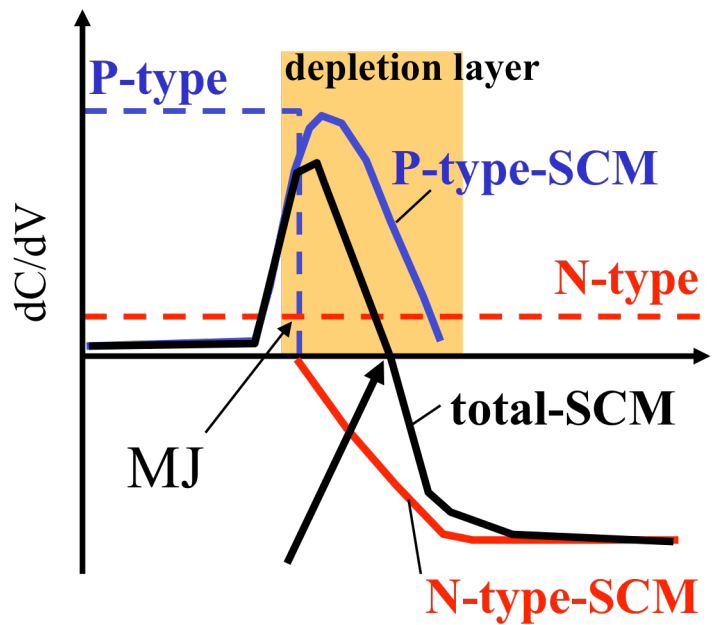
(b) SCM measurement with phase

Fig. 5.8 Schematic illustrations of SCM measurement across an abrupt junction (a) without and (b) with phase information.
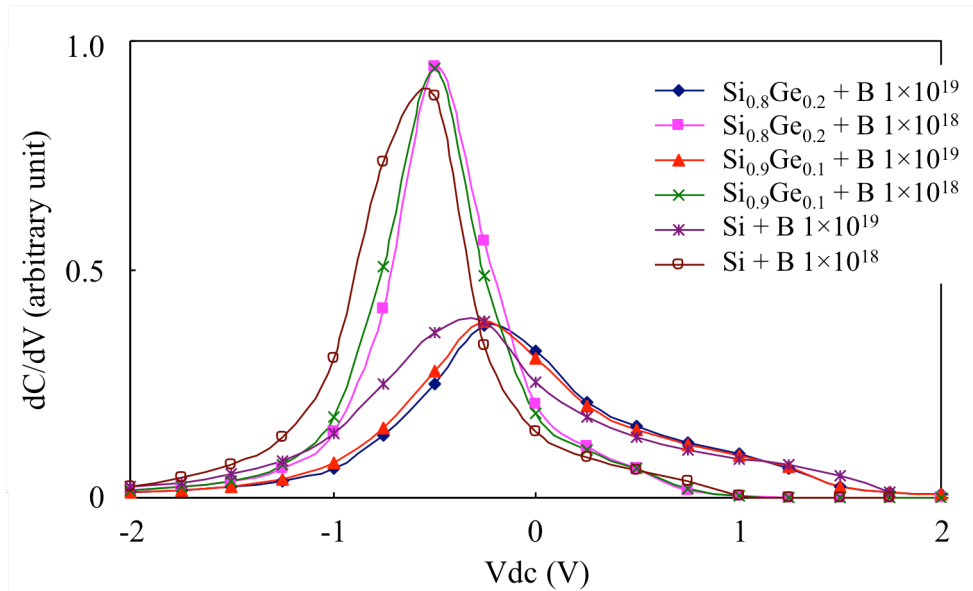
Fig. 5.9 The simulation results of dC/dV – Vdc curve with different Ge Mole fraction and B concentrations.

5.3 Comparison of B diffusion in SiGe and SiGeC

In order to improve high-speed performance of SiGe-HBTs, a SiGeC is used for a base layer material in state-of-the-art HBTs [5.7, 5.8]. One of the features of SiGeC is lower diffusivity of B in it than in SiGe. Therefore, the B profile in and around a base layer could be controlled more precisely by using SiGeC, so that transient time through the base layer becomes shorter.

Low diffusivity of B in SiGeC has been measured by SCM. SiGe and SiGeC epitaxial samples have been prepared. Figure 5.10 shows sample structure common for both samples. There were 6 epitaxial layers; each was 50 nm of the thickness. The Mole fraction of Ge for SiGe and SiGeC was 0.9 and C concentration was 0.25 % for SiGeC.

Three layers included B whose concentration are 1×10^{17}, 1×10^{18}, and 1×10^{19} atoms/cm^3 respectively, and each layer was separated by a buffer layer including no B atoms.

Si0.9Ge0.1（C0.0025）　B=0　50nm
Si0.9Ge0.1（C0.0025）　B=1e17　50nm
Si0.9Ge0.1（C0.0025）　B=0　50nm buffer layer
Si0.9Ge0.1（C0.0025）　B=1e18　50nm
Si0.9Ge0.1（C0.0025）　B=0　50nm buffer layer
Si0.9Ge0.1（C0.0025）　B=1e19　50nm
Si0.9Ge0.1（C0.0025）　B=0　50nm buffer layer
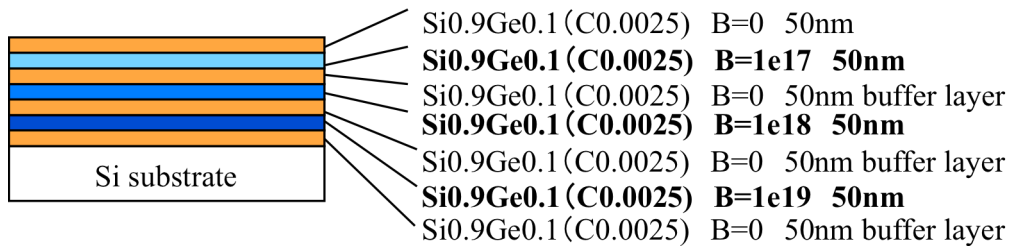
Fig. 5.10 Sample structure of SiGe and SiGeC epitaxial samples. Different B concentrations layers were separated by 50 nm buffer layers including no boron.

These two samples were glued each other and cross-sectioned as described in the Section 4.1.2, and then measured at the same time. Figure 5.11 shows the results of SCM measurements of the cross-sectioned surface of SiGe and SiGeC. Two measurements were shown for each material. In the results of SCM measurements for SiGeC, there were three dips corresponding three different B concentrations layers. On the contrary there was no clear dip in the result of SCM measurement for SiGe. This indicates that B has diffused deeper into buffer layers in SiGe than in SiGeC, namely B diffusivity is larger in SiGe than in SiGeC. Considering tip radius of SCM, which is approximately 30 nm in this measurement, the diffusion distance of B in SiGeC is estimated to be less than 10 nm.
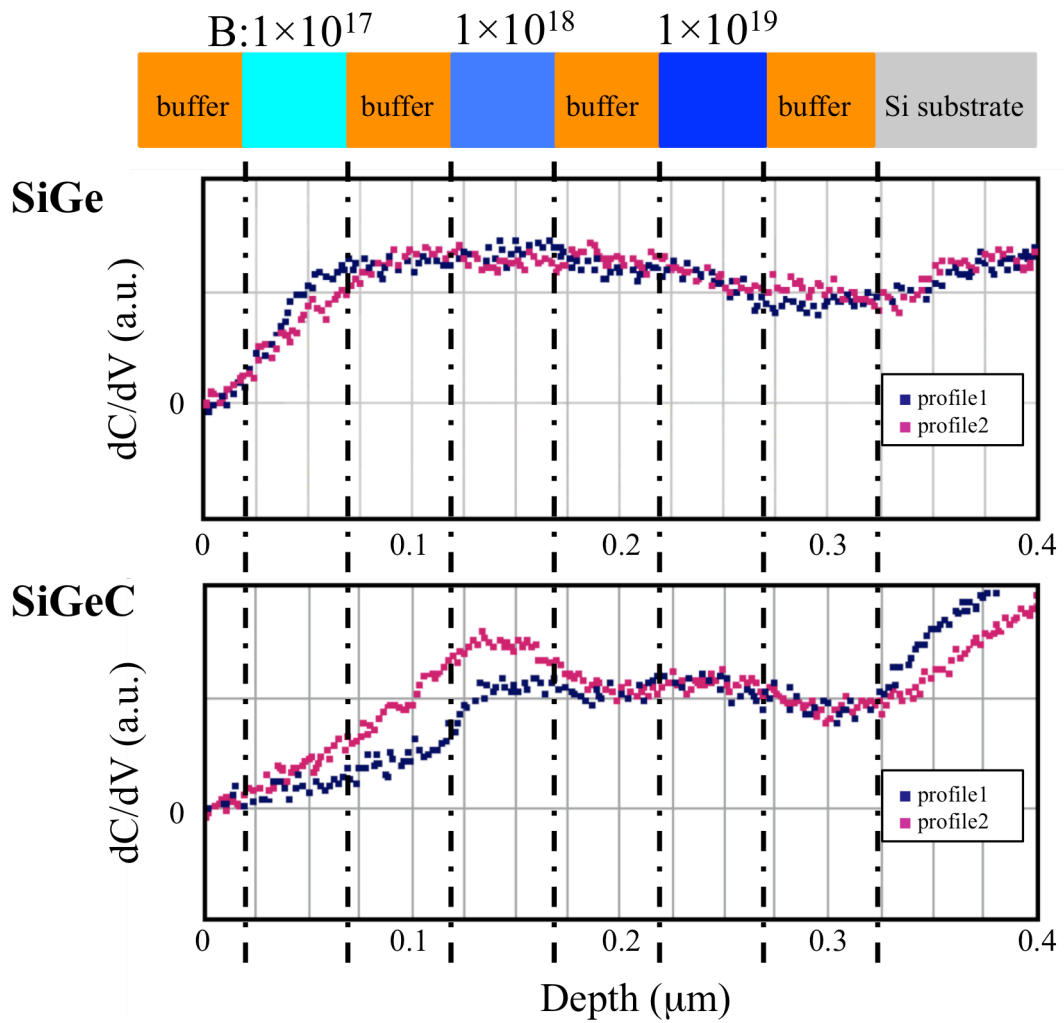
Fig. 5.11 The results of SCM measurements of the cross sectioned surface of SiGe and SiGeC. Both samples were measured two times as profile 1 and 2 in the figure.

In this chapter, the application of SCM measurements to SiGe and SiGeC was described. The SCM could be applicable to any semiconductor materials, which could have a flat surface and a thin insulating layer on it. There have been reports on various materials including GaN, SiC, and GaAs [5.9 – 5.12].

References

[5.1] J. Singh, Semiconductor Devices An Introduction, McGraw-Hill, 1994.

[5.2] Y. M. Sheu, S. J. Yang, C. C. Wang, C. S. Chang, L. P. Huang, T. Y. Huang, M. J. Chen and C. H. Diaz, "Modeling mechanical stress effect on dopant diffusion in scaled MOSFETs", IEEE Transactions on Electron Devices, vol. 52, pp. 30-38, 2005.

[5.3] K. M. Wong, W. K. Chim, K. W. Ang and Y. C. Yeo, "Spatial distribution of interface trap density in strained channel transistors using the spread of the differential capacitance characteristics in scanning capacitance microscopy measurements", Applied Physics Letters, vol. 90, pp. 153507-153507, 2007.

[5.4] J. A.Jackman, L. Dignard-Bailey, R. S. Storey, C. MacPherson, S. Rolfe, L.Van Der Zwan and T. E. Jackman, "Matrix effects in sims depth profiles of SiGe superlattices", Nuclear Instruments and Methods in Physics Research Section B, vol. 45,pp. 592-596, 1990.

[5.5] J. D. Cressler, "SiGe HBT technology: a new contender for Si-based RF and microwave circuit applications", IEEE Transactions on Microwave Theory and Techniques, vol. 46, pp. 572-589, 1998.

[5.6] H. K.Liou, P. Mei, U. Gennser and E. S. Yang, "Effects of Ge concentration on SiGe oxidation behavior", Applied Physics Letters, vol. 59, pp.1200-1202, 1991.

[5.7] H. J. Osten, G. Lippert, P. Gaworzewski and R. Sorge, "Impact of low carbon concentrations on the electrical properties of highly boron doped SiGe layers", Applied

Physics Letters, vol. 71, pp. 1522-1524, 1997.

[5.8] P. Chevalier, C. Fellous, B. Martinet, F. Leverd, F. Saguin, D. Dutartre and A.Chantre, "180 GHz f/sub T/and f/sub max/self-aligned SiGeC HBT using selective epitaxial growth of the base", ESSDERC'03, pp. 299-302. 2003.

[5.9] S. Das Bakshi, J. Sumner, M.J. Kappers and R.A. Oliver, "The influence of coalescence time on unintentional doping in GaN/sapphire", Journal of Crystal Growth, vol. 311, pp. 232-237, 2009.

[5.10] J. Sumner, R. A. Oliver, M. J. Kappers and C. J. Humphreys, "Practical issues in carrier-contrast imaging of GaN structures", physica status solidi (c), vol.4, pp. 2576-2580, 2007.

[5.11] P. Fiorenza, F. Giannazzo, M. Vivona, A. La Magna and F. Roccaforte, "SiO2/4H-SiC interface doping during post-deposition-annealing of the oxide in N2O or POCl3", Applied Physics Letters, vol.103, pp.153508, 2013.

[5.12] Z. Y. Zhao, W. M. Zhang, C. Yi, A. D. Stiff-Roberts, B. J. Rodriguez and A. P. Baddorf, "Doping characterization of InAs∕ GaAs quantum dot heterostructure by cross-sectional scanning capacitance microscopy", Applied Physics Letters, vol.92, pp. 092101, 2008.

Chapter 6
Discussion

6.1 Junction position in lateral direction

6.2 Defect distribution

There have been described our two major studies of computational simulation method for prediction of an ultra-shallow junction position in Chapter 2 and of quantitative SCM measurement of a doping profile in Chapters 3 − 5. In this chapter, advantages and necessity of the combination of these two aspects will be discussed.

6.1 Junction position in lateral direction

As described in the Section 1.3, a doping profile and its junction position directly influences on the electrical properties of a semiconductor device. The importance of a two-dimensional doping profile of a source/drain region has been increased in the smaller MOSFETs in which the short channel effect becomes remarkable. However, the prediction of a doping profile and a junction position, formed by a low-energy doping process, in the lateral direction, i.e. across the channel width, of a MOSFET has not been established well. One reason is that we do not have an adequate simulation model that predicts a dopant distribution in the lateral direction in a doping process at the low-energy range. As for the vertical direction, we could obtain a measured doping profile by SIMS that has enough accuracy for the calibration of the parameters of a doping process simulation model in the vertical, or one-dimensional, direction. On the other hand, we do not have had a good measurement method for the lateral direction or 2D for the calibration of the doping simulation parameters. The SCM method would be an alternative to SIMS method for a profile measurement in the lateral direction.

A simulation model for low-energy doping process should handle the behavior of the dopant atoms in three-dimensions. In Chapter 2, the hybrid method of the quantum molecular dynamics and the classical molecular dynamics was shown to be applicable to a silicon structure with the depth of more than 10nm that is needed for direct prediction of a junction position in the depth direction. This hybrid method has an advantage that could apply to a doping profile prediction in 3D without changing any

simulation parameter except a silicon substrate structure model that has a wider size in the lateral direction and an additional patterned layer for a mask. That would be performed by using, for example, a silicon substrate model with dimensions of 20 nm (in x-direction) × 10 nm (in y-direction) × 10 nm (in z-direction) and a mask layer with dimensions of 10 nm (in x-direction) × 10 nm (in y-direction) × 20 nm (in z-direction), and at least 100000 dopant atoms.

Therefore, the combination of the hybrid molecular dynamics method and the SCM technique would be used effectively in the prediction and the design of a pn junction position of source/drain extension in the lateral direction of a MOSFET.

6.2 Defect distribution

The SCM is basically an electrical measurement and affected not only by carriers generated from activated dopants but also by defects in semiconductors. This is a big difference between SCM and SIMS measurement.

Thus far, an influence of damages on a SCM measurement has not been described well. The damages would be generated in a doping process or in a sample preparation. Figure 6.1 shows the results of SCM measurement of the boron-implanted sample with and without a thermal annealing after the doping process. The annealed sample is the same of Section 4.2.3. Both samples were glued each other, cross-sectioned, and measured by SCM with different dc voltages. The dashed line at about 3.2 μm in Fig. 6.1 indicates the glue layer between the two samples. The left side of the glue layer is the annealed sample and the right side of it is the non-annealed one. The two dotted lines in this figure indicate the peak positions of doped boron concentration. The results of SCM measurement of the sample with and without annealing were different in the doped region and almost same in the deeper region. In the Fig. 6.1, the position at 0.7 μm or 5.7 μm in the horizontal axis is located 2.5 μm from the glued layer, i.e. the

surface of each sample, where the concentration of boron are less than the n-type silicon substrate as shown in Fig. 4.15. At this depth, the SCM signals of the both samples strongly depended on the dc bias because of the low carrier concentration. The intensity of the dC/dV signal at the peak concentrations was 0.08 for the annealed sample and 1.67 for the non-annealed sample at Vdc = 0 V. This dC/dV value of 1.67 was corresponded to 4.8×10^{17} atoms/cm^3 boron or carrier concentrations in the annealed sample. According to the V_{dc} change, the corresponding concentrations changed up to 1.5×10^{18} atoms/cm^3.

From the SCM measurement, we could not tell whether these carriers come from the activated boron atoms or from the defects generated during a doping process so far. On the contrary, this kind of data shown in Fig. 6.1 could not be measured by a SIMS analysis. This is because that SIMS method is destructive analysis and does not distinguish an activated or a non-activated atom.

From the hybrid molecular dynamics method described in Chapter 2, we could estimate a defect distribution as shown in Fig. 2.5. Although we could not describe whether a defect is an electrical active or not so far, this method has a potential to describe them by using a higher ratio of the quantum calculation part to the classical one.

It would be useful to investigate a silicon substrate doped by silicon atoms by using both the SCM measurement and the hybrid molecular dynamics method to distinguish carriers generated from defects during a doping process from activated atoms.
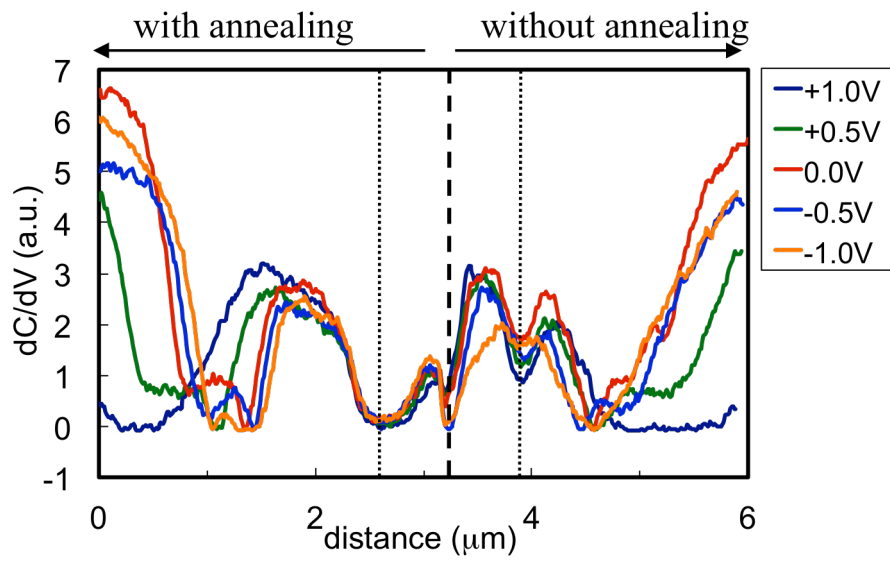
Fig. 6.1 The results of SCM measurements of boron implanted samples with and without thermal annealing after the implantation process. The dashed line indicates the glue layer of the two samples. The dotted lines indicate the positions of peak boron concentration of the samples.

Chapter 7
Summary and Conclusions of this work

7.1 Summary

7.2 Conclusions

     7.2.1 Low-energy doping simulation

     7.2.2 Methodology of quantitative SCM

7.3 Future Perspective

References

7.1 Summary

In this work, the methodologies of evaluation of the doping profiles in semiconductor devices were studied by using computational simulations and the scanning capacitance microscopy measurement.

As for the computational simulation, the original hybrid method combining the tight-binding quantum chemical and the classical molecular dynamics was first applied to the low-energy doping process of boron into a silicon substrate, which has a depth of more than 10 nm that is needed to evaluate an ultra-shallow junction position. A comparison of the junction position with a plasma doping experiment was carried out. Good agreement between the simulation and the experimental results indicates that the hybrid molecular dynamics method is applicable to the doping profile prediction in a silicon structure with a depth of more than 10 nm that is needed to evaluate ultra-shallow junction formation [7.1].

The repeatable and reproducible SCM measurements were established by using dry oxidation of the sample surface and diamond-coated probes [7.2]. Using this stable measurement, the methodology of quantitative SCM measurement and analysis with the combination of the device simulator was performed. Applying this method to the boron implanted silicon sample, we got the results in good agreement with SIMS measurement over the range four orders of magnitude of boron concentrations [7.3].

This work had been done mainly from 2000 to 2002 for the scanning capacitance measurements and from 2005 to 2007 for the doping simulation. After these periods, many progresses have been made and new techniques have been developed in the field of scanning probe microscopy. However, the repeatability and reproducibility of the measurements and data conversion from the measured into desired properties have been always the most important aspect of SCM and any other kinds of SPM in practical uses. Therefore, the importance of this work is still the same or much more increasing.

7.2 Conclusions

7.2.1 Low-energy doping simulation

- Hybrid method of the tight-binding quantum chemical and the classical molecular dynamics (MD) was first applied to the prediction of an ultra-shallow junction position of a low-energy boron doping process.

- The junction position of 200 eV boron doping process was 6.2 nm in the hybrid MD simulation result and 6.4 nm in the experimental result of plasma doping. This good agreement showed the availability of the hybrid MD method for the low-energy doping process.

- The hybrid MD method has advantages of (1) treating many-body collision effect, which is important in the low-energy region, comparing with the Monte Carlo method in binary-collision approximation, (2) having information of the electron states, which is useful for the defect analysis, comparing with the classical MD method, and (3) taking shorter computational time comparing with the first-principles method.

- The hybrid MD method reproduced the increase of the retained boron dose with increasing initial energy in the low energy region of less than 200 eV.

7.2.2 Methodology of quantitative SCM

- Repeatable and reproducible SCM measurement was achieved by using a diamond-coated probe. The shifts of SCM signals during 10 successive measurements of a Si sample having doping concentration among 4.0×10^{15} and 6.0×10^{19} atoms/cm^3 were improved to 0.2 – 8 % by the diamond-coated probe from 5

- 15% by the conventional metal-coated probe.

- The methodology of quantitative SCM measurement was established by using the combination of the concentration standard sample and 3D device simulation. The doping concentration converted from SCM signal was in good agreement with the result of SIMS measurement over the range of four orders of magnitude for a boron doping profile. It was better than the reported results at around year 2002 by one or two orders of magnitude.

- SCM measurement was shown to be suitable for the delineation of abrupt pn junction positions.

- SCM measurement was applied to SiGe and SiGeC, and directly demonstrated the difference of carrier distribution, i.e. boron diffusion, in SiGe and SiGeC.

7.3 Future Perspective

After this work performed mainly from 2000 to 2007, many progresses have been performed in the field of scanning probe microscopy. Scanning spreading resistance microscopy (SSRM) and Kelvin force microscopy (KFM) has shown major improvements [7.4]. Scanning Microwave Microscopy (SMM) has also developed as a dopant profiler [7.5]. These scanning probe techniques use different electrical characters and we still do not understand enough the interaction between probes and sample surfaces of these SPMs [7.6]. This should be studied in the future for us to measure many materials appearing in semiconductor device research and industry.

Nowadays, the SCM measurement is used as one of the standard doping profile measurements in the semiconductor industry. In this work, cross-sectioned samples have been prepared with the method of cleaving and polishing. Recently, a focused ion beam (FIB) method is used for preparing the cross-sectioned samples in device development and manufacturing. This FIB method is essential for a failure analysis of a

device. After electrical measurements of devices in a wafer, the positions of defective devices in the wafer are recorded. The wafer or a part of it is located in FIB equipment and the position of the defective device is identified. Then it is processed with ion beams to make the cross-sectioned sample. Using the FIB method, we can measure dopant profile in the cross-sectioned device sample with SCM, which corresponds one-to-one to the electrical device properties.

References

[7.1] H. Yabuhara and A. Miyamoto, "Prediction of low-energy boron doping profile for ultra-shallow junction formation by hybrid molecular dynamics method", Japanese Journal of Applied Physics, vol. 55, pp. 016503, 2015.

[7.2] H. Yabuhara, M. Ciappa and W. Fichtner, "Diamond-coated cantilevers for scanning capacitance microscopy applications", Microelectronics Reliability, vol. 41, pp. 1459-1463, 2001.

[7.3] H. Yabuhara, M. Ciappa and W. Fichtner, "Scanning capacitance microscopy measurements using diamond-coated probes", Journal of Vacuum Science and Technology B, vol. 20, pp. 783-786, 2002.

[7.4] D. A. Bonnell, D. N. Basov, M. Bode, U. Diebold, S. V. Kalinin, V. Madhavan, L. Novotny, M. Salmeron, U. D. Schwarz and P. S. Weiss, "Imaging physical phenomena with local probes: From electrons to photons", Reviews of Modern Physics, vol. 84, pp. 1343-1381, 2012.

[7.5] A.Imtiaz, T. M. Wallis, S. H. Lim, H. Tanbakuchi, H. P. Huber, A.Hornung, P. Hinterdorfer, J. Smoliner, F. Kienberger and P. Kabos, "Frequency-selective contrast on variably doped p-type silicon with a scanning microwave microscope", Journal of Applied Physics, vol. 111, pp. 093727. 2012.

[7.6] A. Sadeghi, A. Baratoff and S. Goedecker, "Electrostatic interactions with dielectric samples in scanning probe microscopies", Physical Review B, vol. 88, pp.035436, 2013.

List of Publications

Journal Papers

[1] H. Yabuhara, M. Ciappa, and W. Fichtner, "Diamond-coated cantilevers for scanning capacitance microscopy applications", Microelectronics Reliability, vol. 41, pp. 1459-1463, 2001.

[2] H. Yabuhara, M. Ciappa, and W. Fichtner, "Scanning capacitance microscopy measurements using diamond-coated probes", Journal of Vacuum Science and Technology B, vol. 20, pp. 783-786, 2002.

[3] H. Yabuhara and A. Miyamoto, "Prediction of low-energy boron doping profile for ultra-shallow junction formation by hybrid molecular dynamics method", Japanese Journal of Applied Physics, vol. 55, pp. 016503, 2015.

[4] H. Tsuboi, A. Sagawa, H, Iga, K. Sasata, T. Masuda, M. Koyama, M. Kubo, E. Broclawik, H. Yabuhara, and A. Miyamoto, "Tight-Binding Quantum Chemical Molecular Dynamics Study on Depth Profile Prediction in Low Energy Boron Implantation Process", Japanese Journal of Applied Physics, vol. 44, pp. 2288-2293, 2005.

Presentations in international conference

[5] H. Yabuhara, M. Ciappa, and W. Fichtner, "Diamond-coated cantilevers for scanning capacitance microscopy applications", 12th European Symposium on the Reliability of Electron Devices, Failure Physics and Analysis (ESREF 2001), Bordeaux, France, 1-5 October, 2001.

[6] H. Yabuhara, M. Ciappa, and W. Fichtner, "Comparison of boron diffusion in SiGe and SiGeC by scanning capacitance microscope", Seeing at the Nanoscale European Conference II, France, 13-15 October, 2004.

Presentations in domestic conference

[7] H. Yabuhara, M. Ciappa, and W. Fichtner, "Quantitative scanning capacitance microscopy measurement using diamond-coated probes", Extended Abstracts of the 63rd Autumn Meeting of the Japan Society of Applied Physics and Related Societies, 2002.

Others

[1] H. Yabuhara and Y. Kataoka, "Evaluation of n^+a-Si contact with indium tin oxide by X-ray photoelectron spectroscopy valence band measurement", Japanese Journal of Applied Physics, vol. 38, pp. 5232-5235, 1999.

[2] S. Kinoshita, S. Takagi, H. Yabuhara, H. Nishimura, H. Kawaguchi, and N. Shigyo, "Calibration Method for High-Density-Plasma Chemical Vapor Deposition Simulation", Japanese Journal of Applied Physics, vol. 41, pp. 1974-1980, 2002.

[3] H. Yabuhara, H. Okumura, M. Higuchi, and Y. Baba, "Characterization of annealed a-Si films for poly-Si diode", Extended Abstracts of the 43rd Spring Meeting of the Japan Society of Applied Physics and Related Societies, p665, 1996.

[4] H. Yabuhara, R. Saito, and K. Makino, "Increase in ITO/Si contact resistance caused by Indium Diffusion", Extended Abstracts of the 44th Spring Meeting of the Japan Society of Applied Physics and Related Societies, p463, 1997.

[5] H. Yabuhara, M. Honda, M. Morita, and H. Ezawa, "Improvement of aluminum texture using long throw sputtered Ti/TiN underlayer", Extended Abstracts of the 46th Spring Meeting of the Japan Society of Applied Physics and Related Societies, p891, 1999.

[6] H. Yabuhara, K. Tsutsumi, K. Nishitani, and H. Ezawa, "Effect of surface micro roughness of dielectric under layer on aluminum crystal orientation", Extended Abstracts of the 47th Spring Meeting of the Japan Society of Applied Physics and Related Societies, p867, 2000.

Acknowledgments

Finally, I would like to express my profound gratitude to my wife Naoko, my daughter Hinako, my parents and all of my family members for their invaluable support and encouragement throughout this study.